CT-917-551
Doc. 7016

Centro de Investigación y de Estudios Avanzados
del Instituto Politécnico Nacional
Unidad Guadalajara

Un Enfoque Estadístico a la Estimación Modal de Sistemas de Potencia Sujetos a Excitación Ambiente

Tesis que presenta:

Juan Antonio Medina Rosas

para obtener el grado de:

Maestro en Ciencias

en la especialidad de:

Ingeniería Eléctrica

Director de Tesis:

Dr. Arturo Román Messina

CINVESTAV del IPN Unidad Guadalajara, Guadalajara, Jalisco, Agosto de 2015.

CLASIF.. CTOO818
ADQUIS.. CT917-551
FECHA: 25-04-2016
PROCED.. DONA 2016
$

Centro de Investigación y de Estudios Avanzados
del Instituto Politécnico Nacional
Unidad Guadalajara

A Stochastic Approach to Power System Ambient Mode Estimation

A thesis presented by:

Juan Antonio Medina Rosas

to obtain the degree of:

Master of Science

in the subject of:

Electrical Engineering

Thesis Advisor:

Dr. Arturo Román Messina

CINVESTAV del IPN Unidad Guadalajara, Guadalajara, Jalisco, August 2015.

Un Enfoque Estadístico a la Estimación Modal de Sistemas de Potencia Sujetos a Excitación Ambiente

Tesis que presenta:
Juan Antonio Medina Rosas

Por:
Juan Antonio Medina Rosas
Ingeniero en Electricidad y Automatización
Universidad Autónoma de San Luis Potosí
2008-2013

Becario de CONACYT, expediente no. 300937

Director de Tesis:
Dr. Arturo Román Messina

CINVESTAV del IPN Unidad Guadalajara, Agosto de 2015

A stochastic Approach to Power System Ambient Mode Estimation

Master of Science Thesis
In Electrical Engineering

By·
Juan Antonio Medina Rosas
Electrical Engineer
Universidad Autónoma de San Luis Potosí
2008-2013

Scholarship granted by CONACYT, No. 300937

Thesis Advisor:
Dr. Arturo Román Messina

CINVESTAV del IPN Unidad Guadalajara, August 2015.

Acknowledgments

I would like to express my sincere gratitude to my advisor, Ph.D. Arturo Román Messina, for sharing his knowledge, understanding and patience, and for providing me a valuable global perspective on scientific discovery and innovation.

I would also like to thank my family for the support that they provided me every day of my entire life.

To my professors and friends at CINVESTAV Guadalajara, as well as to my friends

Finally, acknowledgements are also due to CONACYT for its support.

Resumen

Las características modales electromecánicas de los sistemas de potencia proporcionan información crítica para estimar la confiabilidad en la operación y la seguridad del sistema. El monitoreo continuo de la evolución temporal de la respuesta del sistema permite detectar condiciones que vulneran la estabilidad dinámica de la red, así como las etapas críticas para su análisis y control. La extracción de estas propiedades a partir de mediciones ambiente, es un problema difícil que necesita mayor investigación.

En esta tesis, se propone un método novedoso basado en el análisis lineal estocástico, que extiende los métodos existentes de análisis lineal a un ambiente probabilístico. El método propuesto es particularmente útil para la estimación de las características modales a partir de la respuesta del sistema a la excitación aleatoria de las cargas, proporcionando observabilidad completa del sistema. A si mismo, el marco teórico propuesto permite complementar la información proporcionada por las técnicas de estimación basadas en mediciones, así como la ubicación óptima de sensores para el monitoreo de las variables que contienen mayor cantidad de información.

En esta tesis, se desarrolla primero, un modelo lineal del sistema de potencia que incorpora explícitamente el comportamiento aleatorio de la carga. A continuación, se proponen, técnicas para determinar la distribución de la respuesta del sistema.

A partir de este modelo se identifican los modos y las excitaciones que contribuyen de manera dominante en el comportamiento dinámico del sistema. Se identifica, asimismo, la distribución espacial de los modos.

La metodología propuesta se aplica a modelos realistas de sistemas de potencia y los resultados obtenidos se comparan con otros métodos convencionales de análisis.

Abstract

Power system's modal electromechanical properties provide critical information for assessing operational reliability and security of interconnected power grids. By tracking the evolving dynamics of the underlying modal properties, the onset of system instability can be determined and the critical stages for analysis and control can be identified. Extraction of modal properties from ambient operation, however, is very challenging issue.

In this thesis, a novel analytical framework based on linear stochastic analysis that extends the existing linear analysis methods to the stochastic setting, is proposed. The method is especially well suited to estimate modal properties from measured, ambient system response to random load variations and provides full observability of system dynamics. As a result, the developed framework can be used to supplement information to measurement-based modal estimation techniques as well as to place sensors.

A multi-machine linear power system model with a stochastic forcing term that explicitly accounts for random load behavior is first developed. Techniques to determine the distribution of the system response are then introduced. Using this framework, the modes that dominate the system dynamic behavior and the forcing functions that contribute most to this response are directly calculated. Further, the spatial distribution of the modes is identified.

The proposed methodology is tested on realistic power system models and the results are compared with those obtained from conventional analysis methods.

Index

Index of Figures

Chapter 1

Introduction

This introductory chapter presents a brief description of the research work contained in the thesis.

The background and motivations are explained as well as the statement to the problem that is attached in this document.

Further, a concise review of the previous work related to the topics treated in this thesis is presented. Also, the pursued objectives, the obtained results and the limitation of the approach are then stated.

Moreover, the main contributions are summarized.

The last part of the chapter is an outline of the general structure of the thesis.

1.1 Background and motivation.

The stability of power system oscillations, inherent to large interconnected systems, is one of the most important power industry concerns. Consequently, great effort has been made by many researchers to understand and control such complex phenomena [1],[2].

In this pursuit, mathematical models have played an important role, and one basic tool used to analyzed power system oscillatory behavior has been the concept of oscillatory modes [3],[4].

Of special interest are the fundamental electromechanical oscillation modes that underlie system behavior. They can be of two types: local and inter-area. Inter-area oscillations are the main concern in power systems dynamic security studies [3],[4].

Inter-area modes, involve groups of generators exchanging energy through the transmission system. Modal properties such as modal frequency, modal damping and shape provide critical information for improved operational reliability of power grids and can be used to place and design controllers [5]. If these slow modes, in the range of 0.1 to 2 Hz, are not sufficiently damped, unstable operation may occur, potentially leading to uncontrolled separation of the system into islands and consequently blackouts [6]. As a result of the critical characteristics of the physical phenomena that inter-area modes describe, the primary aim of dynamic security studies is to extract and characterize the key dynamic properties of these oscillations. Two main approaches are found to this purpose: *modal-based* and *measurement-based* approaches.

Model-based approaches assume that an accurate non-linear model of the power system is available and that this can be linearized around an operating condition of interest. As a consequence, the modal properties are obtained by using linear system concepts; this method is referred to as modal system analysis or small signal stability analysis [3],[4]. Probabilistic extensions of modal analysis also exist, and they account for uncertainty in model [7].

Measurement-based approaches do not require an analytic model of the grid. Instead, signal-processing techniques are implemented to conduct modal estimation by using data collected from wide-area monitoring systems [8],[9]. These measurement-based techniques are classified according to the system response that they are able to analyze, and two main categories are found in power systems literature: the first group embodies the analysis of measurements from transient operations, i.e., the response of a power system after a fault has occurred or a large disturbed [4] has been initiated. The second group estimates electromechanical modes from measurements describing the ambient system response, i.e., when there are continuous random changes occurring in the system, and that these changes provide a small excitation to the electromechanical dynamics [10].

Modal identification techniques when applied to ambient data present a main advantage over other existent modal identification methods using probing signals [11]: they work in a non-intrusive manner [12]. However, depending on the distribution of system sensors, they can provide a limited perspective of large system dynamic behavior [13].

In this thesis, a novel analytical framework based on linear stochastic analysis that extends the existing linear analysis methods to the stochastic setting, is proposed. A key advantage of this approach is its ability to provide full observability of the system. As a result, the proposed analytical framework can be used to describe inherent properties of the system that cannot be obtained from conventional measurement-based modal estimation techniques.

The model is especially well suited to analyzing the system response to random load and generation variations and can be used to identify the transmission and generation elements that contribute most to the oscillations as well as to extract key modal information.

1.2 Problem statement

Ambient conditions (ambient noise) [8], [10]-[17].is a widely used term in power systems literature and usually refers to the observed low-amplitude stochastic time series resulting from random load variations.

It assumes that, in absence of large disturbances such as fault, generator trip or load trip, the dynamic system behavior, over a time span of few minutes, is forced by small-amplitude varying-load processes, varying generation effects, system switching effects [14]. In practice, however, it is commonly accepted that load variations are the primary excitation to the system [10]-[17].

The principal assumption adopted for the analysis of ambient operation conditions in power systems, is that in the range of electromechanical oscillations, the çomposite load changes exhibit uncorrelated or pure white noise behavior [14],[16]-[20].

Probabilistic and statistical analyses play an important role to understand stochastic behavior of power systems [21]-[27]. The statistical analysis of the ambient response provides information about the most likely critical modes that dominate the system response. Also, the participation of an individual machine or groups of machines in one particular mode can be determined through these methods. These inherent properties of the system are of vital importance in security assessment and with the current ambient analysis techniques, an extensive number of estimations and the corresponding statistical analysis of them needs to be performed.

In power system monitoring, it is highly desirable to identify the potentially harmful oscillations before they occur, rather than when the oscillation modes are already excited [13],[28]. To attain this objective, previous knowledge about modal observability is needed. More precisely, a statistical approach to determine in which system measurement an oscillatory mode is more visible (observable) is a theoretical problem of practical interest [29]. This will optimize

the placement of measurement units for monitoring critical modes from ambient data .

Understanding the effects of stochastically excited disturbances on system dynamic behavior provides valuable information that could be used to determine the impact that forcing functions representing random load or generation variations such as renewable generation has on the power system response [32]-[33]. This, in turn, allows the detection of the spatial distribution of the critical stochastic perturbations that should be constantly monitored.

In this research, an analytical framework based on linear stochastic systems theory [34],[35] is proposed to estimate power system electromechanical dynamics under ambient operating conditions. With this approach, the modes that dominate the system response, and the forcing functions that contribute most to this response can be directly estimated.

1.3 A brief review of previous work

Recently there has been intensive research on stochastic analysis of the ambient power system response to random load variations. The idea behind this research is that the parameters of the process generating a time series can be described by a low-amplitude stochastic excitation [15]-[19]. The description and understanding of variability in the observed system response is a central question in power system stability analysis. A variety of research based on Monte Carlo simulation analysis has been proposed for power systems transient stability analysis considering uncertainties; much of this research, however, has been focused on the analysis of the system response to disturbances and changes in operating point conditions [20]-[26]. These approaches combine deterministic simulation techniques with stochastic analysis to compute the probability that the power system will have a stable operating [14].

Only a handful of work addresses the identification of the most influential sources of variability [30],[31]. These methodologies are used to reduce the

number of simulations required to approximate results obtained by conventional analysis techniques [20]-[26].

This thesis focuses on the study of the power systems response to ambient perturbations; the approach adopted is based on research developed in the field of atmospheric science and control theory. [34],[35]. Through this formulation the stochastically maintained variance of the perturbations, the structures that dominate system response, the modes of deterministic dynamics, and the forcing functions that contribute most to the statistically stationary response can be estimated.

Asymptotic properties of linear randomly excited models originally developed for linear stochastic systems are extended and generalized to study the system response to random inputs. The methodology proposed is general and could be expanded to assess the combined effect of random load and generator variations on system response.

1.4 Thesis objectives

1) The development of a new analytic framework to estimate the predominant electromechanical modes of the system response under ambient operating conditions.

2) The development of an analytical methodology to assess the effects of stochastically excited disturbances on system dynamic behavior. Using this framework, the modes that dominates the system response, and the forcing functions that contribute most to this response are directly calculated.

3) The identification of transmission and generation elements that contribute most to the observed oscillations.

4) The extension and generalization of existing analysis techniques to study the statistically stationary response and the initial forcing conducive to instability of the system.

1.5 Research contributions

The following issues constitute original contributions:

1) The development of a rigorous linear statistical framework for analyzing power systems subject to small random load and generation variations, along with performance and sample diagnostic.

2) The development of a linear model with a stochastic forcing term that explicitly accounts for small-random load behavior. The main advantage of this framework is linearity, and automatic identification of key system modal parameters.

3) The identification of predominant electromechanical modes of the system response under ambient operating conditions.

4) The determination of the forcing functions associated with dominant ambient system behavior.

5) The detection of the most energetic oscillation modes that are presented in the ambient power system response.

1.6 Organization of the thesis

The thesis is structured as follows:

Chapter 2 provides a general overview of previous research developed in the field of ambient-mode estimation. Ambient operating conditions are briefly contextualized within the field of power system dynamics.

Chapter 3 discusses theory involved in the study of stochastically driven linear systems. Modal response expressions are generalized to the case of ran-

dom excitation. The statistics that describe this stochastic response are derived, and basic concepts used to interpret these moments are reviewed.

Chapter 4 introduces a new methodology used for the direct mode shape identification of the modes that dominate the system response of a white noise driven linear system.

Chapter 5 develops an analytical methodology based on the decomposition of system response energy to identify the stochastic forcing functions that most contribute to the response of a linear dynamical system.

Chapter 6 develops a new flexible approach to performing state-space analysis of a simplified multi-machine power system that explicitly accounts for random load behavior.

The application of the novel model-based approach developed through Chapters 4-6 is presented in Chapter 7. Results obtained show the feasibility of the proposed methodology to understand power system dynamic behavior as a result of stochastically excited load disturbances.

Finally, some concluding remarks and suggestions for future research are presented in Chapter 8.

Additional information used to develop the proposed methodology and further material describing POD analysis and stochastic numerical integration are presented in the Appendix.

1.7 References

[1] Morison, K., Wang, L., & Kundur, P. (2004). Power system security assessment. Power and Energy Magazine, IEEE, 2(5), 30-39

[2] Sterpu, S., Lu, W., Besanger, Y., & Hadjsaid, N. (2006, June). Power systems security analysis. In Power Engineering Society General Meeting, 2006. IEEE (pp. 5-pp). IEEE.

[3] Rogers, G. (2012). Power system oscillations. Springer Science & Business Media

[4] Kundur, P. (1994). Power system stability and control (Vol. 7). N. J. Balu, & M. G. Lauby (Eds.). New York: McGraw-hill.

[5] Pal, B., & Chaudhuri, B. (2006). Robust control in power systems. Springer Science & Business Media.

[6] Andersson, G., Donalek, P., Farmer, R., Hatziargyriou, N., Kamwa, I., Kundur, P., ... & Vittal, V. (2005). Causes of the 2003 major grid blackouts in North America and Europe, and recommended means to improve system dynamic performance. Power Systems, IEEE Transactions on, 20(4), 1922-1928.

[7] Bu, S. Q., Du, W., Wang, H. F., Chen, Z., Xiao, L. Y., & Li, H. F. (2012). Probabilistic analysis of small-signal stability of large-scale power systems as affected by penetration of wind generation. Power Systems, IEEE Transactions on, 27(2), 762-770.

[8] Messina, A. R. (Ed.). (2009). Inter-area oscillations in power systems: a nonlinear and nonstationary perspective. Springer Science & Business Media.

[9] Thambirajah, J., Barocio, E., & Thornhill, N. F. (2010). Comparative review of methods for stability monitoring in electrical power systems and vibrating structures. Generation, Transmission & Distribution, IET, 4(10), 1086-1103.

[10] Ledwich, G., & Palmer, E. (2000). Modal estimates from normal operation of power systems. In Power Engineering Society Winter Meeting, 2000. IEEE (Vol. 2, pp. 1527-1531). IEEE.

[11] Zhou, N., Pierre, J., & Hauer, J. (2008, July). Initial results in power system identification from injected probing signals using a subspace method. In Power and Energy Society General Meeting-Conversion and Delivery of Electrical Energy in the 21st Century, 2008 IEEE (pp. 1-1). IEEE.

[12] Liu, G., & Venkatasubramanian, V. M. (2008, May). Oscillation monitoring from ambient PMU measurements by frequency domain decomposition. In Circuits and Systems, 2008. ISCAS 2008. IEEE International Symposium on (pp. 2821-2824). IEEE.

[13] Larsson, M., & Laila, D. S. (2009, July). Monitoring of inter-area oscillations under ambient conditions using subspace identification. In Power & Energy Society General Meeting, 2009. PES'09. IEEE (pp. 1-6). IEEE

[14] Pierre, J. W., Trudnowski, D. J., & Donnelly, M. K. (1997). Initial results in electromechanical mode identification from ambient data. Power Systems, IEEE Transactions on, 12(3), 1245-1251.

[15] Jingmin, N., Chen, S., & Feng, L. (2011, July). Estimating the electromechanical oscillation characteristics of power system based on measured ambient data utilizing stochastic subspace method. In Power and Energy Society General Meeting, 2011 IEEE (pp. 1-7). IEEE.

[16] Wies, R. W., Pierre, J. W., & Trudnowski, D. J. (2004, June). Use of least mean squares (LMS) adaptive filtering technique for estimating low-frequency electromechanical modes in power systems. In Power Engineering Society General Meeting, 2004. IEEE (pp. 1863-1870). IEEE.

[17] Zhou, N., Pierre, J. W., Trudnowski, D. J., & Guttromson, R. T. (2007). Robust RLS methods for online estimation of power system electromechanical modes.Power Systems, IEEE Transactions on, 22(3), 1240-1249.

[18] Korba, P., Larsson, M., & Rehtanz, C. (2003, June). Detection of oscillations in power systems using Kalman filtering techniques. In Control Applica-

tions, 2003. CCA 2003. Proceedings of 2003 IEEE Conference on (Vol. 1, pp. 183-188). IEEE.

[19] Turunen, J., Haarla, L., & Rauhala, T. (2010, August). Performance of wavelet-based damping estimation method under ambient conditions of the power system. In Bulk Power System Dynamics and Control (iREP)-VIII (iREP), 2010 iREP Symposium (pp. 1-9). IEEE.

[20] Billinton, R., & Kuruganty, P. R. S. (1978, January). Probabilistic index for transient stability. In IEEE Transactions on Power Apparatus and Systems(Vol. 97, No. 4, pp. 1012-1012). 345 E 47TH ST, NEW YORK, NY 10017-2394: IEEE-INST ELECTRICAL ELECTRONICS ENGINEERS INC.

[21] Anderson, P. M., & Bose, A. (1983). A probabilistic approach to power system stability analysis. Power Apparatus and Systems, IEEE Transactions on, (8), 2430-2439.

[22] Timko, K. J., Bose, A., & Anderson, P. M. (1983). Monte Carlo simulation of power system stability. Power Apparatus and Systems, IEEE Transactions on, (10), 3453-3459.

[23] Wu, F. F., Tsai, Y. K., & Yu, Y. X. (1988). Probabilistic steady-state and dynamic security assessment. IEEE Trans. Power Syst.;(United States), 3(1).

[24] Leite da Silva, A. M., Endrenyi, J., & Wang, L. (1993). Integrated treatment of adequacy and security in bulk power system reliability evaluations. IEEE Transactions on Power Systems (Institute of Electrical and Electronics Engineers);(United States), 8(1).

[25] Hockenberry, J. R., & Lesieutre, B. C. (2004). Evaluation of uncertainty in dynamic simulations of power system models: The probabilistic collocation method. Power Systems, IEEE Transactions on, 19(3), 1483-1491.

[26] Loparo, K., & Blankenship, G. L. (1985). A probabilistic mechanism for small disturbance instabilities in electric power systems. Circuits and Systems, IEEE Transactions on, 32(2), 177-184... (inestabilidad por variaciones de

[27] Dhople, S. V., Chen, Y. C., DeVille, L., & Domínguez-García, A. D. (2013). Analysis of power system dynamics subject to stochastic power injections.Circuits and Systems I: Regular Papers, IEEE Transactions on, 60(12), 3341-3353

[28] Larsson, M., Korba, P., Sattinger, W., & Owen, P. (2012, August). Monitoring and control of power system oscillations using FACTS/HVDC and wide-area phasor measurements. In Proc. of CIGRE Conf.-SC B5 PS1, Paris, France.

[29] Chan, S. M. (1984). Modal controllability and observability of power-system models. International Journal of Electrical Power & Energy Systems, 6(2)

[30] Hockenberry, J. R., & Lesieutre, B. C. (2004). Evaluation of uncertainty in dynamic simulations of power system models: The probabilistic collocation method. Power Systems, IEEE Transactions on, 19(3), 1483-1491.

[31] Hiskens, I., & Alseddiqui, J. (2006). Sensitivity, approximation, and uncertainty in power system dynamic simulation. Power Systems, IEEE Transactions on, 21(4), 1808-1820.

[32] Loparo, K., & Blankenship, G. L. (1985). A probabilistic mechanism for small disturbance instabilities in electric power systems. Circuits and Systems, IEEE Transactions on, 32(2), 177-184...

[33] Dhople, S. V., Chen, Y. C., DeVille, L., & Domínguez-García, A. D. (2013). Analysis of power system dynamics subject to stochastic power injections.Circuits and Systems I: Regular Papers, IEEE Transactions on, 60(12), 3341-3353

[34] Nolan, D. S., & Farrell, B. F. (1999). The intensification of two-dimensional swirling flows by stochastic asymmetric forcing. Journal of the atmospheric sciences, 56(23), 3937-3962.

[35] Farrell, B. F., & Ioannou, P. J. (1993). Stochastic forcing of the linearized Navier–Stokes equations. Physics of Fluids A: Fluid Dynamics (1989-1993), 5(11), 2600-2609.

Chapter 2

Ambient Analysis of Measured Data

This chapter examines the application of measurement-based identification methods to estimate electromechanical modal properties. First, the notion of power system ambient mode identifications is introduced in the context of this research and a structure for information sources in the identification process is reviewed.

Then, a brief review of methods used to estimate modal properties from measured data is presented including the use of ambient analysis of power system data followed by a review of signal processing methods for small-signal analysis.

The chapter concludes with a brief review of linear power system models for system identification.

2.1 Ambient operation

Ambient oscillations are the result of complex random variations and interactions between many system components. Measurements from the system during ambient operation show that there is always a constant level of ambient noise present in the data in the bandwidth of electromechanical dynamics [1].

A common and reasonable assumption in most cases is that the excitation is primarily caused by changes in the system load. Over a time span of a few minutes, load changes are seen as primarily random and Gaussian. Nonetheless, generation and system switching effects are primarily planned and therefore deterministic; thus, these variations are not significant in a time interval of several minutes [2].

Assuming that the stochastically excited load variations are white, i.e., independent sources of uncertainty are considered, and stationary over an analysis window, it is possible to estimate the electromechanical modal frequencies and damping from the spectral content of the ambient noise [3].

Analyzing and estimating power-system electromechanical dynamic effects are a challenging problem because of various factors [3].

1) The system is nonlinear, high order, and time varying,

2) It contains many electromechanical modes of oscillation close in frequency.

3) It is primarily stochastic in nature, especially over a given time interval

Additionally, since the load cannot be measured everywhere in the system and is constantly changing, the input is assumed to be unknown or white.

Knowledge about dynamic processes in power systems can be obtained from a number of information sources including known and unknown dynamics. Figure 2.1 shows a conceptual view of the problem of process identification illustrating the various known and unknown dynamics and the output data [3]. The key point to emphasize is that the response of the power system contains information about the power system's electromechanical model properties and can be used for stability monitoring. Discussion of this representation is deferred to section 2.4.

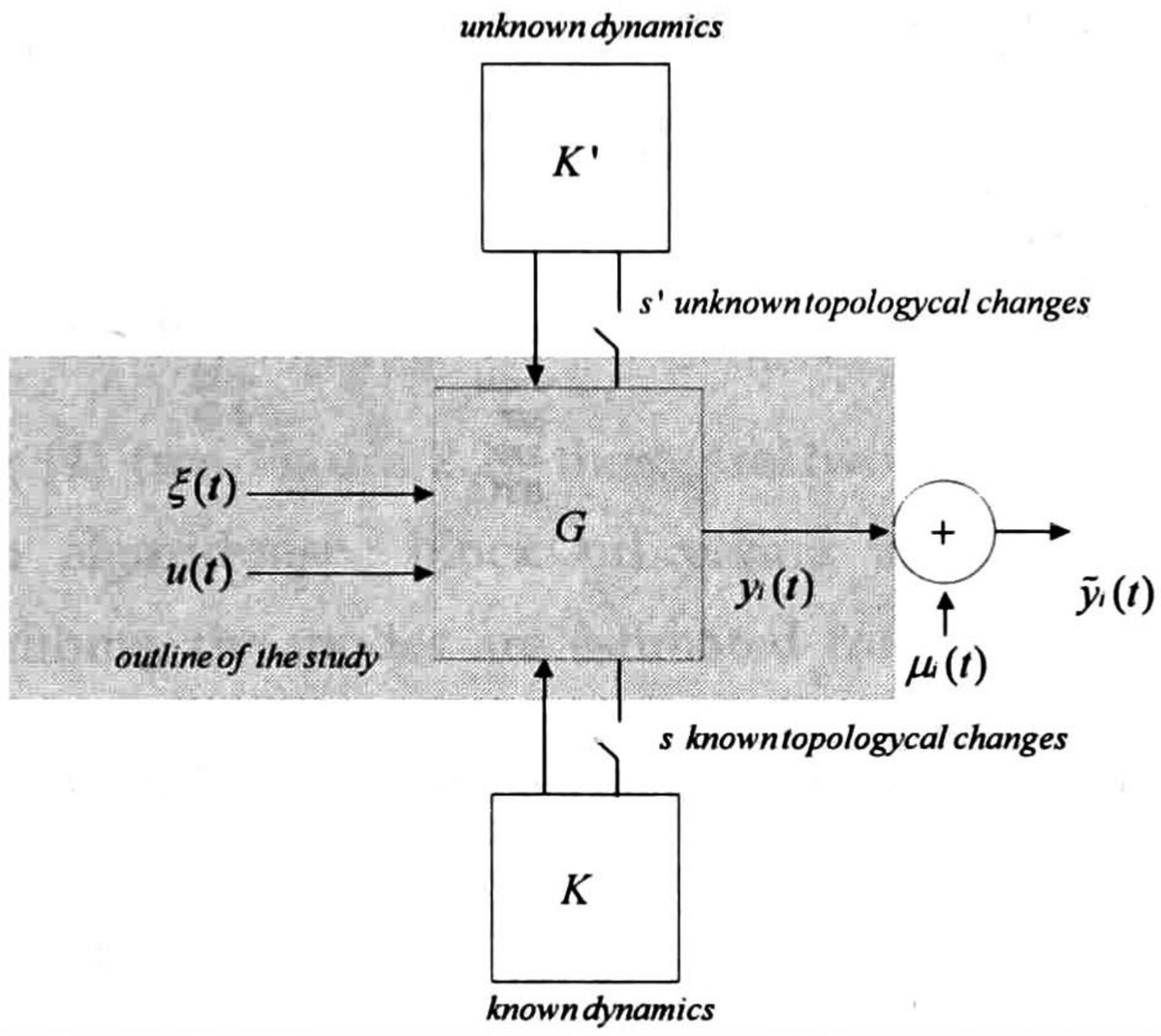

Figure 2.1. A structure for information sources in process identification [3]

2.2 Measurement-based methods system analysis

In recent years, several methods to characterized modal behavior have been developed. Most of this research focuses on measurement-based analysis methods that can be broadly classified into two categories: Ringdown analysis (Transient analysis), and ambient analysis [3],[4].

Figure 2.2 provides a taxonomy of existing measurement-based approaches to system identification [4] Showing the nature of the intended contribution.

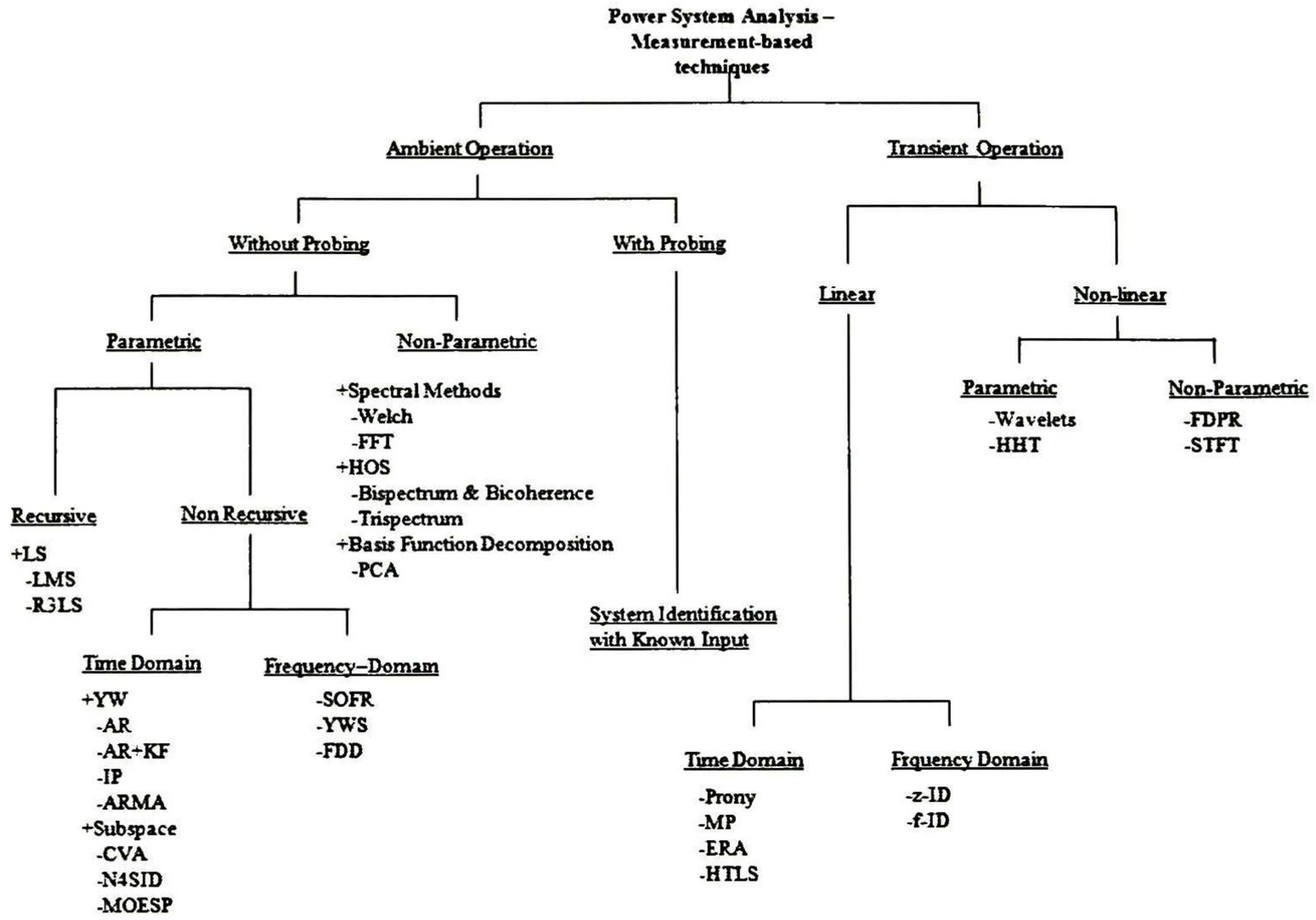

Figure 2.2.Basic overview of methods for system identification

As this research concerns ambient analysis, identification methods based on transient responses are out of the scope of this work; However, as way to give a complete description of Figure 2.2 , these methods are briefly mentioned in the Appendix, section A.

2.3 Brief review of ambient analysis methods

Approaches to the statistical characterization of system variability are of ongoing interest. Ambient response can be observed in all system variables (e.g.,voltages, currents, powers, and frequency), even under quasisteady-state operation. Information about system transfer functions, and, consequently, system modes, are contained in the spectrum of ambient responses.

In this sense, non-parametric spectral-estimation methods have been used to estimate electromechanical mode properties due to their robustness and simplicity. Perhaps, the most widely used non-parametric method is the Welch periodogram spectrum [5],[6], which provides an estimate of a signal's strength as a function of frequency, and can be used to estimate mode shapes. Other non-parametric methods are reviewed in [3] and include higher order spectral methods and basis function decomposition methods such as principal component analysis and its variants.

Non-parametric methods, however, do not provide direct numerical estimates of modal properties, which limits their usefulness. This has led to the development of parametric methods with the ability to estimate the amplitude and frequency of the observed oscillations.

Following [4] (see Figure 2.2), there are two basic types of parametric mode-estimation algorithms: block processing and recursive. In block-processing algorithms, the modes are estimated from a window of data. For each new window of data, a new estimate is calculated. A limitation of these approaches is the amount of data that is required for an accurate estimate of modal dynamics. A new mode estimate can be calculated as often as required; but, each calculation requires several minutes of the most recent data.

The first application of block processing used the Yule-Walker algorithm to estimate modes using an Autoregressive (AR) model [2]. The method was then extended to the over-determined modified Yule-Walker method (YW) [7] to estimate an Autoregressive Moving Average (ARMA) model [8]. Extensions to the case of multiple signals are discussed in [9].

Block processing methods using subspace methods CVA (Canonical Variate Algorithm) and N4SID (Numerical algorithm for Subspace state-space system identification) were first introduced in [10], [11]. A variation of the YW approach that estimates the autocorrelation function using a frequency-domain

calculation is introduced in [12] and is termed the Yule-Walker-Spectrum (YWS) method.

In [12], the YW, YWS, and N4SID algorithms are compared. Along these lines, another frequency domain method is the Frequency Domain Decomposition (FDD) method described in [14], which decomposes the signals estimated power spectrum.

For recursive methods (refer to Figure 2.2), the estimated modes are updated for each new arriving data. The new estimate is obtained using a combination of the new data point and the previous mode estimate. A forgetting factor is employed to discount information based on previous data; as a result, new data is weighted more in each calculation.

Similar to the block-processing methods, all recursive methods tested to date require many minutes of data to converge to a steady-state solution. Published results include the Least-Mean Squares (LMS) method [15] and the Regularized Robust Recursive Least Squares (R3LS) method [16],[17].

The R3LS method described in [17] offers several advances to previous algorithms. First, it accommodates an Autoregressive Moving Average Exogenous (ARMAX) model to account for ambient noise as well as a known input, which can enhance performance during probing. Second, it has a robust objective function to reduce the impact of missing or outlier data; and third, it can incorporate a-priori knowledge of the modes. The full impact of these advances is the subject of current and future research.

There are other approaches to ambient analysis for electromechanical mode identification that have been applied to simulated and measured data. These include hybrid analysis techniques based on the combined application of linear statistical analysis techniques and the random decrement method, blind source separation [18] and Kalman filter-based approaches [19] among others.

In a departure from previous work, this thesis addresses the problem of system identification from a model-based perspective. The use of model-based ambient identification techniques provides an alternative view to the problem of ambient identification that can provide additional insight into the nature of system response to random inputs.

2.4 Linear power system models

The effects of random forcing on system behavior can be estimated using a linearized power system representation. Following Trudnowski *et al.*[12], the underlying assumption is that small motions of the power system can be described by a set of ordinary differential equations of the form

$$\begin{aligned} \dot{\mathbf{x}} &= \mathbf{A}\mathbf{x}(t) + \mathbf{F}_{\xi}\xi(t) + \mathbf{F}_{E}\mathbf{u}_{E}(t) \\ \mathbf{y} &= \mathbf{C}\mathbf{x}(t) + \mathbf{D}_{\xi}\xi(t) + \mathbf{D}_{E}\mathbf{u}_{E}(t) + \boldsymbol{\mu}(t) \end{aligned} \tag{2.1}$$

where $\xi(t)$ is a hypothetical random vector perturbing the system, vector $\mathbf{x}(t)$ contains all system states including generator angles and speeds, and t is time.

Control actions that can be described as smooth functions of the state $\mathbf{x}(t)$ are embedded in the system **A** matrix; all other actions are represented by the exogenous input vector $\mathbf{u}_E.(t)$. These include set-point changes, low-level probing signals (e.g., a low-level probing signal into a DC converter [13]), and load pulses that are applied to examine system dynamics as suggested in Figure 2.1.

Measurable signals are represented by $\mathbf{y}(t)$ which contains measurement noise $\boldsymbol{\mu}(t)$ that includes effects from instruments, communication channels, recording systems, and similar devices. In general, measurement noise has a relatively small amplitude when quality instrumentation is employed. Changes which are breaker actuated may produce system topology changes that alter the system **A** matrix to various degrees.

The assumption for $\xi(t)$ is that it is a vector of small-amplitude random perturbations typically conceptualized as noise-produced load switching. It has

been hypothesized that the load switching is primarily integrated stationary Gaussian white noise with each element of ξ independent [11]. This assumption is certainly open to more research.

In this dissertation a simplified version of model (2.1) is adopted; due the generator model (classical-generator model) implemented in this work, and because no probing signals are used, the term $\mathbf{u}_E$ in (2.1) is not taken into account. Furthermore, no changes in network topology are considered and the measurement noise is negligible. From these assumptions, the linear power system model adopted is mathematically described by :

$$\begin{aligned} \dot{\mathbf{x}} &= \mathbf{A}\mathbf{x}(t) + \mathbf{F}_\xi \xi(t) \\ \mathbf{y} &= \mathbf{C}\mathbf{x}(t) + \mathbf{D}_\xi \xi(t) \end{aligned} \tag{2.2}$$

the conceptual representation of this model corresponds to the elements inside the blue chart in Figure 2.1.

In the following, mathematical expressions to describe the response of system (2.2) in a statistical sense are developed.

2.5 References

[1] Hauer, J. F., & Cresap, R. L. (1981). Measurement and modeling of pacific AC intertie response to random load switching. Power Apparatus and Systems, IEEE Transactions on, (1), 353-359.

[2] Pierre, J. W., Trudnowski, D. J., & Donnelly, M. K. (1997). Initial results in electromechanical mode identification from ambient data. Power Systems, IEEE Transactions on, 12(3), 1245-1251.

[3] Messina, A. R. (Ed.). (2009). Inter-area oscillations in power systems: a nonlinear and nonstationary perspective. Springer Science & Business Media.

[4] Thambirajah, J., Barocio, E., & Thornhill, N. F. (2010). Comparative review of methods for stability monitoring in electrical power systems and vibrating structures. Generation, Transmission & Distribution, IET, 4(10), 1086-1103

[5] Pierre, J., & Kubichek, R. F. (2002). Spectral analysis: Analyzing a signal spectrum. Tektronix Application Note.

[6] Proakis John, G., & Manolakis Dimitris, G. (1996). Digital Signal Processing, principles, algorithms, and applications. Pentice Hall.

[7] Stoica, P., & Moses, R. L. (1997). Introduction to spectral analysis (Vol. 1, pp. 3-4). Upper Saddle River: Prentice hall.

[8] Wies, R. W., Pierre, J. W., & Trudnowski, D. J. (2003). Use of ARMA block processing for estimating stationary low-frequency electromechanical modes of power systems. Power Systems, IEEE Transactions on, 18(1), 167-173.

[9] Anderson, M. G., Zhou, N., Pierre, J. W., & Wies, R. W. (2005). Bootstrap-based confidence interval estimates for electromechanical modes from multiple output analysis of measured ambient data. Power Systems, IEEE Transactions on, 20(2), 943-950.

[10] Zhou, N., Pierre, J. W., & Wies, R. W. (2003, October). Estimation of low-frequency electromechanical modes of power systems from ambient measurements using a subspace method. In *Proceedings of the North American Power Symposium*. Sn.

[11] Zhou, N., Pierre, J., & Hauer, J. (2008, July). Initial results in power system identification from injected probing signals using a subspace method. In Power and Energy Society General Meeting-Conversion and Delivery of Electrical Energy in the 21st Century, 2008 IEEE (pp. 1-1). IEEE.

[12] Trudnowski, D. J., Pierre, J. W., Zhou, N., Hauer, J. F., & Parashar, M. (2008). Performance of three mode-meter block-processing algorithms for automated dynamic stability assessment. Power Systems, IEEE Transactions on, 23(2), 680-690.

[13] Zhou, N., Pierre, J., & Hauer, J. (2008, July). Initial results in power system identification from injected probing signals using a subspace method.

In Power and Energy Society General Meeting-Conversion and Delivery of Electrical Energy in the 21st Century, 2008 IEEE (pp. 1-1). IEEE.

[14] Liu, G., & Venkatasubramanian, V. M. (2008, May). Oscillation monitoring from ambient PMU measurements by frequency domain decomposition. In Circuits and Systems, 2008. ISCAS 2008. IEEE International Symposium on (pp. 2821-2824). IEEE.

[15] Wies, R. W., Pierre, J. W., & Trudnowski, D. J. (2004, June). Use of least mean squares (LMS) adaptive filtering technique for estimating low-frequency electromechanical modes in power systems. In Power Engineering Society General Meeting, 2004. IEEE (pp. 1863-1870). IEEE.

[16] Zhou, N., Pierre, J. W., Trudnowski, D. J., & Guttromson, R. T. (2007). Robust RLS methods for online estimation of power system electromechanical modes.Power Systems, IEEE Transactions on, 22(3), 1240-1249.

[17] Zhou, N., Trudnowski, D. J., Pierre, J. W., & Mittelstadt, W. (2008). Electromechanical mode online estimation using regularized robust RLS methods. Power Systems, IEEE Transactions on, 23(4), 1670-1680.

[18] Ayon, J. J., Barocio, E., & Messina, A. R. (2015). Blind extraction and characterization of power system oscillatory modes. Electric Power Systems Research, 119, 54-65.

[19] Korba, P., Larsson, M., & Rehtanz, C. (2003, June). Detection of oscillations in power systems using Kalman filtering techniques. In Control Applications, 2003. CCA 2003. Proceedings of 2003 IEEE Conference on (Vol. 1, pp. 183-188). IEEE

Chapter 3

Linear Stochastic Forcing Model of System Motion

Modal analysis is one of the most effective techniques to extract modal information from linear power system models. This chapter presents a review of the theory involved in the study of stochastically forced linear systems (uncorrelated white noise). In this approach, modal response expressions are generalized to the case of random excitation. The concept of statistical steady state of the moments of a stochastic process is discussed and analytic expressions for the covariance function and the ensemble average energy function of the state and output responses of a linear stochastic state space model are derived.

Properties of linear stochastic systems are discussed, and a complete proof of the main results used in this research is provided. Various other extensions to this analysis are briefly discussed, and references are provided for further detail.

The notation utilized throughout the dissertation is also summarized.

3.1 Linear dynamical system with stochastic forcing

To introduce the adopted model, consider a linear dynamical system with stochastic forcing of the form [1],[2]

$$\begin{aligned} \dot{\mathbf{x}}(t) &= \mathbf{A}\mathbf{x}(t) + \mathbf{F}\xi(t) \\ \mathbf{y}(t) &= \mathbf{C}\mathbf{x}(t) + \mathbf{D}\xi(t) \end{aligned} \tag{3.1}$$

where $\mathbf{x}$ is an n-dimensional vector representing the state of the system, $\xi(t)$ is a m-dimensional vector representing a stochastic forcing (random process), $\mathbf{y}$ is the r-dimensional vector of outputs (vector of measurements).

Matrix $\mathbf{A}$ represents the deterministic dynamics, and matrix $\mathbf{F}$ represents the spatial distribution of the forcing vector. For simplicity it is assumed that the state matrix $\mathbf{A}$ is time independent and asymptotically stable, i.e., all the eigenvalues of the state matrix have negative real parts.

In physical models, vector $\xi(t)$ represents uncertainties or stochastic effects perturbing the system (3.1). More formally, vector $\xi(t)$ is modeled as a stochastic process evolving probabilistically or more precisely, represented by time-dependent random variables [3],[4].

We assume that, ξ is represented by a sequence of uncorrelated samples (white noise) with zero mean and unit variance [1], *i.e.*,

$$\begin{aligned} \langle \xi(t) \rangle &= 0 \\ \langle \xi_i(t_m)\xi_j(t_n) \rangle &= \delta_{ij}\delta(t_m - t_n) \end{aligned} \tag{3.2}$$

where angle brackets denote an ensemble average, δ_{mn} is the delta Kronecker function used to denote independence between the i-th and j-th elements of $\xi(t)$, and δ is the delta Dirac function (see Appendix, section B.1) used to denote no correlation in time [4].

3.2 Modal response

Much insight into the nature of stochastic behavior can be obtained from linear analysis of the stochastic linear model. Let the solution of (3.1) with a deterministic initial condition $\mathbf{x}(t_0)=\mathbf{x}_0$, be expressed as

$$\mathbf{x}(t) = \underbrace{e^{\mathbf{A}t}\mathbf{x}(t_o)}_{\substack{\text{Deterministic}\\ \text{response}}} + \underbrace{\int_0^t e^{\mathbf{A}(t-\tau)}\xi(\tau)d\tau}_{\substack{\text{Random noise}\\ \text{forcing}}} \tag{3.3}$$

from which the output response can be readily determined as

$$\mathbf{y}(t) = \mathbf{C}\left[e^{\mathbf{A}t}\mathbf{x}(t_o) + \int_0^t e^{\mathbf{A}(t-\tau)}\xi(\tau)d\tau\right] + \mathbf{D}\xi(t) \tag{3.4}$$

where τ is the lead time [1].

The first term on the right-hand side *(rhs)* represents the effect of the initial conditions, and it vanishes for a stable system; the second term, represents the influence of random noise forcing on system behavior.

It follows that, when all the eigenvalues of the deterministic dynamics in **A** are negative, the first term tends to zero as $t \to \infty$, and the system state response is described by

$$\mathbf{x}(t) = \int_0^t e^{\mathbf{A}(t-\tau)}\xi(\tau)d\tau \tag{3.5}$$

Under these assumption, (3.4) becomes

$$\mathbf{y}(t) = \mathbf{C}\left[\int_0^t e^{\mathbf{A}(t-\tau)}\xi(\tau)d\tau\right] + \mathbf{D}\xi(t) \tag{3.6}$$

Figure 3.1 illustrates the state response of a stochastic forcing linear system such as that expressed in (3.1). This response is composed of the transient and stochastic forced responses. For a stable system, the transient response decays after a few time constants [5], and as $t \to \infty$, the forced response becomes predominant.

Clearly, the random response, **x** and **y**, are linearly dependent on $\xi(t)$, and consequently are also Gaussian distributed. As a result, both signals are fully characterized by their first two moments [3].

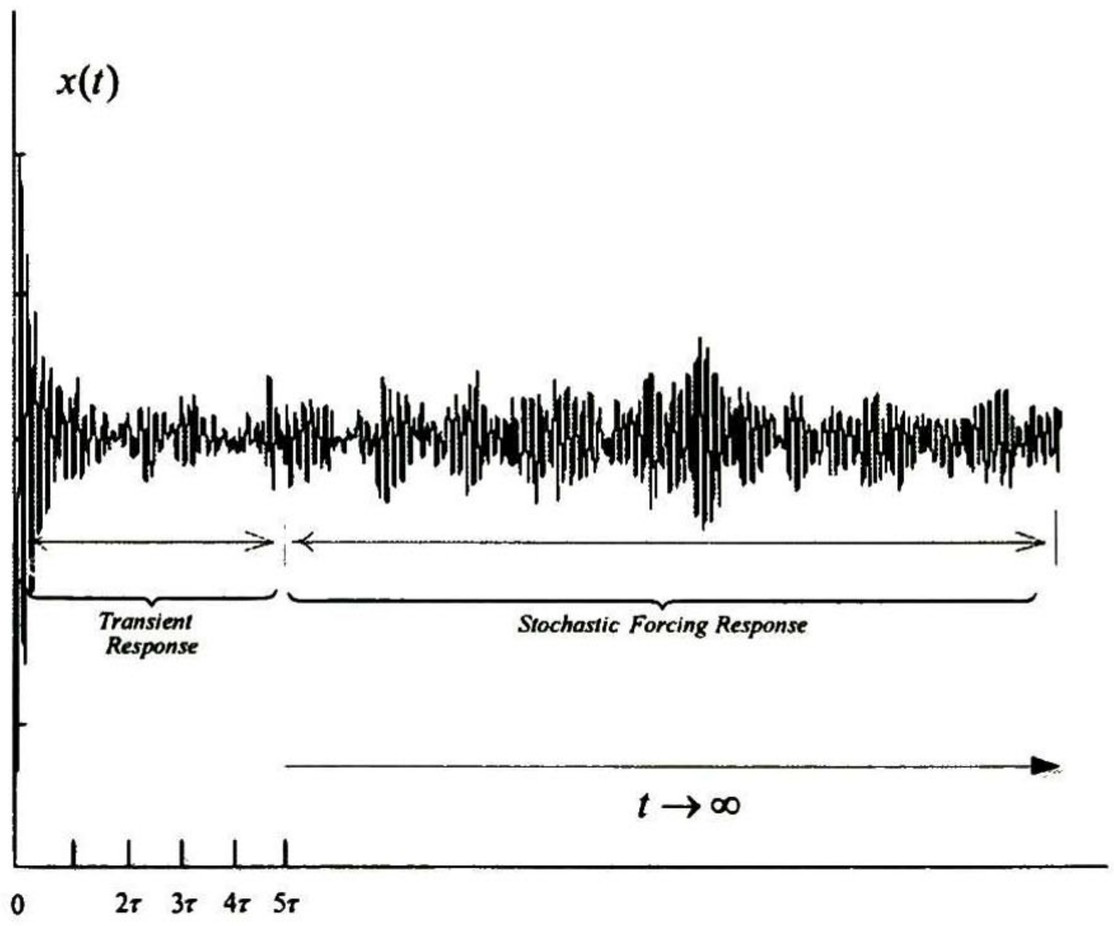

Figure 3.1.Dynamical response of a linear stochastic system

3.3 First and second moments of the state and output responses

The first moment of the state and output responses are the ensemble average of the $\mathbf{x}(t)$ and $\mathbf{y}(t)$ vectors respectively, and they are defined by

$$\eta_x{}^t(t) = \langle \mathbf{x}(t) \rangle, \tag{3.7}$$

$$\eta_y{}^t(t) = \langle \mathbf{y}(t) \rangle, \tag{3.8}$$

where $\eta_x{}^t(t)$ and $\eta_y{}^t(t)$ are time dependent vectors of appropriate dimensions.

When they are used to describe the state and output responses in (3.5) and (3.6), it can be demonstrated that $\eta_x{}^t(t)$ and $\eta_y{}^t(t)$, satisfy

$$\lim_{t\to\infty} \eta_x{}^t(t) = \eta_x{}^\infty = \lim_{t\to\infty} \langle \mathbf{x}(t) \rangle = \mathbf{0}, \tag{3.9}$$

$$\lim_{t\to\infty} \eta_y{}^t(t) = \eta_y{}^\infty = \lim_{t\to\infty} \langle \mathbf{y}(t) \rangle = \mathbf{0}. \tag{3.10}$$

These results follow from the linearity of the expected value and the direct substitution of the statistics of the forcing (3.2) when the integrals on the *rhs* of (3.5) and (3.6) take the form of Riemann integrals [3].

The second order central moment of the state response **x**, which is a vector-valued stochastic process, is given by the $n \times n$ matrix, $\mathbf{R}_x^t$

$$\mathbf{R}_x^t(t) = \left\langle \mathbf{x}(t)\mathbf{x}(t)^* \right\rangle, \tag{3.11}$$

Similarly, the vector of observations, $\mathbf{R}_y^t$ is given by

$$\mathbf{R}_y^t(t) = \left\langle \mathbf{y}(t)\mathbf{y}(t)^* \right\rangle, \tag{3.12}$$

where $\mathbf{R}_y^t$ is an $r \times r$ matrix.

Definitions (3.11) and (3.12) are called the covariance matrices of vectors **x**(t) and **y**(t), respectively [3]. Another important concept to understand is that of the second *central moment* $\mathbf{C}^t$, which is defined in terms of $\mathbf{R}^t$ and η^t (the covariance of decentralized vectors **x**(t) and **y**(t) and ensemble average of a general multidimensional stochastic process) [3]. From previous results, we have

$$\begin{aligned} \mathbf{C}_x^t(t) &= \left\langle \left(\mathbf{x}(t) - \eta_x^t(t)\right)\left(\mathbf{x}(t) - \eta_x^t(t)\right)^* \right\rangle \\ &= \mathbf{R}_x^t(t) - \eta_x^t(t)\eta_x^t(t)^* \end{aligned} \tag{3.13}$$

and

$$\begin{aligned} \mathbf{C}_y^t(t) &= \left\langle \left(\mathbf{y}(t) - \eta_y^t(t)\right)\left(\mathbf{y}(t) - \eta_y^t(t)\right)^* \right\rangle \\ &= \mathbf{R}_y^t(t) - \eta_y^t(t)\eta_y^t(t)^* \end{aligned} \tag{3.14}$$

In this work, both matrices $\mathbf{C}^t$ and $\mathbf{R}^t$ are called covariance matrices [9]; the difference between them is that $\mathbf{C}^t$ is formulated in terms of decentralized vectors, i.e., **x**(t)-$\eta_y(t)$ and **y**(t)-$\eta_y(t)$, and $\mathbf{R}^t$ is defined in terms of **x**(t) and **y**(t).

It follows from (3.9), that when $t \to \infty$, $\mathbf{C}_x^\infty$ simplifies to

$$\mathbf{C}_x^\infty = \lim_{t\to\infty} \left\langle \mathbf{x}(t)\mathbf{x}(t)^* \right\rangle = \lim_{t\to\infty} \mathbf{R}_x^t \tag{3.15}$$

and

$$\mathbf{C}_y^{\infty} = \lim_{t\to\infty}\left\langle \mathbf{y}(t)\mathbf{y}(t)^* \right\rangle = \lim_{t\to\infty} \mathbf{R}_y^t \tag{3.16}$$

From (3.15) and (3.16) the equality between $\mathbf{R}^t$ and $\mathbf{C}^t$ (when $t \to \infty$), is evident; for this reason $\mathbf{C}^t$ and $\mathbf{R}^t$ are used indistinctly.

Through the body of the text, the definition of covariance matrix is widely used; the study of matrices $\mathbf{C}_x^{\infty}$ and $\mathbf{C}_y^{\infty}$ will play an important role in the development of the theory addressed in this work. Specifically, eigenanalysis of $\mathbf{C}_x^{\infty}$ and $\mathbf{C}_y^{\infty}$ allows to find the structures that represent an ordered decomposition of the responses **x** and **y** to the response of the system to the stochastic forcing, usually referred to as empirical orthogonal functions (EOFs) [1],[6].

Another important definition related to the covariance matrix is that given by the transient ensemble energy, E^t. In its most basic form (following references [1],[2]) E_x^t and E_y^t are given by

$$E_x^t(t) = \left\langle \|\mathbf{x}(t)\|^2 \right\rangle \tag{3.17}$$

$$E_y^t(t) = \left\langle \|\mathbf{y}(t)\|^2 \right\rangle \tag{3.18}$$

where $\|\cdot\|$ denotes the L^2-norm.

The meaning of these definitions is intuitively clear and easy to understand; in a statistical sense, they determine what magnitude of fluctuation can be expected over a period of time. As a side result, when the transient response of the system (3.1) vanishes- $t \to \infty$, they can be used to measure the level of excitation of responses $\mathbf{x}(t)$ and $\mathbf{y}(t)$.

For large values of time, we can write

$$E_x^{\infty} = \lim_{t\to\infty}\left\langle \|\mathbf{x}(t)\|^2 \right\rangle = trace(\mathbf{C}_x^{\infty}) \tag{3.19}$$

$$E_y^{\infty} = \lim_{t\to\infty}\left\langle \|\mathbf{y}(t)\|^2 \right\rangle = trace(\mathbf{C}_y^{\infty}) \tag{3.20}$$

These results follow from the fact that the elements in the main diagonal of the matrix $\mathbf{C}_x^{\infty}$ are of the form

$$c_{x-ii} = \left\langle x_i^{*} x_i \right\rangle \text{ for } i = 1,\ldots,n \tag{3.21}$$

where x_i is the *i-th* elment of the vector $\mathbf{x}(t)$. A similar interpretation can be made for the ensemble average energy of the output response, E_y^{∞}

3.4 Ensemble and statisticall steady state concepts

The analytic results presented in subsequent sections represent the behavior of the system in a probabilistic sense; this means that they will describe the statistical behavior of the system when an infinite number of outputs are under study (see law of the large numbers [3]).

Figure 3.2 displays a set of synthetic signals (1,2,...,*N*) obtained from repeated experiments, e.g., multiple numerical solutions of the system (3.1) at different forcing inputs. This set of responses is said to conform an ensemble, and this ensemble is statistically characterized by the theoretical results $\mathbf{R}^t$, $\mathbf{C}^t$ η^t, and E^t . when the number of experiments *N* tends to infinity.

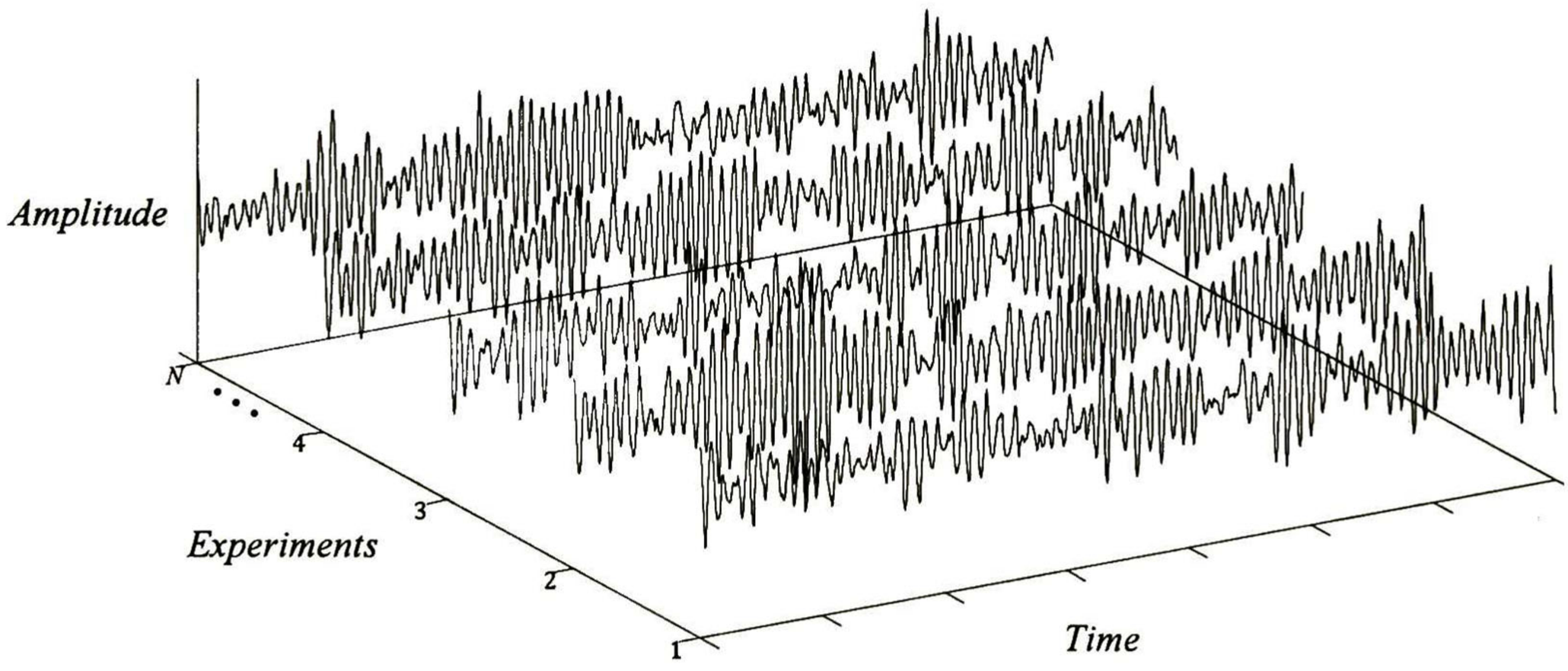

Figure 3.2. Statistical ensemble

In the previous section definitions of the first and second moments ($\mathbf{R}^t$, $\mathbf{C}^t$ η^t), and also the definition of E^t where given. Because they describe the behavior of stochastic processes, they are time dependent matrices, vectors and scalars functions respectively.

In our analysis, especial emphasis was focused on the interpretation of $\mathbf{R}^t$, $\mathbf{C}^t$, η^t, and E^t when $t \to \infty$, *i.e.*, when the transient response of system (3.1) vanishes. In this condition, the statistics ($\mathbf{R}^t$, $\mathbf{C}^t$. η^t, and E^t) of the responses $\mathbf{x}(t)$ and $\mathbf{y}(t)$ are said to reach an *statistically steady state condition*, and definitions (3.9)-(3.10), (3.15)-(3.16) and (3.19)-(3.20) become time independent (this time independency will be formally demonstrated in later sections).

The notion of a statistically steady state must not be confused with the concept of a steady state condition reached in a deterministic linear system. Since the forcing term $\xi(t)$ is randomly changing for every time, it provides a constant random excitation of the dynamics of (3.1) even if the statistically steady state is reached. This can be seen from equations (3.5) and (3.6), which explicitly show the dependency of $\mathbf{x}$ and $\mathbf{y}$ on the stochastic process ξ.

Figure 3.3 is used to explain the notion of the statistical steady state of a linear system from the practical point of view of multiple experiments. Let us choose a general instant of time, say t_k , and let the corresponding value of x at that time instant be denoted as $x(t_k)$. If this procedure is repeated at each experiment (1,2,...,N) conforming the ensemble (see Figure 3.2) , then a random variable $X_k = \{x^1(t_k), x^2(t_k), \ldots, x^N(t_k)\}$ can be defined (the upper-index of x correspond to the experiment number).

Furthermore, a statistical analysis of the random variable X_k (e.g., mean and variance,) for each time t_k in the range [0 T] will yield discrete values for $\eta^t(t_k)$ and $E^t(t_k)$ and the time evolution of η^t and E^t can be obtained by plotting $\{\eta^t(t_1), \eta^t(t_2), \ldots\}$ and $\{E^t(t_1), E^t(t_2), \ldots\}$ respectively.

In Figure 3.3 there exists a transient behavior of η^t and E^t in $t \in [0\ tss=5\tau]$, after that η^t and E^t adopt constant values, or the same the system reaches an statistical steady state condition.

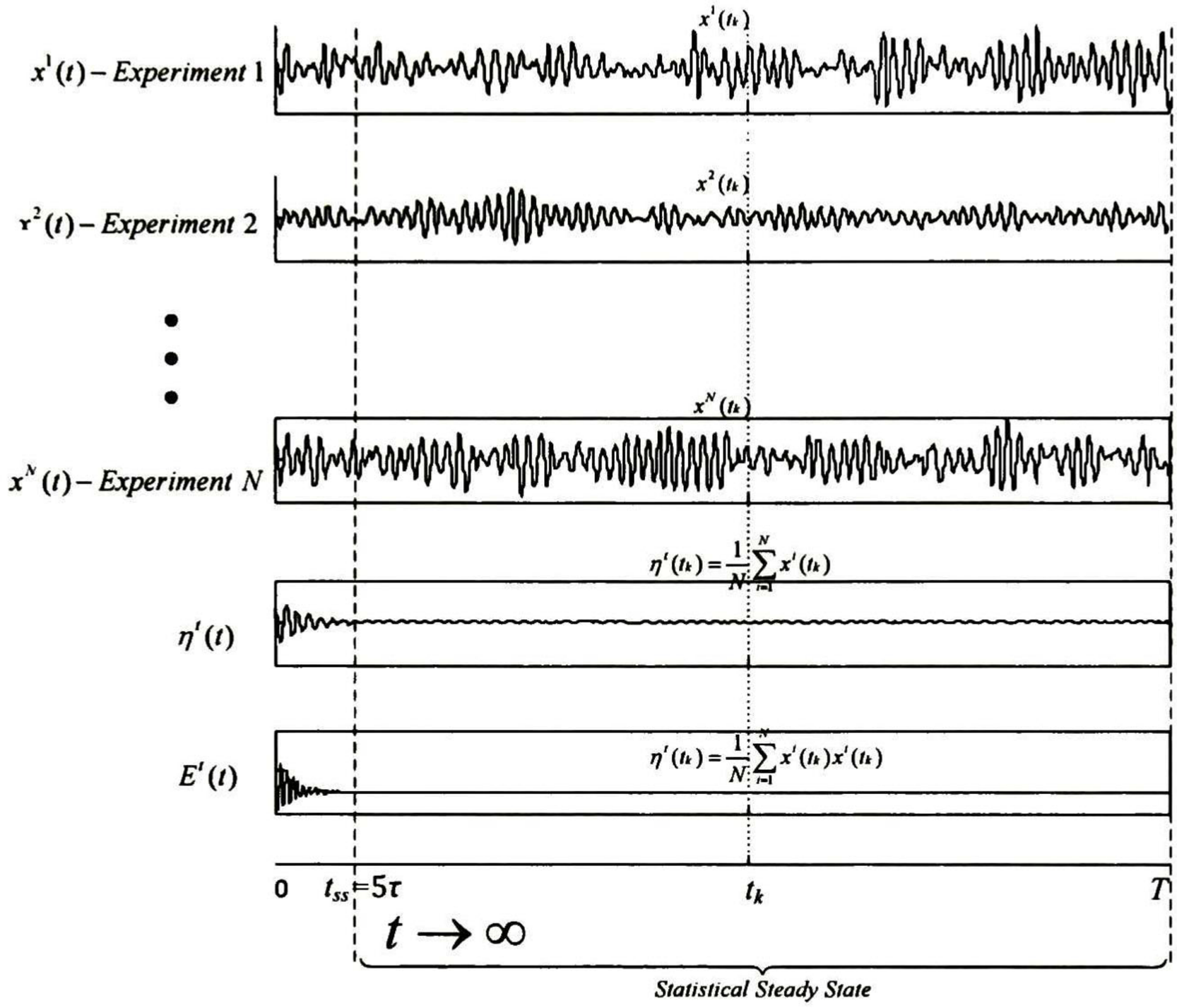

Figure 3.3. Statistical steady state.

The study developed in this thesis is focused on the dynamics of system (3.1) when it reaches a statistical steady state condition. This assumption and that of modeling $\xi(t)$ as uncorrelated white noise, allow for analytical solutions that help to understand the response of physical systems to stochastic forcing and to obtain global information with multiple applications.

3.5 Analytical development of the covariance function

The principal motivation for studying $\mathbf{C}^{\infty}$ is to compute the mode shapes associated with the modes with strong presence in the dynamical response of system (3.1) (see Chapter 4). Clearly, when the system is excited by an stochastic forcing, it is of vital importance in power systems [6]; in the more general case, however, the study of $\mathbf{C}^{\infty}$ provides insight into the patterns of oscillation of the responses **x** and **y** of a linear system.

3.5.1 Statistical steady state covariance of the state response

In this section, a practical form of computing $\mathbf{C}_x^{\infty}$ and its interpretation is provided. The major result is that $\mathbf{C}_x^{\infty}$ can be obtained by solving a Lyapunov equation of the form [2]

$$\mathbf{A}\mathbf{C}_x^{\infty} + \mathbf{C}_x^{\infty}\mathbf{A}^T = -\mathbf{F}\mathbf{F}^H \tag{3.22}$$

Several observations can be made about this result. From linear systems theory [7], matrix **A** is directly linked with the dynamics of linear systems; modal analysis characterizes the natural system response (modes and mode shapes) and the modal parameters e.g. damping a frequency of oscillation can be known from their study.

The other component, **F**, represents the spatial distribution of the stochastic forcing. Thus, matrix $\mathbf{C}_x^{\infty}$ depends on the inherent dynamics of (3.1) and the spatial distribution of the forcing $\xi(t)$. Consequently, $\mathbf{C}_x^{\infty}$ provides information of how the distribution of a spatial pattern of stochastic forcings (now considered to have equal level of energy) excites certain modes of the system.

Lyapunov equations (3.22) play an essential role in control theory. Efficient ways to solve these equations exist in the literature (e.g. [8]). The procedure followed in this work to derive (3.22) is that described in references [1],[2]. Reference [9] shows an alternative form of analysis, with a nice interpretation of the ideal white noise phenomena and it can be reviewed to enrich the study.

Proof of (3.22):

Proof of equation (3.22) begins with the direct substitution of (3.5) in (3.11). This yields

$$\mathbf{R}_x{}' = \left\langle \left(\int_0^t e^{\mathbf{A}(t-\tau_m)} \mathbf{F} \xi(\tau_m) d\tau_m \right) \left(\int_0^t \xi(\tau_n)^* \mathbf{F}^H e^{\mathbf{A}^H (t-\tau_n)} d\tau_n \right) \right\rangle, \tag{3.23}$$

Rearranging terms inside brackets results in

$$\mathbf{R}_x{}' = \int_0^t \int_0^t e^{\mathbf{A}(t-\tau_m)} \mathbf{F} \left\langle \xi(\tau_m) \xi(d\tau_n)^* \right\rangle \mathbf{F}^H e^{\mathbf{A}^H (t-\tau_n)} d\tau_m d\tau_n, \tag{3.24}$$

Finally, combing equations (3.24) and (3.2), it is easily seen that

$$\mathbf{R}_x{}' = \int_0^t \int_0^t \delta(\tau_m - \tau_n) e^{\mathbf{A}(t-\tau_m)} \mathbf{F}\mathbf{F}^H e^{\mathbf{A}^H (t-\tau_n)} d\tau_m d\tau_n . \tag{3.25}$$

At this point, it is necessary to make use of the properties of the delta function (impulse function) $\delta(t)$ to simplify (3.25) [4],[5]. In this regard, these properties are briefly reviewed in the Appendix, section B.1, where special attention should be paid to results (B.1.12)-(B.1.13).

Define the function, $\varphi(\tau_m, \tau_n)$

$$\varphi(\tau_m, \tau_n) = e^{\mathbf{A}(t-\tau_m)} \mathbf{F}\mathbf{F}^H e^{\mathbf{A}^H (t-\tau_n)} \tag{3.26}$$

An alternative form of the internal integral with respect to τ_m in (3.25) is

$$\begin{aligned} \int_0^t \delta(\tau_m - \tau_n) \varphi(\tau_m, \tau_n) d\tau_m &= \varphi(\tau_m, \tau_n)\big|_{\tau_m = \tau_n} \\ &= e^{\mathbf{A}(t-\tau_n)} \mathbf{F}\mathbf{F}^H e^{\mathbf{A}^H (t-\tau_n)} \end{aligned} \tag{3.27}$$

where use has been made of (B.1.12), and τ_n has been treated as a constant parameter.

Substituting (3.27) into (3.25), yields

$$\mathbf{R}_x{}' = \int_0^t e^{\mathbf{A}(t-\tau_n)} \mathbf{F}\mathbf{F}^H e^{\mathbf{A}^H (t-\tau_n)} \tau_n . \tag{3.28}$$

This is the time-dependent expression of the covariance matrix of the state response. In practice, alternate forms that avoid the computation of the integral in (3.28) are preferred.

In what follows, an alternative expression that describes $\mathbf{R}_x^{\infty} = \mathbf{C}_x^{\infty}$ is derived. Taking the derivative of (3.28), gives

$$\frac{d}{dt}\mathbf{R}_x^{\,t} = \frac{d}{dt}\int_0^t e^{\mathbf{A}(t-\tau_n)}\mathbf{F}\mathbf{F}^H e^{\mathbf{A}^H(t-\tau_n)}d\tau_n = \frac{d}{dt}\int_0^t \varphi(\tau_m,\tau_n)\Big|_{\tau_m=\tau_n} d\tau_n, \tag{3.29}$$

where use has been made of definition (3.26).

A useful result that can be used to compute the derivative of the integral in the *rhs* of (3.29) is the so-called Leibniz integration rule [10], defined in its general form in the Appendix, section B.2

By applying the Leibniz rule to (3.29), one has that

$$\frac{d}{dt}\mathbf{R}_x^{\,t} = \frac{d}{dt}\left(\int_0^t \varphi(\tau_m,\tau_n)\Big|_{\tau_m=\tau_n} d\tau_n\right) = \varphi(\tau_m,\tau_n)\Big|_{\tau_m=t,\tau_n=t} + \int_0^t \frac{\partial\,\varphi(\tau_m,\tau_n)\big|_{\tau_m=\tau_n}}{\partial t} d\tau_n \tag{3.30}$$

in which

$$\varphi(\tau_m,\tau_n)\Big|_{\tau_m=t,\tau_n=t} = e^{\mathbf{A}(t-t)}\mathbf{F}\mathbf{F}^H e^{\mathbf{A}^H(t-t)} = \mathbf{F}\mathbf{F}^H \tag{3.31}$$

and

$$\frac{\partial\,\varphi(\tau_m,\tau_n)\big|_{\tau_m=\tau_n}}{\partial t} = \mathbf{A}e^{\mathbf{A}(t-\tau_n)}\mathbf{F}\mathbf{F}^H e^{\mathbf{A}^H(t-\tau_n)} + e^{\mathbf{A}(t-\tau_n)}\mathbf{F}\mathbf{F}^H e^{\mathbf{A}^H(t-\tau_n)}\mathbf{A}^H \tag{3.32}$$

where use has been made of the result (B.3.2).

Inserting now (3.31)-(3.32) into (3.30), gives

$$\frac{d}{dt}\mathbf{R}_x^{\,t} = \mathbf{A}\left(\int_0^t e^{\mathbf{A}(t-\tau_n)}\mathbf{F}\mathbf{F}^H e^{\mathbf{A}^H(t-\tau_n)}d\tau_n\right) + \left(\int_0^t e^{\mathbf{A}(t-\tau_n)}\mathbf{F}\mathbf{F}^H e^{\mathbf{A}^H(t-\tau_n)}d\tau_n\right)\mathbf{A}^H + \mathbf{F}\mathbf{F}^H \tag{3.33}$$

where from (3.28) it is evident that (3.33) can be simplified to ,

$$\frac{d}{dt}\mathbf{R}_x^{\,t} = \mathbf{A}\mathbf{R}_x^{\,t} + \mathbf{R}_x^{\,t}\mathbf{A}^H + \mathbf{F}\mathbf{F}^H \tag{3.34}$$

Eq. (3.35) represents a differential equation of the form (3.28), and is useful under the assumption of asymptotic stability of the system (3.1). It immediately follows that the limit $\mathbf{R}_x^{\infty} = \lim_{t\to\infty} \mathbf{R}_x^{t}$ exists and satisfies

$$\frac{d}{dt}\mathbf{R}_x^{\infty} = 0\,. \tag{3.36}$$

Finally making use of the condition (3.36) in (3.34) and because of (3.15), (3.34) turns into (3.22) and the proof is complete.

3.5.2 Statistical steady state covariance of the output response

The covariance matrix $\mathbf{C}_y^{\infty}$ of the output response can be computed from knowledge of the value of $\mathbf{C}_x^{\infty}$ (3.22). In terms of these matrices, the output covariance matrix can be written as

$$\mathbf{C}_y^{\infty} = \mathbf{C}\mathbf{C}_x^{\infty}\mathbf{C}^H + \mathbf{D}\mathbf{Q}\mathbf{D}^H \tag{3.37}$$

in which, **C** and **D** are the matrices of the set of algebraic equations that combine the state variables into the output variables of the system (3.1), and matrix **Q** corresponds to the covariance of the input vector ξ.

Proof of (3.37):

The proof of (3.37) is obtained by direct substitution of (3.6) into (3.12). Thus,

$$\mathbf{R}_y^{\,t} = \mathbf{C}\mathbf{C}_x^{\,t}\mathbf{C}^H + \mathbf{C}\mathbf{R}^{t}_{x\xi}\mathbf{D}^H + \mathbf{D}\mathbf{R}^{t}_{\xi x}\mathbf{C}^H + \mathbf{D}\mathbf{R}^{t}_{\xi\xi}\mathbf{D}^H \tag{3.38}$$

where $\mathbf{C}_x^{\,t}$ was defined in (3.11) and $\mathbf{R}^{t}_{\xi\xi}$ is the covariance matrix of the input vector $\xi(t)$.

Here, the appearance of cross-correlation terms (to see cross-correlation definition see [3]) of vectors **x** and $\xi(t)$, deserves special attention. The cross-covariance of the vectors involved is denoted as $\mathbf{R}^{t}_{x\xi}$, and can be computed as

$$\mathbf{R}^{t}_{x\xi} = \left(\mathbf{R}^{t}_{\xi x}\right)^H = \left\langle \mathbf{x}(t)\xi(t)^* \right\rangle \tag{3.39}$$

and by the direct substitution of (3.5) into (3.39), turns into

$$\begin{aligned}\mathbf{R}'_{x\xi} &= \int_0^t e^{\mathbf{A}(t-\tau)}\mathbf{F}\left\langle \xi(t)\xi(\tau)\right\rangle d\tau \\ &= \int_0^t \delta(\tau - t)e^{\mathbf{A}(t-\tau)}\mathbf{F}d\tau \\ &= 0\end{aligned} \tag{3.40}$$

where result (B.1.13) has been used for the correlation of $\xi(t)$ and $\xi(\tau)$.

Let now (3.38) be rewritten as

$$\mathbf{R}_y' = \mathbf{C}\mathbf{C}_x'\mathbf{C}^H + \mathbf{D}\mathbf{Q}\mathbf{D}^H \tag{3.41}$$

where use has been made of (3.2) for the correlation of $\xi(t)$ to get $\mathbf{R}_{\xi\xi}$=$\mathbf{Q}$.

By taking the limit of expression (3.41) when $t \to \infty$, and from (3.15) then expression (3.37) is easily derived and the proof is complete.

3.6 Ensemble average energy function

The results of the preceding paragraphs will be used in subsequent sections to develop a procedure to identify the stochastic forcing terms that excite the most, some outputs or a group of them in the system (3.1). The identification criteria is basically formulated based on a ratio of ensemble average energies.

3.6.1 Ensemble average energy of the system state response

Following references [1],[2], the expressions that describe the transient ensemble energy behavior of the state response can be easily derived. The main results is the following Lyapunov equation,

$$\mathbf{A}^H\mathbf{B}_x{}^\infty + \mathbf{B}_x{}^\infty\mathbf{A} = -\mathbf{I}, \tag{3.42}$$

An alternative form of (3.19) given in terms of the solution of (3.42) for $\mathbf{B}_x{}^\infty$ and the matrix $\mathbf{F}$, $E_x{}^\infty$, is

$$E_x{}^\infty = trace\left(\mathbf{F}^H\mathbf{B}_x{}^\infty\mathbf{F}\right). \tag{3.43}$$

Proof of (3.42)

With reference to the original definition of E_x^{∞} in (3.17), substitution of (3.5) into this equation gives

$$E^t = \left\langle \left(\int_0^t e^{\mathbf{A}(t-\tau_m)} \mathbf{F} \xi(\tau_m) ds \right)^* \left(\int_0^t e^{\mathbf{A}(t-\tau_n)} \mathbf{F} \xi(\tau_n) d\tau_n \right) \right\rangle, \tag{3.44}$$

Rearranging terms and simplifying, one has that

$$E^t = \left\langle \left(\int_0^t \int_0^t \xi(\tau_m)^* \mathbf{F}^\dagger e^{\mathbf{A}^\dagger(t-\tau_m)} e^{\mathbf{A}(t-\tau_n)} \mathbf{F} \xi(\tau_m) d\tau_n d\tau_m \right) \right\rangle. \tag{3.45}$$

An appropriate form of (3.45) is needed to make use of the statistics of ξ, given in (3.2). Expansion of the matrix product inside brackets (see Appendix, section B.4), results in

$$\begin{aligned} E^t &= \int_0^t \int_0^t \sum_i^m \sum_j^m \left\langle \xi_i(\tau_m)^* \xi_j(\tau_n) \right\rangle \psi_{ij}(\tau_m, \tau_n) d\tau_m d\tau_n \\ &= \int_0^t \int_0^t \sum_i^m \delta(\tau_m - \tau_n) \psi_{ii}(\tau_m, \tau_n) d\tau_m d\tau_n \end{aligned} \tag{3.46}$$

where ξ_i is the *i-th* element of ξ and ψ_{ij} is the *ij*-th element of the matrix ψ, defined as

$$\psi(\tau_m, \tau_n) = \mathbf{F}^H e^{\mathbf{A}^H(t-\tau_m)} e^{\mathbf{A}(t-\tau_n)} \mathbf{F}. \tag{3.47}$$

Eq. (3.46) is similar to (3.25). Therefore, from property (B.1.12), E_x^t can be rewritten as

$$\begin{aligned} E_x^t &= trace\left(\int_0^t \psi_{ii}(\tau_m, \tau_n) \Big|_{\tau_m = \tau_n} \tau_n \right) \\ &= trace\left(\mathbf{F}^H \left(\int_0^t e^{\mathbf{A}^H(t-\tau_n)} e^{\mathbf{A}(t-\tau_n)} d\tau_n \right) \mathbf{F} \right) \\ &= trace\left(\mathbf{F}^H \mathbf{B}_x{}^t \mathbf{F} \right) \end{aligned} \tag{3.48}$$

where the time dependent matrix $\mathbf{B}_x{}^t$ has been defined as

$$\mathbf{B}_x{}^t = \int_0^t e^{\mathbf{A}^H(t-\tau_n)} e^{\mathbf{A}(t-\tau_n)} \tau_n. \tag{3.49}$$

Result (3.48) describes the transient behavior of the ensemble average of the state response; as can be seen the time dependency is given by the matrix $\mathbf{B}_x{}^t$.

When system (3.1) reaches a statistical steady state condition, $\mathbf{B}_x^t$ becomes a constant matrix, and it satisfies the condition $\mathbf{B}_x^\infty$

$$\frac{d}{dt}\mathbf{B}_x^\infty = 0. \tag{3.50}$$

Thus the derivative of $\mathbf{B}_x^t$ may be found to be

$$\begin{aligned}\frac{d}{dt}\mathbf{B}_x^t &= \frac{d}{dt}\int_0^t e^{\mathbf{A}(t-\tau_n)}e^{\mathbf{A}^H(t-\tau_n)}d\tau_n = \frac{d}{dt}\int_0^t \psi(\tau_m,\tau_n)\Big|_{\tau_m=\tau_n}\tau_m \\ &= \frac{d}{dt}\left(\int_0^t \psi(\tau_m,\tau_n)\Big|_{\tau_m=\tau_n}d\tau_n\right) = \psi(\tau_m,\tau_n)\Big|_{\tau_m=\tau_n=t} + \int_0^t \frac{\partial}{\partial t}\psi(\tau_m,\tau_n)\Big|_{\tau m=\tau n}d\tau_n\end{aligned} \tag{3.51}$$

in which

$$\psi(\tau_m,\tau_n)\Big|_{\tau_m=\tau_n=t} = e^{\mathbf{A}(t-t)}e^{\mathbf{A}^H(t-t)} = \mathbf{I} \tag{3.52}$$

and

$$\psi(\tau_m,\tau_n)\Big|_{\tau m=\tau n} = \mathbf{A}^H e^{\mathbf{A}^H(t-\tau_n)}e^{\mathbf{A}(t-\tau_n)} + e^{\mathbf{A}^H(t-\tau_n)}e^{\mathbf{A}(t-\tau_n)}\mathbf{A} \tag{3.53}$$

where use has been made of; (B.2.1), (B.3.2), and the definition of ψ given in (3.47). So that the time evolution of $\mathbf{B}_x^t$, is written in its differential form as

$$\frac{d}{dt}\mathbf{B}_x^t = \mathbf{A}^H\mathbf{B}_x^t + \mathbf{B}_x^t\mathbf{A} + \mathbf{I}. \tag{3.54}$$

Consequently, result (3.42) and (3.43), become evident.

3.6.2 Ensemble average energy of the system output response

Similar results to those presented in the previous section are developed here for ensemble average energy of the observations vector, **y**. In this case, the solution of the Lyapunov equation is sought of the form

$$\mathbf{A}^H\mathbf{B}_y^\infty + \mathbf{B}_y^\infty\mathbf{A} = -\mathbf{C}^T\mathbf{C}, \tag{3.55}$$

The solution for the ensemble average energy, E_y^∞ is given by

$$E_y^\infty = trace\left(\mathbf{F}^H\mathbf{B}_y^\infty\mathbf{F}\right) + trace(\mathbf{D}^H\mathbf{Q}\mathbf{D}). \tag{3.56}$$

This last expression differs from (3.43) because a second term has been added; it represents the direct effect of the stochastic forcing terms on the amount of energy of the output vector.

Proof of (3.55) and (3.56)

Most of the developments used in the previous section are used in this derivation. From definitions (3.18) and (3.6) it is found that in its general form, $E_y{}^t$ can be expressed as

$$E_y{}^t = \left\langle \mathbf{x}(t)^* \mathbf{C}^H \mathbf{C}\mathbf{x}(t) \right\rangle + \left\langle \mathbf{x}(t)^* \mathbf{C}^H \mathbf{D}\xi(t) \right\rangle + \left\langle \xi(t)^* \mathbf{D}^H \mathbf{C}\mathbf{x}(t) \right\rangle + \left\langle \xi(t)^* \mathbf{D}^H \mathbf{D}\xi(t) \right\rangle . \quad (3.57)$$

An expansion of the matrix product of second term on the *rhs* yields

$$\begin{aligned} \left\langle \mathbf{x}(t)^* \mathbf{C}^H \mathbf{D}\xi(t) \right\rangle &= \left\langle \xi(t) \mathbf{D}^H \mathbf{C}\mathbf{x}(t) \right\rangle^* \\ &= \left\langle \int_0^t \xi(\tau_m)^* \mathbf{F}^\dagger e^{\mathbf{A}^\dagger (t-\tau_m)} \mathbf{C}^H \mathbf{D}\xi(t) d\tau_m \right\rangle \\ &= \int_0^t \sum_i^m \sum_j^m \left\langle \xi_i(\tau_m) \xi_j(t) \right\rangle \phi_{ij}(\tau_m) d\tau_m \qquad (3.58) \\ &= \int_0^t \sum_i^m \left\langle \xi_i(\tau_m) \xi_i(t) \right\rangle \phi_{ii}(\tau_m) d\tau_m \\ &= \sum_i^m \int_0^t \delta(\tau_m - t) \phi_{ii}(\tau_m) d\tau_m = 0 \end{aligned}$$

In the procedure above, results; (B.1.13), (B.4.1), and the auxilar matrix, ϕ

$$\phi(\tau_m) = \mathbf{F}^\dagger e^{\mathbf{A}^\dagger (t-\tau_m)} \mathbf{C}^H \mathbf{D}, \qquad (3.59)$$

have been used.

Thus, (3.57) is rewritten as

$$E_y{}^t = \left\langle \mathbf{x}(t)^* \mathbf{C}^H \mathbf{C}\mathbf{x}(t) \right\rangle + \left\langle \xi(t)^* \mathbf{D}^H \mathbf{D}\xi(t) \right\rangle , \qquad (3.60)$$

and from (3.2) and (B.4.1), it can be easily proved that

$$\left\langle \xi(t)^* \mathbf{D}^H \mathbf{D}\xi(t) \right\rangle = trace(\mathbf{D}^H \mathbf{Q}\mathbf{D}) . \qquad (3.61)$$

The first term in the *rhs* of (3.60) can be rewritten as

$$\left\langle \mathbf{x}(t)^{*}\mathbf{C}^{H}\mathbf{C}\mathbf{x}(t)\right\rangle = \int_0^t\int_0^t \sum_j^m \left\langle \xi_i\left(\tau_m\right)^{*}\xi_i\left(\tau_n\right)\right\rangle \theta_{ii}(\tau_m,\tau_n)d\tau_m d\tau_n$$

$$= \int_0^t\int_0^t \sum_i^m \delta(\tau_n-\tau_m)\theta_{ii}(\tau_m,\tau_n)d\tau_n \qquad (3.62)$$

$$= \sum_i^m \int_0^t \theta_{ii}(\tau_m,\tau_n)\Big|_{\tau_m=\tau_n} d\tau_n$$

in which,

$$\theta(\tau_m,\tau_n) = \mathbf{F}^{H}e^{A^{H}(t-\tau_m)}\mathbf{C}^{H}\mathbf{C}e^{A(t-\tau_n)}\mathbf{F}\,. \qquad (3.63)$$

Then

$$\left\langle \mathbf{x}(t)^{*}\mathbf{C}^{H}\mathbf{C}\mathbf{x}(t)\right\rangle = trace\left(\mathbf{F}^{H}\left(\int_0^t e^{A^{H}(t-\tau_m)}\mathbf{C}^{H}\mathbf{C}e^{A(t-\tau_n)}d\tau_n\right)\mathbf{F}\right). \qquad (3.64)$$

As it was done in (3.49), the time dependent part of (3.64) is isolated and defined by $\mathbf{B}_y{}^t$

$$\mathbf{B}_y{}^t = \int_0^t e^{A^{H}(t-\tau_m)}\mathbf{C}^{H}\mathbf{C}e^{A(t-\tau_n)}d\tau_n\,. \qquad (3.65)$$

Therefore, in analogy wit (3.50), a statistical steady state condition is reached when

$$\frac{d}{dt}\mathbf{B}_y{}^{\infty} = 0 \qquad (3.66)$$

Following the same procedure as in (3.51)-(3.53), the time evolution of $\mathbf{B}_y{}^t$, can be expressed as

$$\frac{d}{dt}\mathbf{B}_y{}^t = \mathbf{A}^{H}\mathbf{B}_y{}^t + \mathbf{B}_y{}^t\mathbf{A} + \mathbf{C}^{H}\mathbf{C}\,. \qquad (3.67)$$

where $\mathbf{B}_y{}^{\infty}$ satisfies (3.55).

From results (3.58), (3.61) and (3.55), in a statistical steady state condition the ensemble average energy of the output vector is given by (3.56). This completes the proof of the above statement.

3.7 References

[1] Nolan, D. S., & Farrell, B. F. (1999). The intensification of two-dimensional swirling flows by stochastic asymmetric forcing. *Journal of the atmospheric sciences*, 56(23), 3937-3962.

[2] Farrell, B. F., & Ioannou P. J. (1993). Stochastic forcing of the linearized Navier–Stokes equations. *Physics of Fluids A: Fluid Dynamics (1989-1993)*,5(11), 2600-2609.

[3] Papoulis, A., & Pillai, S. U. (2002).*Probability, random variables, and stochastic processes*. Tata McGraw-Hill Education.

[4] Gardiner, C. W. (1986). *Handbook of stochastic methods for physics, chemistry and the natural sciences*. Springer series in synergetics, 13, 149-168.

[5] Lathi, B. (1998). Signal processing and linear systems. Oxford University Press, USA.

[6] Messina, A. R., & Vittal, V. (2007). Extraction of dynamic patterns from wide-area measurements using empirical orthogonal functions. Power Systems, IEEE Transactions on, 22(2), 682-692.

[7] Chen, C. T. (1995). Linear system theory and design. Oxford University Press Inc.

[8] Penzl, T. (1998). Numerical solution of generalized Lyapunov equations.Advances in Computational Mathematics, 8(1-2), 33-48.

[9] Bryson, A. E. (1975). Applied optimal control: optimization, estimation and control. CRC Press.

[10] Flanders, H. (1973). Differentiation under the integral sign. American Mathematical Monthly, 615-627.

Chapter 4

Extraction of Dominant Spatial Structures

Electromechanical oscillations are inherent to large interconnected power systems. Much recent effort has been devoted to estimating the electromechanical modes of oscillation from measured (simulated) data. Mode shapes, in particular, provide important information on the participation of an individual machine or a group of machines in a particular mode and can be associated with the observability of the mode in the electromechanical states. In a multimachine system, the electromechanical mode shapes can be used to determine coherent groupings of machines.

In this section, a new analytic methodology for the direct mode shape identification of the modes that dominate the response of a stochastically driven linear system is suggested. The procedure described combines the advantages of the statistical steady state covariance matrix and the Proper Orthogonal Decomposition (POD) method to extract mode shapes and modal coordinates from the random response of a linear stochastically forced model of the system.

4.1 POMs interpreted as mode shapes

The Proper Orthogonal Decomposition (POD) method is an optimal technique to extract a set of basis functions or modes, which capture spatial correlations in the system response. These modes will be referred to as POD modes.

In what follows, a flexible analytical framework is proposed to identify a set of POD modes that accurately describe spatial correlations in the response of a linear stochastically forced system. The reader is referred to Appendix C for a detailed treatment of the POD method.

To introduce the proposed framework, let $x_i(t)$ be the continuous version of $\mathbf{x}_i$. From linear systems theory, $x_i(t)$ can be decomposed in terms of its POD modes as

$$x_i(t) \approx \sum_{j=1}^{p} \alpha_{ij}(t)\mathbf{w}_j \tag{4.1}$$

Equation (4,1) shows that, for each $x_i(t)$ i=1,2,..., the spatial distribution is described by the vector $\mathbf{w}$ and the time dependency is given by the coefficient $\alpha_{ij}(t)$.

In analogy with conventional linear analysis, POMs can be interpreted as mode shapes while $\alpha(t)$ provides the temporal amplitude evolution of the POD modes [1].

4.2 Statistical steady state covariance matrix and POD analysis

Proper orthogonal decomposition analysis is taken as the point of departure for the analysis of ambient system response. Let to this end, the dynamic behavior of the power system be approximated by the linear time-invariant model

$$\begin{aligned} \dot{\mathbf{x}}(t) &= \mathbf{A}\mathbf{x}(t) + \mathbf{F}\xi(t) \\ \mathbf{y}(t) &= \mathbf{C}\mathbf{x}(t) + \mathbf{D}\xi(t) \end{aligned} \tag{4.2}$$

where the coefficients of the linear model have the usual interpretation (refer to Chapter 3).

The solution of **x**(t) is given by

$$\mathbf{x}(t) = \int_0^t e^{\mathbf{A}(t-\tau)} \xi(\tau) d\tau \tag{4.3}$$

and

$$\mathbf{y}(t) = \mathbf{C}\left[\int_0^t e^{\mathbf{A}(t-\tau)} \xi(\tau) d\tau \right] + \mathbf{D}\xi(t). \tag{4.4}$$

Under an statistical steady state condition, the covariance matrix of $\mathbf{x}(t)$ and $\mathbf{y}(t)$ can be defined as

$$\mathbf{C}_x{}^{\infty} = \lim_{t \to \infty} \int_0^t e^{\mathbf{A}(t-\tau_n)} \mathbf{F}\mathbf{F}^H e^{\mathbf{A}^H (t-\tau_n)} \tau_n \tag{4.5}$$

and

$$\mathbf{C}_y{}^{\infty} = \mathbf{C}\mathbf{C}_x{}^{\infty}\mathbf{C}^H + \mathbf{D}\mathbf{Q}\mathbf{D}^H \tag{4.6}$$

respectively.

The expression on the *rhs* of (4.5) is referred to as the controllability Grammian.

It is easy to demonstrate that when the number of samples building $\mathbf{x}_i$ i=1,2,…,n in (C.1.4) tends to infinity, i.e., $N \rightarrow \infty$, then (C.1.11) converges to $\mathbf{C}_x{}^{\infty}$ or $\mathbf{C}_y{}^{\infty}$ when the spatio-temporal phenomena under study are the state response $\mathbf{x}(t)$ and the vector of measurements **y**(t) respectively.

As a proof let $\mathbf{C}_s$ (see Appendix, section C.1) be rewritten as

$$\mathbf{C}s = \frac{1}{N}\mathbf{X}\mathbf{X}^T = \begin{bmatrix} \frac{1}{N}\mathbf{x}_1{}^{*}\mathbf{x}_1 & \cdots & \frac{1}{N}\mathbf{x}_1{}^{*}\mathbf{x}_n \\ \vdots & & \vdots \\ \frac{1}{N}\mathbf{x}_n{}^{*}\mathbf{x}_1 & \cdots & \frac{1}{N}\mathbf{x}_n{}^{*}\mathbf{x}_n \end{bmatrix}$$

$$= \begin{bmatrix} \frac{1}{N}\sum_{k=1}^{N} x_1(t_k)x_1(t_k) & \cdots & \frac{1}{N}\sum_{k=1}^{N} x_1(t_k)x_n(t_k) \\ \vdots & & \vdots \\ \frac{1}{N}\sum_{k=1}^{N} x_n(t_k)x_1(t_k) & \cdots & \frac{1}{N}\sum_{k=1}^{N} x_n(t_k)x_n(t_k) \end{bmatrix}. \tag{4.7}$$

It follows that, from the law of the large numbers [2]:

$$\frac{1}{N}\sum_{k=1}^{N} x_i(t_k)x_j(t_k) \rightarrow \left\langle \mathbf{x}_i(t)^* \mathbf{x}_j(t) \right\rangle \text{ when } N \rightarrow \infty . \tag{4.8}$$

This means that the sampling mean tends to the expected value of the product of the continuous functions $\mathbf{x}_i(t)$ and $\mathbf{x}_j(t)$. More formally, when $N \rightarrow \infty$, (4.7) can be rewritten as

$$\lim_{N\to\infty} \mathbf{C}s = \lim_{N\to\infty} \frac{1}{N}\mathbf{X}\mathbf{X}^T = \begin{bmatrix} \left\langle \mathbf{x}_1(t)^* \mathbf{x}_1(t) \right\rangle & \cdots & \left\langle \mathbf{x}_1(t)^* \mathbf{x}_n(t) \right\rangle \\ \vdots & & \vdots \\ \left\langle \mathbf{x}_n(t)^* \mathbf{x}_1(t) \right\rangle & \cdots & \left\langle \mathbf{x}_n(t)^* \mathbf{x}_n(t) \right\rangle \end{bmatrix} \tag{4.9}$$
$$= \mathbf{C}_x.$$

POD analysis allows to find the POM's $\mathbf{w}_{x1}, \mathbf{w}_{x2},\ldots,\mathbf{w}_{xn}$ from the linear expression

$$\mathbf{C}_x^{\infty} \mathbf{w}_x = \lambda_x \mathbf{w}_x \tag{4.10}$$

In an analogous manner, the corresponding POM's $\mathbf{w}_{y1}, \mathbf{w}_{y2},\ldots,\mathbf{w}_{yn}$ for $\mathbf{y}(t)$ can be obtained from

$$\mathbf{C}_y^{\infty} \mathbf{w}_y = \lambda_y \mathbf{w}_y \tag{4.11}$$

In both cases, the predominant spatial structure describing the stochastic forcing responses $\mathbf{x}$ and $\mathbf{y}$ are those right eigenvectors corresponding to the leading POV's of $\mathbf{C}_x^{\infty}$ and $\mathbf{C}_y^{\infty}$ respectively. As a consequence, the mode shape of the mode that dominates the randomly excited response of (4.2) is given by the values of vectors $\mathbf{w}_{x1}$ and $\mathbf{w}_{y2}$ which are associated to the state and output responses respectively.

The application of these criteria are described in subsequent chapters.

4.3 References.

[1] Messina, A. R., & Vittal, V. (2007). Extraction of dynamic patterns from wide-area measurements using empirical orthogonal functions. Power

[2] Papoulis, A., & Pillai, S. U. (2002). *Probability, random variables, and stochastic processes*. Tata McGraw-Hill Education.

Chapter5
Dominant Stochastic Forcing Functions

Power systems are continuously subject to random perturbations. Many recent studies have suggested that random load variations can act to stochastically force the power system and excite the system electromechanical modes.

In this Chapter, a methodology based on the concept of Stochastic Optimals (SO's) for the identification of the stochastic forcing functions that contribute most to the response of a linear dynamical system is suggested.

The analytic approach presented here is formulated for a statistical steady state condition, and focuses on the decomposition of the ensemble average energy in terms of components of energy uniquely associated with each stochastic forcing function.

The identification procedures are well suited to perform analysis of system observability during random operating condition. Such an approach helps to identify the elements and operating conditions that contribute the most to the observed system response.

5.1 Ensemble average energy decomposition

Before presenting details of the proposed framework, some basic definitions for a stochastically driving linear system are introduced. A new analytic approach used to identify the forcing functions that contribute most to the dynamical response of this white-noise excited linear system is then developed.

Consider the ensemble average energy definitions for E_x^t and E_y^t [1],[2]

$$E_x^t(t) = \left\langle \|\mathbf{x}(t)\|^2 \right\rangle \tag{5.1}$$

and

$$E_y^t(t) = \left\langle \|\mathbf{y}(t)\|^2 \right\rangle \tag{5.2}$$

for vectors **x** and **y** respectively.

Expressions (5.1)-(5.2) can be used as a measure of the energy level of the dynamical response of the system and depending on the use of the definition (5.1) or (5.2), this concept of energy can be interpreted in two ways: the energy of the state response vector and the energy of the vector of measurements.

Let (5.1) be expanded as

$$E_x^t(t) = \left\langle x_1(t)^* x_1(t) \right\rangle + \left\langle x_2(t)^* x_2(t) \right\rangle + \ldots + \left\langle x_n(t)^* x_n(t) \right\rangle \tag{5.3}$$

It is easily seen that E_x^t represents the sum of the individual energies of the elements making up the state vector **x**. Consequently, E_x^t is considered to assess the global energy of the linear system response. Similarly for E_y^t, one has that

$$E_y^t(t) = \left\langle y_1(t)^* y_1(t) \right\rangle + \left\langle y_2(t)^* y_2(t) \right\rangle + \ldots + \left\langle y_r(t)^* y_r(t) \right\rangle \tag{5.4}$$

estimates the total energy of the output state vector, and is considered also as a measure of the total amount of energy in the system.

The objective of this chapter is the formulation of a methodology that decomposes E_x^∞ ($E_x^\infty = \lim_{t\to\infty} E_x^t$) in energy contributions associated with the indi-

vidual elements of the forcing vector function ξ, i.e., find an analytic expression of the form:

$$E_x^{\infty} = S_{x1} + S_{x2} + \cdots + S_{xm}, \tag{5.5}$$

where the coefficient S_{xi}, measure the fraction of growth attributable to the forcing function ξ_i.

This decomposition can be be extended to E_y^{∞} as

$$E_y^{\infty} = S_{y1} + S_{y2} + \cdots + S_{ym} \tag{5.6}$$

where S_{yi}, measures the contribution of the energy to the output vector due to the stochastic perturbation ξ_i.

It should be emphasized that this procedure is a particular result valid for a linear system driven by delta-uncorrelated white noise.

5.2 Stochastic optimals

As pointed out in previous sections, the covariance matrix, $\mathbf{C}_x^{\infty}$ depends on the dynamics of the system, given by the linear modes of A, and on the structures and magnitudes of the forcing functions building the matrix **F** [1],[2]. This idea can be extended to the ensemble average energy and becomes evident from the definition, E_x^{∞}

$$E_x^{\infty} = trace\left(\mathbf{F}^H \mathbf{B}_x^{\infty} \mathbf{F}\right) = \sum_{i=1}^{m} \mathbf{f}_i^H \mathbf{B}_x^{\infty} \mathbf{f}_i . \tag{5.7}$$

where $\mathbf{B}_x^{\infty}$ satisfies the equation

$$\mathbf{A}^H \mathbf{B}_x^{\infty} + \mathbf{B}_x^{\infty} \mathbf{A} = -\mathbf{I} . \tag{5.8}$$

In an effort to understand this double dependency, the concept of stochastic optimals (SO's) is introduced in this work [1],[2] and will be used as an important tool to determine the most important random excitations in a linear representation of a physical system.

More formally, the SO's $\{\mathbf{f}_{so\text{-}1}, \mathbf{f}_{so\text{-}2}, \ldots, \mathbf{f}_{so\text{-}n}\}$ are n orthonormal vectors that constitute a *reference frame (SO's reference frame)*, entirely defined by the *dynamical characteristics* of a general linear representation model. The elements of the set $\{\mathbf{f}_{so\text{-}1}, \mathbf{f}_{so\text{-}2}, \ldots, \mathbf{f}_{so\text{-}n}\}$ keep a hierarchical relation between them, determining different directions of growth. Specifically, $\mathbf{f}_{so\text{-}1}$ is said to be associated to the spatial distribution that allows the optimal growth of a one particular perturbation ξ_i and $\mathbf{f}_{so\text{-}2}$ with the second most optimal growth and so forth.

5.2.1 Mathematical definition of stochastic optimals

The mathematical concept of SO's is formulated trough an optimization problem that consists in the computation of the ensemble average energy of a conceptual linear system with a spatial the forcing distribution given by the SO's vectors.

For convenience of notation, we can write the system representation as

$$\dot{\mathbf{x}}(t) = \mathbf{A}\mathbf{x}(t) + \mathbf{F}_{so}\xi_{so}(t) \tag{5.9}$$

where ξ_{so} is an n-dimensional vector (delta uncorrelated white noise) and $\mathbf{F}_{so}$ is the spatial distribution of the forcing matrix composed by the columns $\mathbf{f}_{sox\text{-}1}$, $\mathbf{f}_{sox\text{-}2}, \ldots, \mathbf{f}_{sox\text{-}n}$.

This is formulated in this research as an optimization problem as explained below.

Optimization problem:.

Given the model (5.9), find a set of n-dimensional normalized vectors, $\{\mathbf{f}_{sox\text{-}1}, \mathbf{f}_{sox\text{-}2}, \ldots, \mathbf{f}_{sox\text{-}n}\}$ that maximize, $E^{\infty}_{so\text{-}x}$, i.e., if

$$E^{\infty}_{so-x} = trace\left(\mathbf{F}_{so}{}^{H}\mathbf{B}_{x}{}^{\infty}\mathbf{F}_{so}\right) = \sum_{i=1}^{n}\mathbf{f}_{sox-i}{}^{H}\mathbf{B}_{x}{}^{\infty}\mathbf{f}_{sox-i}\,. \tag{5.10}$$

then

$$\text{Maximize } E^{\infty}_{so-x}\,. \tag{5.11}$$

Subject to

$$\mathbf{f}_{sox-1}{}^{H}\mathbf{f}_{sox-1}=1\,. \tag{5.12}$$

The optimal solution of this optimization problem is developed in Appendix B.5. It is is probed that the solution is given in terms of the eigenvalue problem

$$\mathbf{B}_x{}^{\infty}\mathbf{f}_{sox}=\lambda_{so}\mathbf{f}_{sox}\,. \tag{5.13}$$

Use of result (5.13) in (5.10) gives

$$\begin{aligned} E^{\infty}{}_{so-x} &= \sum_{i=1}^{n}\lambda_{sox-1}\,\mathbf{f}_{sox-i}{}^{H}\mathbf{f}_{sox-i} \\ &= \sum_{i=1}^{n}\lambda_{so-1}\,. \end{aligned} \tag{5.14}$$

It can be seen that the sum of the eigenvalues of $\mathbf{B}_x{}^{\infty}$ determines, in an statistical sense, the energy of the state response of (5.10). Also from (5.14) the $\lambda_{sox\text{-}i}$ can be interpreted as the value of energy in $E^{\infty}{}_{so\text{-}x}$ due the *i-th* element of ξ_{so}, i.e., for the state representation

$$\dot{\mathbf{x}}(t)=\mathbf{A}\mathbf{x}(t)+\mathbf{f}_{sox-1}\xi_{so-1}(t)\,, \tag{5.15}$$

and for, $E^{\infty}{}_{so\text{-}x}$

$$E^{\infty}{}_{so-x}=\lambda_{sox-1}\,. \tag{5.16}$$

Also, from the definition of $\mathbf{B}_x{}^{\infty}$ in Chapter 3, one has that

$$\mathbf{B}_x{}^{\infty}=\lim_{t\to\infty}\int_0^t e^{\mathbf{A}^{H}(t-\tau_n)}e^{\mathbf{A}(t-\tau_n)}\tau_n\,. \tag{5.17}$$

It is seen that $\mathbf{B}_x{}^{\infty}$ is a Hermitian matrix, and therefore, its eigenvectors conform an orthonormal basis with positive and real eigenvalues [3].

From expression (5.13) it can be established the hierarchical nature of the SO's. After sorting the eigenvalues as $\lambda_{sox\text{-}1} > \lambda_{sox\text{-}2} > \ldots > \lambda_{sox\text{-}n}$ it is observed that the respective vectors $\{\mathbf{f}_{sox\text{-}1}, \mathbf{f}_{sox\text{-}2}, \ldots, \mathbf{f}_{sox\text{-}n}\}$ can be ranked according to the level of energy computed in (5.16); the eigenvectors corresponding to the greatest ei-

genvalues of matrix $\mathbf{B}_x^{\infty}$ represent spatial patterns for the stochastic forcing functions that optimize the level of excitation of the state response.

Figure 5.1 displays the relation between $\lambda_{sox\text{-}i}$ and $E^{\infty}_{so\text{-}x}$ in expressions (5.15)-(5.16).

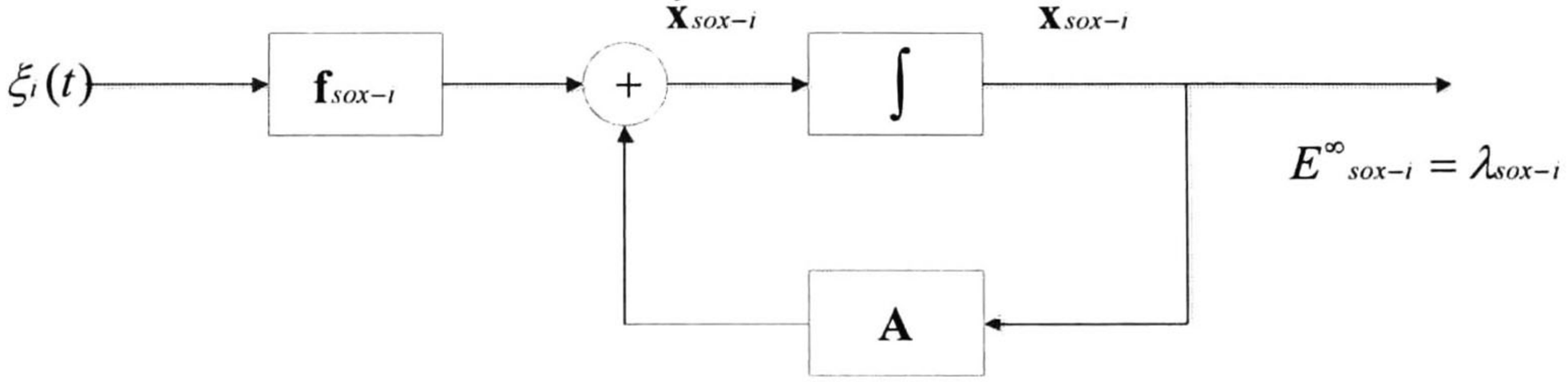

Figure 5.1. Conceptual representation of stochastic optimals.

5.2.2 *State response energy decomposition, SO's approach*

Each column of a general spatial distribution matrix **F** can be expressed as a linear combination of the orthonormal basis $\{\mathbf{f}_{sox\text{-}1}, \mathbf{f}_{sox\text{-}2},\ldots, \mathbf{f}_{so\text{-}n}\}$, namely

$$\mathbf{f}_i = \sum_{k=1}^{n} a_{xk}{}^{i}\mathbf{f}_{sox-k} \tag{5.18}$$

Substituting (5.18) into (5.7) gives

$$\begin{aligned} E_x{}^{\infty} &= \sum_{i=1}^{n}\left[\left(\sum_{j=1}^{n} a_{xj}{}^{i}\mathbf{f}_{sox-j}\right)^{H} \mathbf{B}_x{}^{\infty}\left(\sum_{k=1}^{n} a_{xk}{}^{i}\mathbf{f}_{sox-k}\right)\right] \\ &= \sum_{i}^{n}\sum_{j}^{n}\sum_{k}^{n} a_{xj}{}^{i}\, a_{xk}{}^{i}\mathbf{f}_{sox-j}{}^{H}\mathbf{B}_x{}^{\infty}\mathbf{f}_{sox-k} \qquad (5.19) \\ &= \sum_{i}^{n}\sum_{j}^{n}\sum_{k}^{n} a_{xj}{}^{i}\, a_{xk}{}^{i}\mathbf{f}_{sox-j}{}^{H}\mathbf{f}_{sox-k}\lambda_{sox-k} \end{aligned}$$

Noting now that the elements of the set $\{\mathbf{f}_{so\text{-}1}, \mathbf{f}_{so\text{-}2},\ldots, \mathbf{f}_{so\text{-}n}\}$, are orthonormal, (5.19) can be rewritten as

$$E_x{}^{\infty} = \sum_{i=1}^{m}\sum_{k=1}^{n}\left(a_{xk}{}^{i}\right)^2\lambda_{sox-k}\,, \tag{5.20}$$

Further, defining

$$S_{xi} = \sum_{k=1}^{n} \left(a_{xk}^{i}\right)^2 \lambda_{sox-k}, \; i=1,2,\ldots,n, \tag{5.21}$$

then, expression (5.5) becomes evident.

Physically, the coefficients a^i_k in (5.21)correspond to the projection of the vector **f** onto $\mathbf{f}_{sox\text{-}k}$, and $\lambda_{sox\text{-}k}$ is the corresponding eigenvalue of $\mathbf{f}_{sox\text{-}k}$. The extent of energy to which one input contributes to the ensemble average energy of the state response, is determined by the projection of $\mathbf{f}_i$ onto the SO's $\{\mathbf{f}_{sox\text{-}1}, \mathbf{f}_{sox\text{-}2}, \ldots, \mathbf{f}_{sox\text{-}n}\}$.

If the projection is large in the direction of the SO's corresponding to the greatest eigenvalues $\{\lambda_{sox\text{-}1}, \lambda_{sox\text{-}2}, \ldots, \lambda_{sox\text{-}n}\}$, then the effect of $\xi_i(t)$ onto E_x^{∞} will be predominant. This idea is explained schematically in Fig. 5.2 for a 3-dimensional linear system. Here, the width of the lines is used to distinguish between the distinct levels of growth of the perturbation in the different directions.

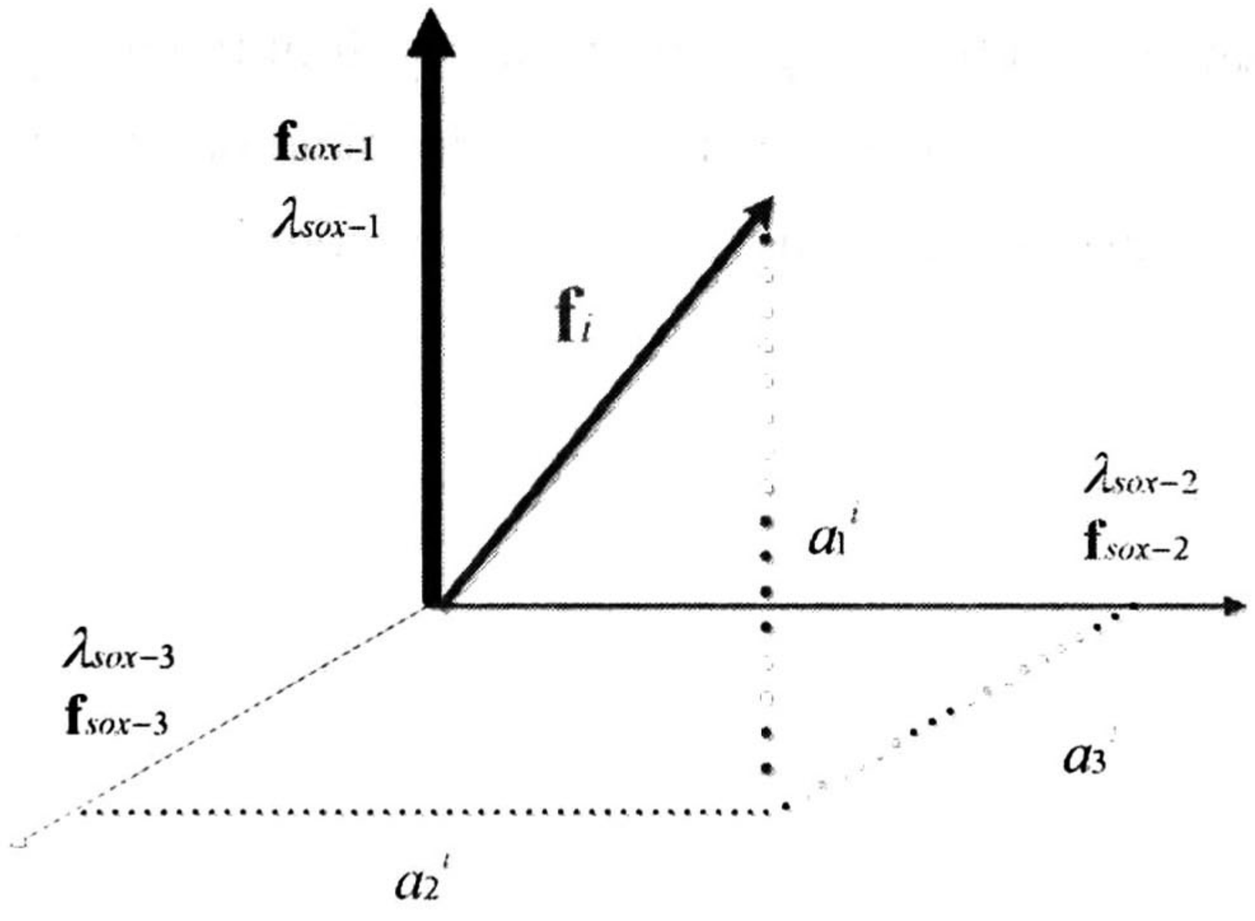

Figure 5.2. Decomposition of an arbitrary spatial distribution

5.2.3 Output response energy decomposition, SO's approach

A similar analysis to that developed for the state energy can be used to study the way that stochastic functions excite the output response of the system. The objective is to decouple ensemble average energy corresponding to the output vector, in terms of the energy contribution of each input.

The analytical study is based on the same assumption of capturing the spatial and dynamical dependency of the output energy and its relationship with the set of inputs that perturbed the linear system.

Let the equation defining the ensemble of average energy of the output vector, E_y^{∞} be rewritten as

$$\tilde{E}_y^{\infty} = \underbrace{trace\left(\mathbf{F}^H \mathbf{B}_y^{\infty} \mathbf{F}\right)}_{\substack{Spatial\ and\ Dynamical \\ Dependency}} + \underbrace{trace(\mathbf{D}^H \mathbf{Q} \mathbf{D})}_{Spatial\ Dependency}. \tag{5.22}$$

It can be seen that E_y^{∞} is constituted by two terms: the first term on the *rhs* represents the spatial and dynamical dependency. The second terms captures spatial dependency. Similar conclusions to those performed for the input-to-state relation about the meaning of SO's concept can be made for the first term on the *rhs* of (5.22).

The second term in the *rhs* of (5.22) can be easily decoupled in components uniquely associated to a single input. As result of the independency of the components of $\xi(t)$, the i-th element in the main diagonal of the matrix $\mathbf{D}^H\mathbf{Q}\mathbf{D}$ defined as $d_{y\text{-}i}$, measures the partial contribution of energy attributable to the i-th input $\xi_i(t)$.

Then the coefficient that measures the whole output energy caused by $\xi_i(t)$ will be defined as

$$\tilde{S}_{yi} = \sum_{k=1}^{n} \left[\left(a_{yk}{}^{i} \right)^2 \lambda_{soy-k} \right] + d_{y-i}. \tag{5.23}$$

where $\lambda_{soy\text{-}i}$ can be obtained from the eigensolution of the linear expression

$$\mathbf{B}_y{}^{\infty} \mathbf{f}_{soy} = \lambda_{soy} \mathbf{f}_{soy} \tag{5.24}$$

and the term $a_{yk}{}^{i}$ is a coefficient to be determined associated to the decomposition of $\mathbf{f}_i$ as a linear combination of the SO's $\{\mathbf{f}_{soy\text{-}1}, \mathbf{f}_{soy\text{-}2}, \ldots, \mathbf{f}_{soy\text{-}n}\}$; $a_{yk}{}^{i}$ satisfies

$$\mathbf{f}_i = \sum_{k=1}^{n} a_{yk}{}' \mathbf{f}_{soy-k} \text{ for } i = 1, 2, \ldots, p. \tag{5.25}$$

Several remarks are in order here. The first term on the *rhs* of (5.23) can be interpreted as follows.

- The extent to which a single input contributes to the ensemble average energy of the output response, is determined by the projection of $\mathbf{f}_i$ onto the SO's $\{\mathbf{f}_{soy\text{-}1}, \mathbf{f}_{soy\text{-}2}, \ldots, \mathbf{f}_{soy\text{-}n}\}$,
- If this projection is large in the direction of SO's corresponding to greatest eigenvalues $\{\lambda_{soy\text{-}1}, \lambda_{soy\text{-}2}, \ldots, \lambda_{soy\text{-}n}\}$ then the effect of $\xi(t)$ onto E_y^{∞} will be predominant.

Furthermore, $d_{y\text{-}i}$ should be interpreted carefully when numerical simulations are performed. For the case of uncorrelated white noise excitation, $d_{y\text{-}i}$ is formally defined as

$$d_{i\text{-}y} = \delta(0) d_{ii} \text{ for } i = 1, 2, \ldots, p. \tag{5.26}$$

where d_{ii} represents the *i-i* element of matrix $\mathbf{D}^H\mathbf{D}$. In addition, the impulse function $\delta(0)$ sets the coefficient $d_{i\text{-}y}$ to an infinite value, which is physically meaningless. However, when numerical approximations for $\delta(0)$ are adopted, this coefficient can be used as a measure of energy.

In general, the fraction of energy that only depends of the forcing functions, can be measured according to the value of d_{ii}.

Further research need to be performed to developed a general expression like (5.23) that jointly accounts for the state-dependent and input-dependent energy terms. Based on numerical simulations, $d_{i\text{-}y}$ can be described as a function of Δt^{-1}, being Δt the time-step integration of certain model under study.

To avoid these difficulties and because this research focuses on the study of the dynamical behavior of the system under randomly excited load changes, this thesis will focus on the state-dependent energy term

$$E_y^{\infty} = \underbrace{trace\left(\mathbf{F}^H \mathbf{B}_y^{\infty} \mathbf{F}\right)}_{\substack{\textit{Spatial and Dynamical} \\ \textit{Dependency}}}, \tag{5.27}$$

and its associated decomposition

$$E_y^{\infty} = \underbrace{trace\left(\mathbf{F}^H \mathbf{B}_y^{\infty} \mathbf{F}\right)}_{\substack{\textit{Spatial and Dynamical} \\ \textit{Dependency}}} = \sum_{i=1}^{p} S_{i-y}, \tag{5.28}$$

with

$$S_{yi} = \sum_{k=1}^{n} \left[\left(a_{yk}{}^{i} \right)^2 \lambda_{soy-k} \right]. \tag{5.29}$$

5.3 Modal energy components

The objective of this approach is to decompose the energy of the state response in terms of energy components associated to the modes that are part of this response. Our principal objective is to find an expression similar to (5.3) and (5.5), where the coefficients resulting from the decomposition are expected to measure the presence of certain mode in the state response of the system, i.e.

$$E_x^{\infty} = S_{\lambda 1-x} + S_{\lambda 2-x} + \cdots + S_{\lambda n-x}, \tag{5.30}$$

In this representation, the coefficient $s_{\lambda i}$ represent the amount of energy measuring the excitation level of the i-th linear mode. As will be demonstrated, this expression results from neglecting the mode-interaction energy terms resulting in the computation of E_x^{∞}. However, these neglected terms can be directly measured and they are small enough to be ignored.

Proof of (5.30)

Let $\mathbf{x}(t)$ to be rewritten in terms of dyadic expansion of $e^{\mathbf{A}t}$, (B.4.2). Then,

$$\mathbf{x}(t) = \int_0^t \sum_{i=1}^{n} e^{\lambda_i (t-s)} \mathbf{v}_i \mathbf{w}_i{}^T \mathbf{F} \xi(\tau_n) d\tau_n . \tag{5.31}$$

Direct substitution of expression (5.31) into the definition E_x^{∞}, yields

$$E_x^{\infty} = \lim_{t\to\infty}\left\langle \left(\int_0^t \sum_{i=1}^{n} e^{\lambda_i (t-\tau_n)} \mathbf{v}_i \mathbf{w}_i{}^T \mathbf{F}\xi(\tau_n) d\tau_n \right)^* \left(\int_0^t \sum_{j=1}^{n} e^{\lambda_j (t-\tau_m)} \mathbf{v}_j \mathbf{w}_j{}^T \mathbf{F}\xi(\tau_m) \tau_m \right) \right\rangle . \quad (5.32)$$

Rearranging terms of (5.32) results in

$$E_x^{\infty} = \lim_{t\to\infty} \sum_{i=1}^{n}\sum_{j=1}^{n} \left\langle \int_0^t \int_0^t \xi(\tau_n)^* \mathbf{F}^T \left(\mathbf{w}_i{}^T\right)^* \mathbf{v}_i{}^* \mathbf{v}_j \mathbf{w}_j{}^T \mathbf{F}\xi(\tau_m) e^{\lambda_i^* (t-\tau_n)} e^{\lambda_j (t-\tau_m)} d\tau_n d\tau_m \right\rangle . (5.33)$$

Also, from the result (B.4.2)

$$E_x^{\infty} = \lim_{t\to\infty} \sum_{i=1}^{n}\sum_{j=1}^{n} \eta_{ij} \int_0^t \int_0^t \delta(\tau_n - \tau_m) e^{\lambda_i^* (t-\tau_n)} e^{\lambda_j (t-\tau_m)} d\tau_n d\tau_m \quad (5.34)$$

with

$$\eta_{ij-x} = trace\left(\mathbf{F}^T \left(\mathbf{w}_i{}^T\right)^* \mathbf{v}_i{}^* \mathbf{v}_j \mathbf{w}_j{}^T \mathbf{F} \right). \quad (5.35)$$

Further, from (B.1.12), (5.34) turns into

$$E_x^{\infty} = \lim_{t\to\infty} \sum_{i=1}^{n}\sum_{j=1}^{n} \eta_{ij} \int_0^t e^{\lambda_i^* (t-\tau_n)} e^{\lambda_j (t-\tau_n)} d\tau_n . \quad (5.36)$$

By solving the integral in the *rhs* of (5.36) yields

$$E_x^{\infty} = \lim_{t\to\infty} \sum_{i=1}^{n}\sum_{j=1}^{n} -\frac{\eta_{ij-x}}{\left(\lambda_i^* + \lambda_j\right)} \left(1 - e^{\left(\lambda_i^* + \lambda_j\right) t} \right). \quad (5.37)$$

And, in an statistical stationary condition

$$E_x^{\infty} = \sum_{i=1}^{n}\sum_{j=1}^{n} -\frac{\eta_{ij-x}}{\left(\lambda_i^* + \lambda_j\right)} = \sum_{i=1}^{n}\sum_{j=1}^{n} \psi_{ij-x} . \quad (5.38)$$

where the coefficient ψ has been defined as

$$\psi_{ij} = -\frac{\eta_{ij-x}}{\left(\lambda_i^* + \lambda_j\right)} . \quad (5.39)$$

Expression (5.38) can be decomposed into energy components associated with a single mode, and energy contributions resulting from the pairwise mode interaction. More precisely,

$$E_x^{\infty} = \sum_{i=1}^{n} \psi_{ii-x} + 2\, real\left\{ \sum_{i=1}^{n-1} \sum_{j=i+1}^{n} \psi_{ij-x} \right\}. \tag{5.40}$$

where use has been made of the property

$$\psi_{ij-x} = \psi_{ji-x} \Rightarrow \psi_{ij-x} + \psi_{ji-x} = 2\, real\left\{ \psi_{ij-x} \right\} \tag{5.41}$$

Now, by assuming that most of the energy is described by the first term in the *rhs* of (5.40), E_x^{∞} can be approximated by

$$E_x^{\infty} \approx \sum_{i=1}^{n} \psi_{ii-x} \,. \tag{5.42}$$

Under this assumption and noting that $s_{\lambda i} = \psi_{ii}$ the proof of (5.30) is straightforward.

Additional information can be extracted from the definitions of ψ and η. Let $s_{\lambda i}$ be a modal energy component of interest, this component can be expressed as

$$s_{\lambda i} = -\frac{\eta_{ii-x}}{\left(\lambda_i^* + \lambda_i\right)}, \tag{5.43}$$

As can be seen in the equation above, the numerator is uniquely linked with a single mode. Here, the coefficient η can be used to describe the effect of the stochastic forcing functions in a particular modal energy component (e.g. the greatest modal energy component). To show this, let η to be decomposed as:

$$\eta_{ii-x} = \mathbf{f}_1^T \left(\mathbf{w}_i^T\right)^* \mathbf{w}_i^T \mathbf{f}_1 + \mathbf{f}_2^T \left(\mathbf{w}_i^T\right)^* \mathbf{w}_i^T \mathbf{f}_2 + \ldots + \mathbf{f}_m^T \left(\mathbf{w}_i^T\right)^* \mathbf{w}_i^T \mathbf{f}_m \,, \tag{5.44}$$

where it is evident that each term is uniquely associated with the stochastic forcing functions $\xi(t)_1$, $\xi(t)_1$ and $\xi(t)_m$, respectively. The sub-index i denotes the *i-th* single mode involved in the decomposition.

A generalization of (5.40) to the case of output quantities can be made, and the procedure results in a relation of the form

$$E_y^{\infty} = S_{\lambda 1-y} + S_{\lambda 2-y} + \cdots + S_{\lambda n-y}, \tag{5.45}$$

where

$$S_{\lambda i-y} = -\frac{\eta_{ii-y}}{\left(\lambda_i^* + \lambda_i\right)} \tag{5.46}$$

with

$$\eta_{ij-y} = traace\left(\mathbf{F}^T \left(\mathbf{w}_i^T\right)^* \mathbf{v}_i^* \mathbf{C}^T \mathbf{C} \mathbf{v}_j \mathbf{w}_j^T \mathbf{F}\right). \tag{5.47}$$

The difference between expression (5.47) and definition (5.35) lies in the central term $\mathbf{C}^T\mathbf{C}$ that is part of the definition of η_y. Equations (5.45)-(5.47) have a similar interpretation to that provided by (5.42)-(5.44), but these equations are applied to measurement quantities.

5.4 References.

[1] Nolan, D. S., & Farrell, B. F. (1999). The intensification of two-dimensional swirling flows by stochastic asymmetric forcing. *Journal of the atmospheric sciences*, 56(23), 3937-3962.

[2] Farrell, B. F., & Ioannou P. J. (1993). Stochastic forcing of the linearized Navier–Stokes equations. *Physics of Fluids A: Fluid Dynamics (1989-1993)*,5(11), 2600-2609.

[3] Grossman, S. I. (1987). Elementary linear algebra. AMC,10, 12

Chapter 6
Power System Model

A new and flexible approach to performing state-space analysis of multimachine power system dynamics that explicitly accounts for random load behavior is described.

The fundamental feature of the approach is that system dynamic behavior is represented by a set of non-linear stochastic differential algebraic system equations (SDAE). For purposes of clarity and visualization, a classical synchronous machine model is adopted; loads are characterized as a stochastic process and included in the above representation. This model is then used to obtain a linear stochastic state space representation.

Typical instantaneous state variables are given in terms of the state response of the linear SDE power system model and the forcing terms modeling random load changes. Techniques to identify the generation and transmission elements that contribute the most of the observed behavior are developed and methods to characterize modal behavior are proposed.

6.1 Power system DAE model

A large class of physical systems, including the quasistationary dynamics of the large electric power systems can be modeled by a parameter dependent differential-algebraic [1] system of the form:

$$\begin{aligned} \dot{\mathbf{x}} &= f(\mathbf{x},\mathbf{y},\mathbf{u}) \\ 0 &= g(\mathbf{x},\mathbf{y}) \end{aligned} \qquad \mathbf{x}\in\mathbb{R}^{2n} \quad \mathbf{y}\in\mathbb{R}^{p} \quad \mathbf{u}\in\mathbb{R}^{2m} \tag{6.1}$$

In this representation, the dynamic state variables **x** and the instantaneous state variables **y** are assumed to describe a two-scale dynamic process. More precisely, the dynamic variables **x** have their associated dynamics explicitly modeled by *f*, and the dynamics of the instantaneous variables **y** is assumed to be so fast that the constrains g =0 are always satisfied. The variables **u** are parameters which are assumed to have no dynamics in the model (6.1).

This representation extends previous work using single-machine infinite-bus models to the multimachine case.

For the electric power system, typical dynamic state variables are the time dependent values of generator flux-linkages and rotor phases, control states, and load dynamic variables. Typical network instantaneous variables are the load-flow variables, (bus voltages and angles), so that the power balance equations or the load-flow equations typically form the set of constrains $g = 0$ [1] Generator dynamic equations

To introduce the model, assume that each generator is represented by a classical synchronous machine model; it has a constant voltage behind the transient reactance and the differential equations describing the dynamic behavior of the *i*-th generator are given by [1]

$$\dot{\delta}_i = \omega_o\left(\omega_i - \omega_s\right) \quad i=1,\ldots,n \tag{6.2}$$

$$\frac{2H_i}{\omega_s}\dot{\omega}_i = T_{mi} - \frac{E_i V_i \sin(\delta_j - \theta_i)}{X'_{di}} - K_{Di}\left(\omega_i - \omega_s\right), \; i=1,\ldots,n \tag{6.3}$$

In the equations above δ is the angular rotor position in electrical rad, ω is the rotor angle velocity in electrical rad/s, T_m is the mechanical power input in *pu*, X'_{di} is the transient reactance in *pu*, E is the internal voltage machine in *pu*, V denotes the bus voltage where the machine is connected, K_D is the damping coefficient, and n is the total number of generators.

Figure 6.1 shows the structure of the adopted multi-machine model [1].

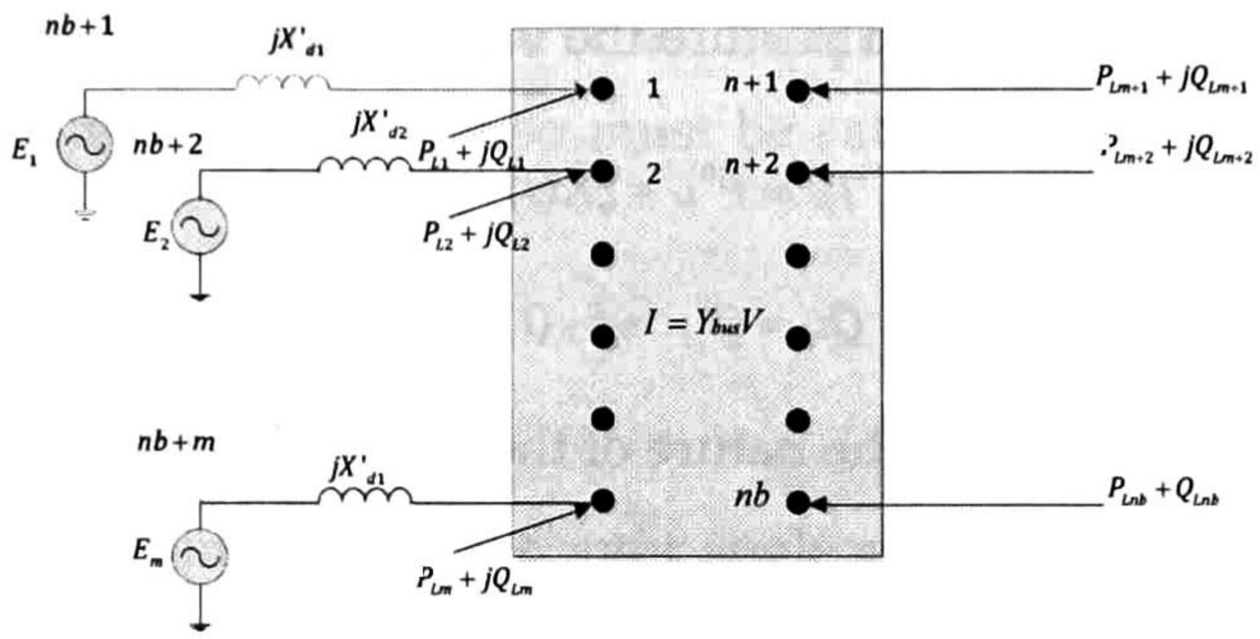

Figure 6.1. Structure-preserving model with constant voltage behind reactance

6.2 Algebraic equations

With reference to Figure 6.1, consider an n-bus transmission network with m generators and nb loads.

For the nodes 1,..,nb the power balance equations can be written as [2],[3]

$$P_{Li} + P_{Gi} = \sum_{k=1}^{nb} V_i V_k Y_{ik} \cos(\theta_i - \theta_k - \alpha_{ik}), \quad i = 1,\ldots,n, \tag{6.4}$$

$$Q_{Li} + Q_{Gi} = \sum_{k=1}^{nb} V_i V_k Y_{ik} \sin(\theta_i - \theta_k - \alpha_{ik}), \quad i = 1,\ldots,n. \tag{6.5}$$

where P_{Gi} and Q_{Gi} are given by the following relations,

$$P_{Gi} = \frac{E_j V_j \sin(\delta_j - \theta_j)}{X'_{dj}}, \; i = 1,\ldots,n \text{ and } P_{Gi} = 0, \; i = n+1,\ldots,nb \tag{6.6}$$

$$Q_{Gi} = \frac{E_i^2}{X'_{dj}} - \frac{E_i V_i \cos(\delta_j - \theta_j)}{X'_{dj}} \quad i = 1,\ldots,m \text{ and } Q_{Gi} = 0,\ i = m+1,\ldots,nb\,. \qquad (6.7)$$

In equations (6.4)-(6.5), Y and α are the magnitude and phase of the elements of $Y_{bus;}$ P_L and P_G are the load and generation active power, and Q_L and Q_G are the reactive components related to demand and generation. It is assumed that each component of active a reactive power can be decomposed in two quantities, one modeled as a constant impedance load and the other one as an independent function of time that perturb the value of the load demand, i.e

$$P_{Li} = P^0{}_{Li} + \xi_{Pi}(t), i = 1,\ldots,nb, \qquad (6.8)$$

$$Q_{Li} = Q^0{}_{Li} + \xi_{Qi}(t), i = 1,\ldots,nb\,. \qquad (6.9)$$

Figure 6.2 illustrates the nature of the adopted model.

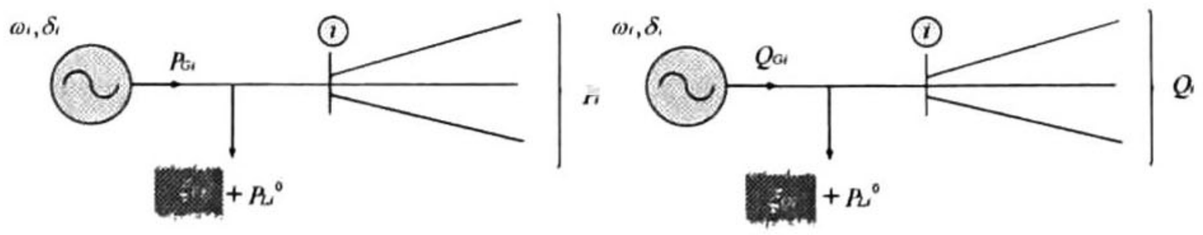

Figure 6.2. Active and reactive power at typical bus i including a classical generator model.

Combining this model with (6.4)-(6.5), the following algebraic equations are obtained

$$P^0{}_{Li} + \xi_{Pi} + P_{Gi} = \sum_{k=1}^{nb} V_i V_k Y_{ik} \cos(\theta_i - \theta_k - \alpha_{ik}),\quad i = 1,\ldots,nb, \qquad (6.10)$$

$$Q^0{}_{Li} + \xi_{Qi} + Q_{Gi} = \sum_{k=1}^{nb} V_i V_k Y_{ik} \sin(\theta_i - \theta_k - \alpha_{ik}),\quad i = 1,\ldots,nb\,. \qquad (6.11)$$

It follows that in (6.10) and (6.11), the elements $P_{Li}{}^0$ and $Q_{Li}{}^0$ can be converted to admittances as, [1]

$$y_{Li} = \frac{-(P_{Li}{}^0 - jQ_{Li}{}^0)}{V_i^2},\ i = 1,\ldots,nb\,. \qquad (6.12)$$

By adding these terms to the diagonal elements of the Y_{bus} matrix, then a modified admittance matrix Y'_{bus} is defined,

$$Y'_{bus} = Y_{bus} + diag[y_{L1} \quad \cdots \quad y_{Lnb}], \tag{6.13}$$

From which it follows that (6.10) and (6.11) can be rewritten as,

$$P^0_{Li} + \xi_{Pi} + P_{Gi} = \sum_{k=1}^{nb} V_i V_k Y'_{ik} \cos(\theta_i - \theta_k - \alpha'_{ik}), \quad i = 1,\ldots,nb, \tag{6.14}$$

$$Q^0_{Li} + \xi_{Qi} + Q_{Gi} = \sum_{k=1}^{nb} V_i V_k Y'_{ik} \sin(\theta_i - \theta_k - \alpha'_{ik}), \quad i = 1,\ldots,nb. \tag{6.15}$$

where Y' and the magnitude and phase of the modified admittance matrix Y'_{bus}. As in (6.4)-(6.5) relations (6.6)-(6.7) also must be satisfied for equations (6.14)-(6.15).

6.3 Power system SDAE model

Let the state vector be composed of the rotor angle and speed deviations, δ and ω as $\mathbf{x}^T=[\delta_1,\ldots,\delta_n\ \omega_1,\ldots,\omega_n]$. Defining $f^T=[f_\delta\ f_\omega]$, according to equation (6.2) the i-th element of the vector f_δ is given by,

$$f_{\delta-i} = \omega_o(\omega_i - \omega_s), \quad i = 1,\ldots,n, \tag{6.16}$$

Using this formulation, and making use of equation (6.3), the *i-th* element of the vector f_ω can be written as,

$$f_{\omega-i} = \frac{\omega_s}{2H_i}\left(T_{mi} - \frac{E_i V_i \sin(\delta_j - \theta_i)}{X'_{di}} - K_{Di}(\omega_i - \omega_s)\right), \quad i = 1,\ldots,m. \tag{6.17}$$

To complete the model, the input vector, is defined by $\mathbf{u}^T=[T_{m1},\ldots,T_{mn}]$.

The instantaneous variables and the constant voltage behind reactance of generators, define the vector $\mathbf{y}^T=[V_1,\ldots,V_{nb+m}\ \theta_1,\ldots,\theta_{nb}]$ where $V_{nb}=E_1,\ldots,V_{nb+m}=E_m$; the nonlinear dynamic model can be written in compact notation as

$$\dot{\mathbf{x}} = f(\mathbf{x},\mathbf{y},\mathbf{u}). \tag{6.18}$$

Now for the constrain equations, if the vector field g is defined as $g^T=[g_P\ g_Q]$, from (6.10) and (6.11), then the i-th element of g_P and g_Q respectively, are written as

$$g_{P-i} = \sum_{k=1}^{nb} V_i V_k Y'_{ik} \cos(\theta_i - \theta_k - \alpha'_{ik}) - \xi_{Pi} - P_{Gi}, \quad i = 1,\ldots,nb, \tag{6.19}$$

$$g_{Q-i} = \sum_{k=1}^{nb} V_i V_k Y_{ik} \sin(\theta_i - \theta_k - \alpha'_{ik}) - \xi_{Qi} - Q_{Gi}, \quad i = 1,\ldots,nb. \tag{6.20}$$

where relations (6.6)-(6.7) must be satisfied.

The independent term $\xi^T=[\xi_P,\xi_Q]$, being $\xi_P{}^T=[\xi_{P\text{-}1},\ldots,\xi_{P\text{-}m}]$ and $\xi_Q{}^T=[\xi_{Q\text{-}1},\ldots,\xi_{Q\text{-}m}]$, explicitly models the effect of random load perturbations in the power system model.

Combining the above equations yields the set of stochastic differential algebraic (SDAE) power system model

$$\begin{aligned} \dot{\mathbf{x}} &= f(\mathbf{x},\mathbf{y},\mathbf{u}) \\ 0 &= g(\mathbf{x},\mathbf{y},\xi) \end{aligned} \qquad \mathbf{x}\in\mathbb{R}^{2n} \quad \mathbf{y}\in\mathbb{R}^{2nb+n} \quad \mathbf{u}\in\mathbb{R}^{n} \quad \xi\in\mathbb{R}^{2nb} \tag{6.21}$$

We now describe a procedure used to find a linear model, which approximate (6.21) in a region near an operating point.

6.4 Power system linear SDE model

Let $\mathbf{x}_0$ to be the initial state vector, $\mathbf{y}_0$ the initial instantaneous variables, $\mathbf{u}_0$ and ξ_0 the input vectors corresponding to the equilibrium point. Use of these assumptions in (6.21) yields,

$$\begin{aligned} \dot{\mathbf{x}}_0 &= f(\mathbf{x}_0,\mathbf{y}_0,\mathbf{u}_0) = 0 \\ 0 &= g(\mathbf{x}_0,\mathbf{y}_0,\xi_0) \end{aligned} \tag{6.22}$$

Letting, $\mathbf{x}_0+\Delta\mathbf{x}$, $\mathbf{y}_0+\Delta\mathbf{y}$,$\mathbf{u}+\Delta\mathbf{u}$, $\xi_0+\Delta\xi$, where the term Δ denotes small deviation, the new states must satisfy,

$$\begin{aligned} \dot{\mathbf{x}}_0 + \Delta\dot{\mathbf{x}} &= f(\mathbf{x}_0 + \Delta\mathbf{x}, \mathbf{y}_0 + \Delta\mathbf{y}, \mathbf{u}_0 + \Delta\mathbf{u}) \\ 0 &= g(\mathbf{x}_0 + \Delta\mathbf{x}, \mathbf{y}_0 + \Delta\mathbf{y}, \xi_0 + \Delta\xi) \end{aligned} \tag{6.23}$$

from which the nonlinear function can be expressed in terms of Taylor's series expansion,

$$\dot{\mathbf{x}}_0 + \Delta\dot{\mathbf{x}} = f(\mathbf{x}_0, \mathbf{y}_0, \mathbf{u}_0) + \frac{\partial f}{\partial \mathbf{x}}\Delta\mathbf{x} + \frac{\partial f}{\partial \mathbf{y}}\Delta\mathbf{y} + \frac{\partial f}{\partial \mathbf{u}}\Delta\mathbf{u}$$
$$0 = g(\mathbf{x}_0, \mathbf{y}_0, \xi_0) + \frac{\partial g}{\partial \mathbf{x}}\Delta\mathbf{x} + \frac{\partial g}{\partial \mathbf{y}}\Delta\mathbf{y} + \frac{\partial g}{\partial \xi}\Delta\xi \qquad (6.24)$$

where second order terms involving powers of $\Delta\mathbf{x}$, $\Delta\mathbf{y}$, $\Delta\mathbf{u}$ and $\Delta\xi$ have been neglected.

From equation (6.22) then expression (6.24) is rewritten as,

$$\Delta\dot{\mathbf{x}} = D_{xf}\Delta\mathbf{x} + D_{yf}\Delta\mathbf{y} + D_{uf}\Delta\mathbf{u} \qquad (6.25)$$

$$0 = D_{xg}\Delta\mathbf{x} + D_{yg}\Delta\mathbf{y} + D_{\xi g}\Delta\xi \qquad (6.26)$$

where

$$D_{xf} = \frac{\partial f}{\partial \mathbf{x}} \in \mathbb{R}^{2n\times 2n} \quad D_{yf} = \frac{\partial f}{\partial \mathbf{y}} \in \mathbb{R}^{2n\times 2ng} \quad D_{uf} = \frac{\partial f}{\partial \mathbf{u}} \in \mathbb{R}^{2n\times m}$$

$$D_{xg} = \frac{\partial g}{\partial \mathbf{x}} \in \mathbb{R}^{2nb\times 2n}, D_{yg} = \frac{\partial g}{\partial \mathbf{y}} \in \mathbb{R}^{2nb\times 2nb} \text{ and } D_{\xi g} = \frac{\partial g}{\partial \xi} \in \mathbb{R}^{2nb\times 2nb}$$

Equation (6.25)-(6.26) represent the DAE linear model of the power system.

Combining expressions (6.25) and (6.26), it is possible to find a reduced linear representation of the form

$$\Delta\dot{\mathbf{x}} = \mathbf{A}\Delta\mathbf{x} + \mathbf{B}_u\Delta\mathbf{u} + \mathbf{B}_\xi\Delta\xi \qquad (6.27)$$

Equation (6.27) can be obtained by solving (6.26) for **y**, and then substitute this result into (6.25). This gives

$$\mathbf{A} = D_{xf} + D_{yf}(D_{yg})^{-1}D_{xg} \in \mathbb{R}^{2n\times 2n}, \mathbf{B}_u = D_{uf} \in \mathbb{R}^{2n\times m} \text{ and } \mathbf{B}_\xi = (D_{yg})^{-1}D_{\xi g} \in \mathbb{R}^{2n\times 2m} \qquad (6.28)$$

Since we are using a classical generator model, in (6.3) the mechanical power input is constant, and then $\mathbf{B}_u = 0$. For this particular case, (6.27) simplifies to

$$\Delta\dot{\mathbf{x}} = \mathbf{A}\Delta\mathbf{x} + \mathbf{B}_\xi\Delta\xi\,, \qquad (6.29)$$

This expression is a first attempt to evaluate the dynamic performance of power systems due the natural variability of load demand.

6.5 Generalized vector of instantaneous variables

Eq. (6.29) represents the linear SDE power system model. Straightforward analysis shows that network variables such as active and reactive power flow, generated power, phase and magnitude of voltages, frequency, which are measures that are constantly monitored to ensure the secure operation of the system can be included in the linear representation.

As an example, let the nonlinear model of the active power flow between nodes m and n be defined as [4]

$$P_{mn} = \mathrm{Re}\{S_{mn}\} = \mathrm{Re}\left\{V_m e^{j\theta_m} I_{mn}^{*}\right\}. \tag{6.30}$$

Figure 6.3 shows and schematic representation of a line transmission model. In terms of the variables of the network. the current I_{mn} can be expressed as

$$I_{mn} = I_l + I_{l0} = y_{mn}(V_m - V_n) + y_{mo}V_m, \tag{6.31}$$

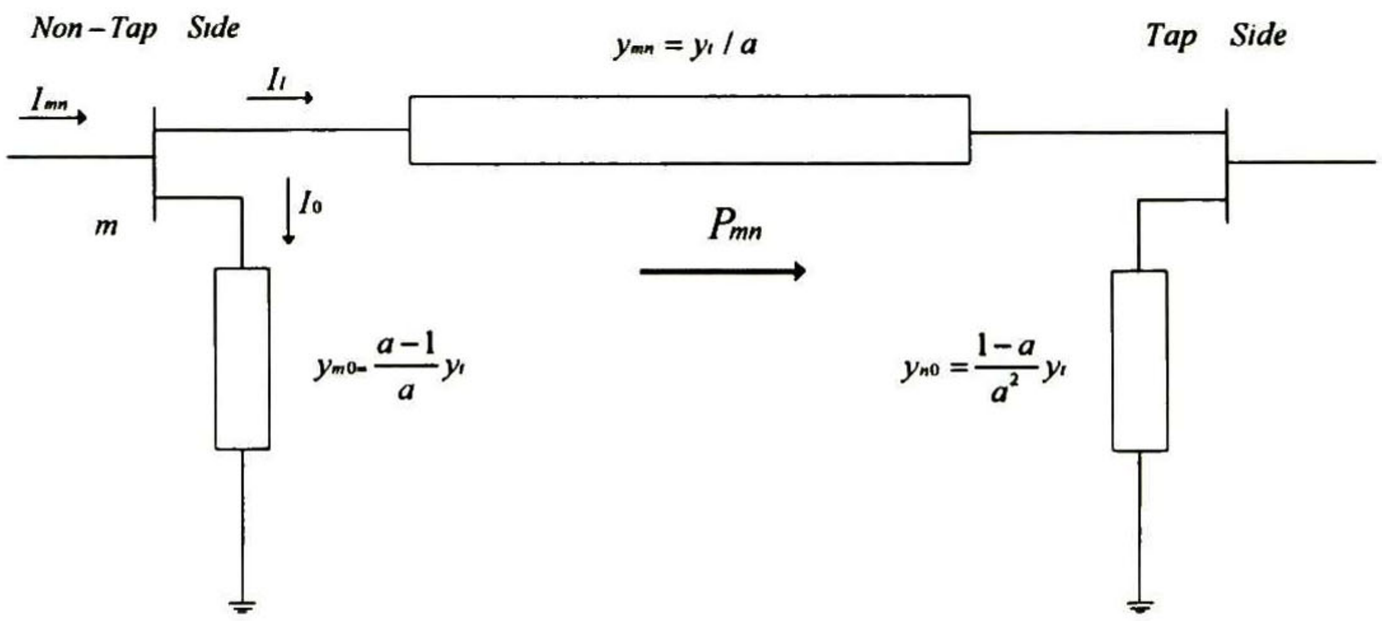

Figure 6.3. Line model used for the computation of the active power flow through a transmission line.

By combining expressions (6.30)-(6.31), P_{mn} turns into,

$$P_{mn}(V_m, V_n, \theta_m, \theta_n) = V_m{}^2 y_{mn}\cos(\alpha_{mn}) + V_m{}^2 y_{mn}\cos(\alpha_0) - V_m V_n \cos(\theta_m - \theta_n). \tag{6.32}$$

As it can be seen, P_{mn} is a non-linear function in terms of the power flow variables V_m, V_n, θ_m and θ_n, which are elements of the vector **y**. So then P_{mn} and many other quantities that can be considered as measures extracted from the grid could be generalized as a **y**-dependent nonlinear function, $h(\mathbf{y})$.

Furthermore, by linearizing $h(\mathbf{y})$ over an operating point, an incremental expression can be found, i.e.,

$$\Delta h = D_{yh} \Delta y \,, \tag{6.33}$$

where D_{yh} is the jacobian of the vector function h with respect to **y**.

Solving (6.26) for $\Delta\mathbf{y}$, results in

$$\Delta\mathbf{y} = (D_{yg})^{-1} D_{xg} \Delta\mathbf{x} + (D_{yg})^{-1} D_{\xi g} \Delta\xi \,. \tag{6.34}$$

If this result is substituted back in (6.33), then a general linear expression for the small signal representation of the functions modeling measured quantities in the grid, is obtained as

$$\Delta h = D_{yh} (D_{yg})^{-1} D_{xg} \Delta\mathbf{x} + D_{yh} (D_{yg})^{-1} D_{\xi g} \Delta\xi \,, \tag{6.35}$$

where depending on the instantaneous variable of interest the value of the matrix D_{yh} will change, while the elements D_{yg}, D_{xg} and $D_{\xi g}$ remain unchanged, e.g., for the magnitude and angle of the bus voltages D_{yh} will be the identity matrix.

For the case of active power flow (6.32), one can show that

$$D_{yh} = \frac{\partial P_{mn}}{\partial \mathbf{y}} \tag{6.36}$$

In order to simplify notation, the prefix Δ on the incremental quantities (e.g., $\Delta\mathbf{x}$, $\Delta\mathbf{y}$, $\Delta\mathbf{u}$ and $\Delta\xi$) will be omitted in subsequent sections.

6.6 References.

[1] Venkatasubramanian, V., Schättler, H., & Zaborszky, J. (1995). Dynamics of large constrained nonlinear systems: a taxonomy theory. Proceedings of the IEEE, 83(11), 1530-1561..

[2] P. W. (1998). Power system dynamics and stability. Prentice Hall.

[3] Kundur, P. (1994). Power system stability and control (Vol. 7). N. J. Balu, & M. G. Lauby (Eds.). New York: McGraw-hill.

[4] Saadat, H. (1999). Power system analysis. WCB/McGraw-Hill.

Chapter 7
Application

This chapter discusses the application of the developed procedures to examine the effect of random load excitation on system behavior.

As a first example, the simplified 189-bus 46-machine model of the Mexican power grid is used to estimate the electromechanical modes of the system under ambient operating conditions. The results obtained from the linear stochastic formulation are compared with those obtained from the application of a measurement-based Blind Source Separation (BSS) technique and linear analysis of the state-space representation of the system.

As a second case, advantages of linear analysis over non-linear analysis are presented based on a simple illustrative example.

The well known, two-area four machine benchmark system is used to verify the ability of the proposed analytic results to predict, in a statistical sense, the effect of the stochastic driving functions on system dynamic behavior.

Finally, a theoretical estimation of the most important forcing functions and a modal energy study for the 189-bus 46-machine model is implemented.

7.1 Outline of the studies

The theory developed in previous sections is applied to the test power systems using a classical representation [1],[2].

The specific objectives of the numerical simulations are:

1. Mode shape computation for dominant modes and comparison between model-based and measurement-based techniques. For this purpose, and by using a realistic test power system model, multiple linear simulations are performed. Blind source separation, a signal processing technique [4], is applied to simulation data (state system response) and the numerical results are compared with the analytic result obtained from the eigenvectors of the state state-response covariance matrix (Chapter 4) .

2. A comparison between linear and non-linear models is performed for a single-machine-infinite-bus representation. In this illustrative example is underlying simplicity that a linear framework gives to the study of power systems operating under ambient conditions.

3. Validate theoretical results used to identify the most important stochastic forcing functions (Chapter 5,sec 5.2). Several simulations are developed, and for each experiment, energy ratios representing the individual effect of certain stochastic forcing function on system behavior are computed. The mean value of these results are compared with the theoretical ratios obtained based on the proposed framework.

4. Extract information of practical interest for power system monitoring from a linear stochastic representation of a test power system. The theory developed for the identification of predominant stochastic forcing functions and the decomposition of the modal energy (Chapter 5, sec. 5.2 and 5.3).are used to describe the characteristics of the power system under ambient operating conditions .

7.2 Mode shape identification

In this section the developed procedures are used to extract the mode shape of 189-bus model of a realistic test power system [3]. For the purpose of this analysis, 1 % a stochastic perturbation of both, active and reactive load is used to excite the system.

Comparisons are provided with other analysis methods.

7.2.1 Small signal analysis of the system

For reference and comparison, linear analysis [2] is used to identify the major characteristics of the inter-area modes of interest. Table 7.1 summarizes the five slowest modes of the system obtained using a conventional small-signal stability program .

Table 7.1. Slowest modes of the system

Inter-Area Mode	*Eigenvalue*	*Frequency (Hz)*	*Damping %*
1	-0.0627 + 2.5106i	0.3996	2.4947
2	-0.0592 + 3.5372i	0.5630	1.6735
3	-0.0627 + 2.5106i	0.7098	1.3868
4	-0.0592 + 3.5372i	0.9164	1.3076
5	-0.0619 + 4.4600i	0.9898	0.9414

The corresponding speed-based mode shapes are displayed in Figure 7.1. For illustrative purposes, the real part is used to indicate the phase angle.

In section 4.2 the state response $\mathbf{x}(t)$ was expressed in terms of their respective POD modes. Associated with each of these modes, a mode shape (spatial pattern) given by the corresponding POM was obtained.

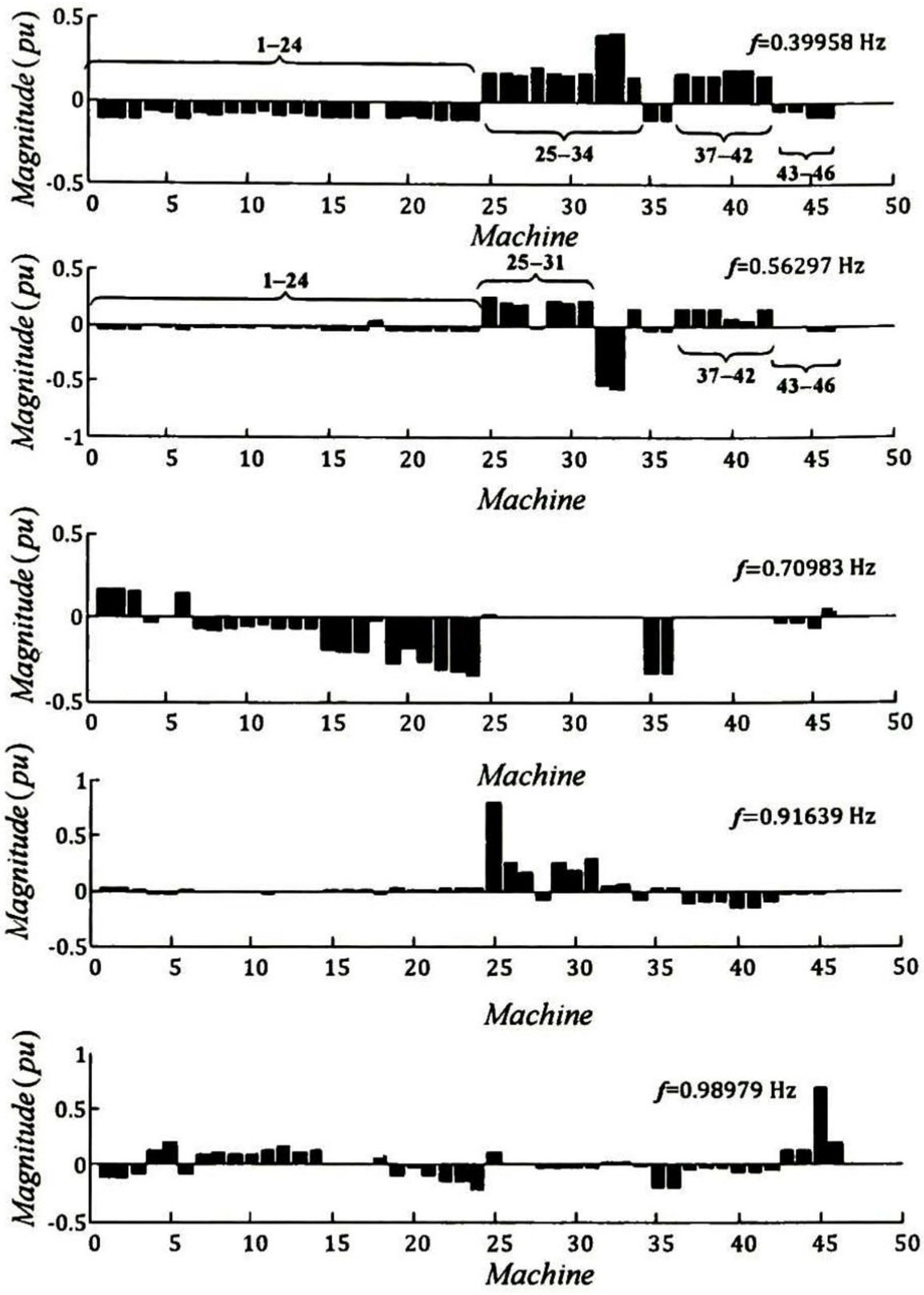

Figure 7.1. Linear mode shape of the 189-bus 46-machine model

To clarify the relationship with the statistical modes, we rewrite $\mathbf{C}_x^{\infty}$ (refer to Appendix C, and Chapter 4) in terms of sub-matrices $\mathbf{C}_{\delta\delta}^{\infty}$ $\mathbf{C}_{\delta\omega}^{\infty}$ $\mathbf{C}_{\omega\delta}^{\infty}$, $\mathbf{C}_{\omega\omega}^{\infty}$ Here,

$$\mathbf{x} = [\omega \quad \delta]^T \tag{7.1}$$

and δ is a vector of relative angles

$$\delta = [\delta_2 - \delta_1 \quad \cdots \quad \delta_n - \delta_1]^T, \tag{7.2}$$

Similarly, the vector of speed machines ω is defined as

$$\omega = [\omega_1 \quad \cdots \quad \omega_n]^T \tag{7.3}$$

Further,

$$\mathbf{C}_x^{\infty} = \begin{bmatrix} \mathbf{C}^{\infty}_{\delta\delta} & \mathbf{C}^{\infty}_{\delta\omega} \\ \mathbf{C}^{\infty}_{\omega\delta} & \mathbf{C}^{\infty}_{\omega\omega} \end{bmatrix}. \tag{7.4}$$

To extract the mode shape corresponding to a set of signals $\{ \omega_1, \omega_2, \ldots \omega_n\}$ constituting the vector ω, a modal analysis of matrix $\mathbf{C}_{\omega\omega}^{\infty}$ (Sec. 4.2) was performed.

Figure 7.2 shows the spectral energy of the POD decomposition of the signals $\{ \omega_1, \omega_2, \ldots \omega_n\}$. As shown in this plot, the first five modes account for about 47.4414% (see Appendix, section C.3) of the total variance (global state-energy). Note worthily, the most important mode accounts for about 14% of the total energy (see Table 7.1).

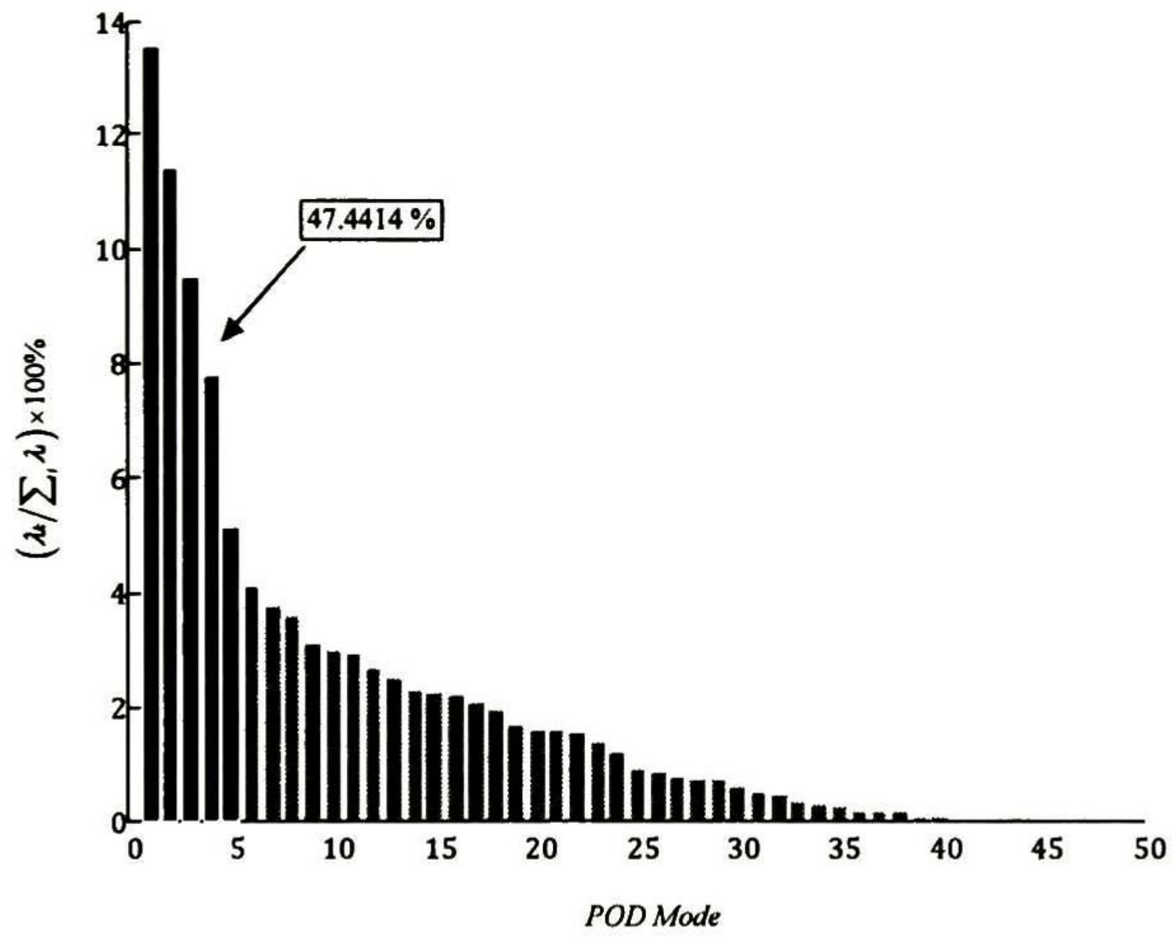

Figure 7.2. Energy captured by the POD modes

Theoretical mode shapes resulting from POD analysis are displayed in Figure 2.1. It is noted that, although, POM 1 and POM 2 have opposite signs, from the eigenvector properties we can see that they are practically the same, i.e., they identify an oscillation between the same groups of machines and they

are most likely associated with the linear mode shapes corresponding to the two slowest modes at 0.39 Hz and 0.56 Hz in Figure 7.1.

Table 7.2. Energy captured by the POD modes (Figure 7.2)

POD MODE	$\lambda_k / \Sigma_i \lambda_i$
1	13.5731 %
2	11.4424 %
3	9.4977 %
4	7.7785 %
5	5.1497 %

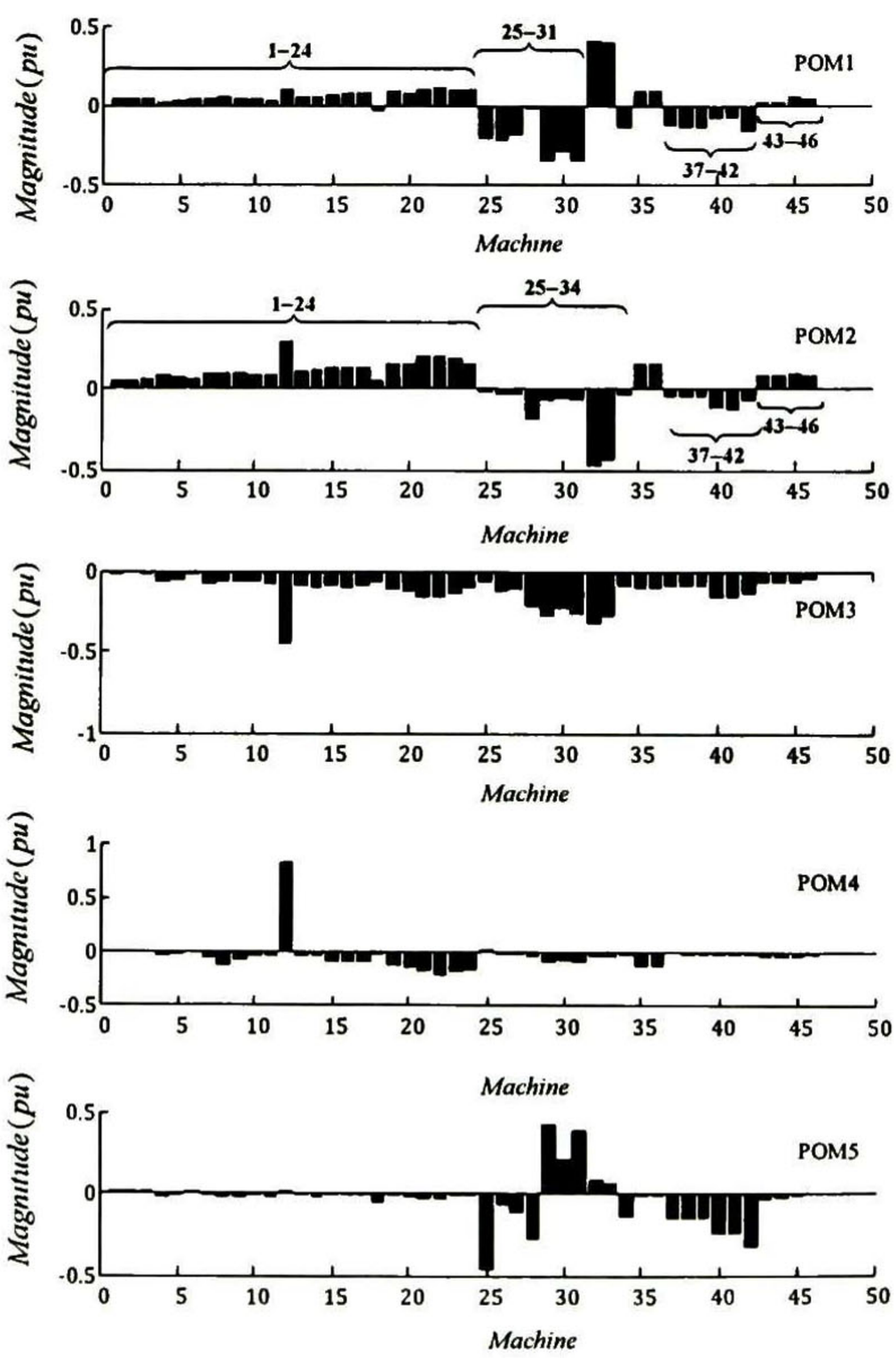

Figure 7.3. Mode shape of the five most important POD modes

Of particular note, in Figure 7.3 POM 1 and POM 2 capture an oscillation involving machines 32 and 33 swinging against machines 25 to 31 in close

agreement with the second slowest linear mode at 0.56297 Hz. in Figure 7.1. Furthermore, coherent machine groups 1-24, 37-42 and 43-46, identified in Figure 7.3, are a common feature observed for the linear modes at f=0.39958 Hz and f=0.56297Hz (see Figure 7.1).

From this graphical description of Figure 7.3, it can be concluded that the linear modes with the highest presence in the system response are the modes at f=0.39958 Hz and f=0.56297Hz. This result will be numerically validated in section 7.5.

In turn, POM 3 can be associated with a mean value different from zero or a tendency of the signals $\{\omega_1, \omega_2, \ldots \omega_n\}$. For practical purposes the other POD modes are neglected.

For validation, a Blind source separation (BSS) method [4], a measurement-based method, is used to extract and identify modal responses and mode shapes from simulation data and the results obtained are compared graphically with the analytic result obtained from POD analysis.

The input data used by BSS is composed of the samples of the speed signals obtained from linear stochastic integration of the linear model defined by expressions (6.29) and (6.35) in Chapter 6. For this numerical procedure, the implicit Euler scheme (see Appendix D) is used to obtain the state response and after that build the data matrix,

$$\Omega = [\Omega_1 \quad \Omega_2 \quad \cdots \quad \Omega_n]. \tag{7.5}$$

where each column of Ω_i ,is an N-dimensional vector of the form

$$\omega_i = [\omega_1(t_1) \quad \omega(t_2) \quad \cdots \quad \omega(t_N)]^T, i = 1,2,...,n. \tag{7.6}$$

For purposes of comparison, the data in Figure 7.4 is presented as it was obtained from the numerical simulations. Keeping this in mind, results Exp-1,2,3,4,5,7,8,9,10 exhibit the same pattern of oscillation as those obtained from POM 1, except Exp-6 that exhibits a different pattern as a result of the stochastic nature of the experiment.

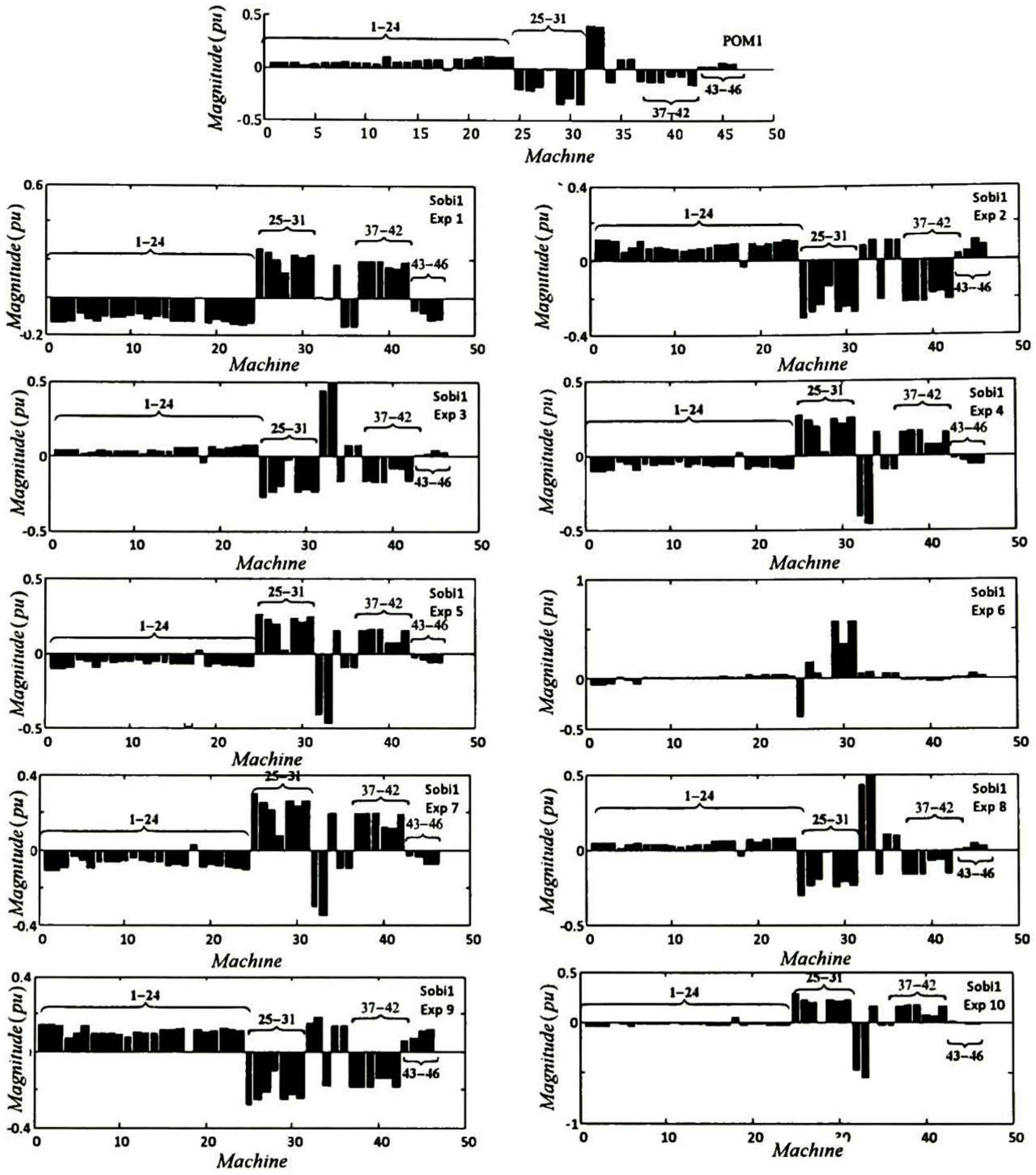

Figure 7.4. Mode shapes comparison between POM1 and Sobi-1 T=100s and $\Delta t=2^{-12}$

For the specific case of mode shapes, a possible application of the results derived in Chapter 5 is that, they could be used to be compared with mode shapes estimated by multi-signal approaches such as those in [6]-[8] when they are applied to real data. This comparison could be used to establish if a spatial distribution of measured units accurately captures the global system behavior predicted from analytic methods.

7.3 Power system response to random load variations

As a second example, a simple case study with a single-machine infinite bus system is used to discuss some basic properties related with the nature of the dynamic behavior of the system following random load perturbations.

In this analysis, the non-linear and linear responses of the system are compared and the practical issues associated with linear stochastic analysis are highlighted.

Since in this thesis stochastic linear and nonlinear models are used (refer to Chapter 6), suitable numerical methods must be used to simulate the solution of the resulting stochastic differential systems. A handful of work have been developed in the area of non-linear stochastic numerical integration for power systems [9]- [11].

In our analysis, the approach introduced in reference [9] by Keyou *et al.*, which deals with the integration of a set of SDAEs, is adopted. In the case of linear SDEs, integration can be performed in a simpler manner by using an implicit Euler scheme [5].

7.3.1 Illustrative example- single machine infinite-bus system

A simple single-machine-infinite-bus (SMIB) power system model is used to gain insight into the response of the system to ambient perturbations. The system data was taken from reference [9]. This system has one generator with a classical representation and one infinite bus with fixed bus voltage magnitude and angle. There are three nodes in this system, a PQ node, a PV node and a slack node for power flow context.

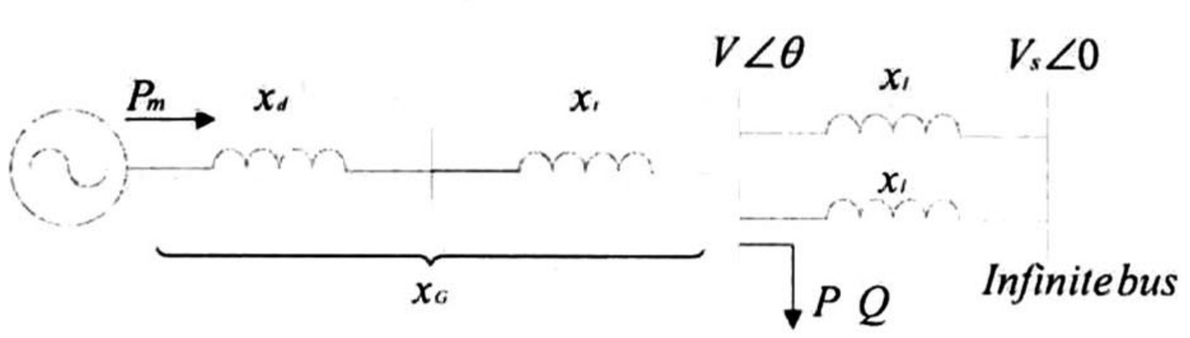

Figure 7.5. Single machine infinite bus system

A single line diagram of the system is shown in Figure 7.5

As it was pointed out earlier, the non-linear behavior of the system can be described by a set of SDAEs as shown in Sec. 6.3, and for the case under study is described in detail in [9]. On the other hand, the linear behavior is described by a set of linear SDEs (see Sec. 6.4).

In general, the models under study in this thesis can adopt the following standard structures:

$$\textit{Non-linear Model} \begin{cases} \dot{x} = f(x,y) \\ 0 = g(x,y) + Q\xi \end{cases} \qquad \textit{Linear Model} \begin{cases} \dot{\mathbf{x}} = \mathbf{A}\mathbf{x} + \mathbf{B}\xi \\ \mathbf{y} = \mathbf{C}\mathbf{x} + \mathbf{D}\xi \end{cases}$$

Although the theory developed in this research was based on linear analysis, under the assumption of small ambient perturbations, it is expected that this theory can be applied to some extent to the non-linear case.

For the power system of Figure 7.5, ambient perturbations were modeled as 0.05 % of random variation of the active and reactive load demand at the PQ node. More precisely, the standard deviation of the stochastic processes ξ_P and ξ_Q was given by λP and λQ , respectively, with $\lambda = 5\times10^{-4}$ P and Q are the corresponding schedules values of active and reactive power demand.

Results from the non-linear and linear simulations of the SMIB-case are displayed in Figure 7.6. It can be observed that, because the relative small value of λ the linear model describes accurately the system response to ambient perturbations, i.e., for the SIMB, linear analysis accurately describes the dynamical behavior of the system under ambient conditions.

For this small size illustrative example more important than accuracy of the linear and non-linear responses is the interpretation of these responses and the flexibility gained from linear framework.

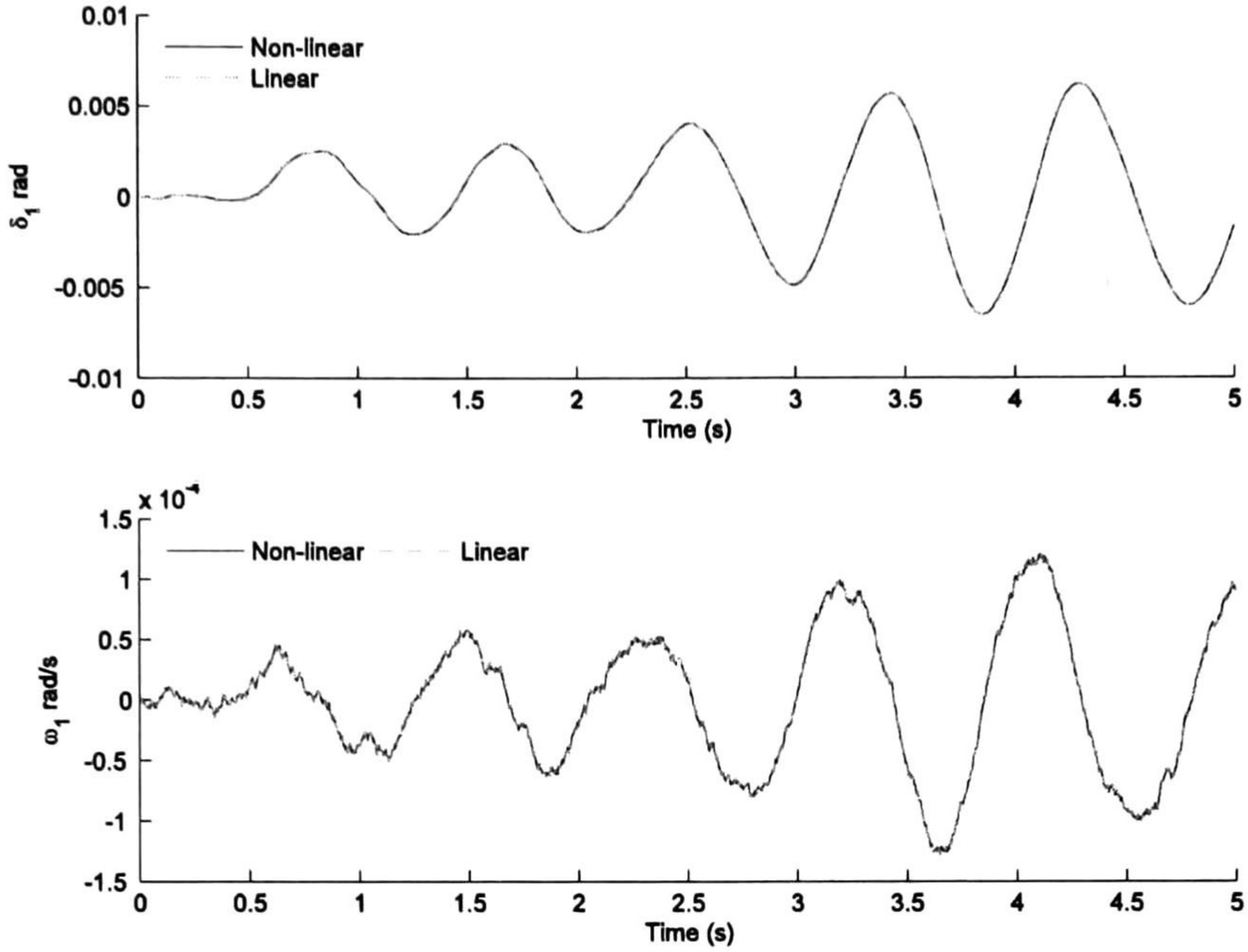

Figure 7.6. Generator state response Δt=0.001s. T=5 s.

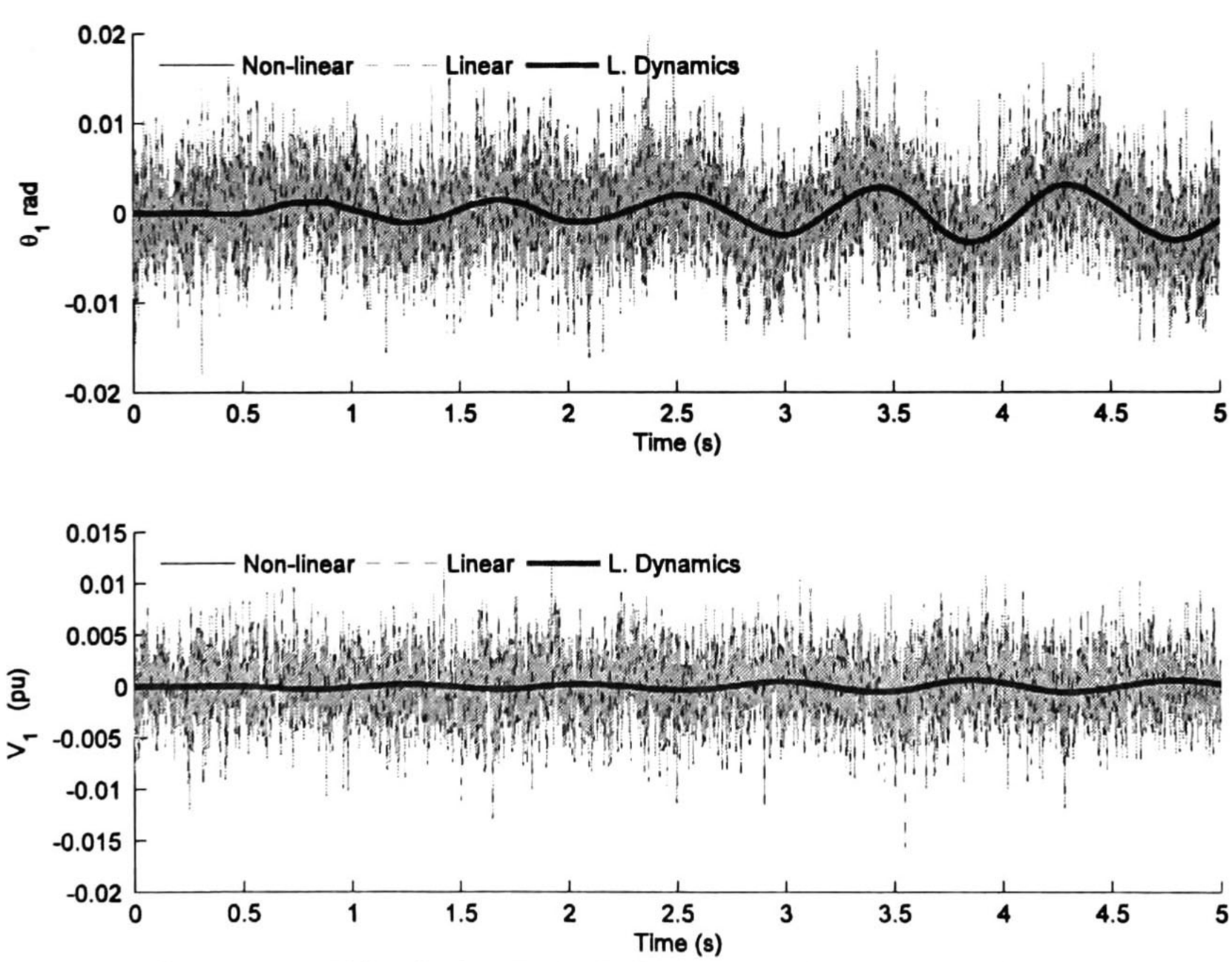

Figure 7.7. PQ algebraic variables Δt=0.001s. T=5 s.

As emphasized in previous research [9], the algebraic variables (θ and V) behave as very fast variables. The deviations caused by random load chances ξ propagate into the algebraic variables almost instantaneously. Figure 7.7 displays the dynamic behavior of the magnitude (V) and angle (θ) at the load node.

In sharp contrast, the speed variables (speed and angle of the generators) behave as relatively slow variables. This fact is easily seen in Figure 7.6 where the time evolution of the dynamical states (δ and ω) is shown.

As discussed in previous sections, linear analysis allows the decomposition of the algebraic quantities in terms of state-dependent and input-dependent components, i.e,

$$\mathbf{y} = \underbrace{\mathbf{Cx}}_{\substack{State-dependent \\ Response}} + \underbrace{\mathbf{D}\xi}_{\substack{Input-dependent \\ Response}} \tag{7.7}$$

The corresponding term of $\mathbf{Cx}$ is shown in solid line in Figure 7.7. As seen in this plot, this state-dependent component captures the oscillatory behavior inherent to the dynamic characteristics of system. Therefore, basic information such as linear mode presence can be obtained from it. By contrast, the term $\mathbf{D}\xi$ accounts for the noisy behavior of switching loads and it provides the fast behavior observed in the time evolution of the algebraic variables.

7.4 Two-area, four generator system

The power system used in this case of study is the two-area four-generator system in [2]. Operating conditions and system parameters are given in [2] for the classical system representation.

A single line diagram of the system is shown in Figure 7.8. The test system consists of two areas interconnected through a radial transmission system. Each area has two generators. For P_4 and P_{14} the active load is modeled as in section 6.2. Thus, the corresponding portion of load used for modeling stochastic

ambient variations is a zero-mean white noise process with a standard deviation given by 1% of the corresponding nominal active power demand at node 4 and 14 respectively.

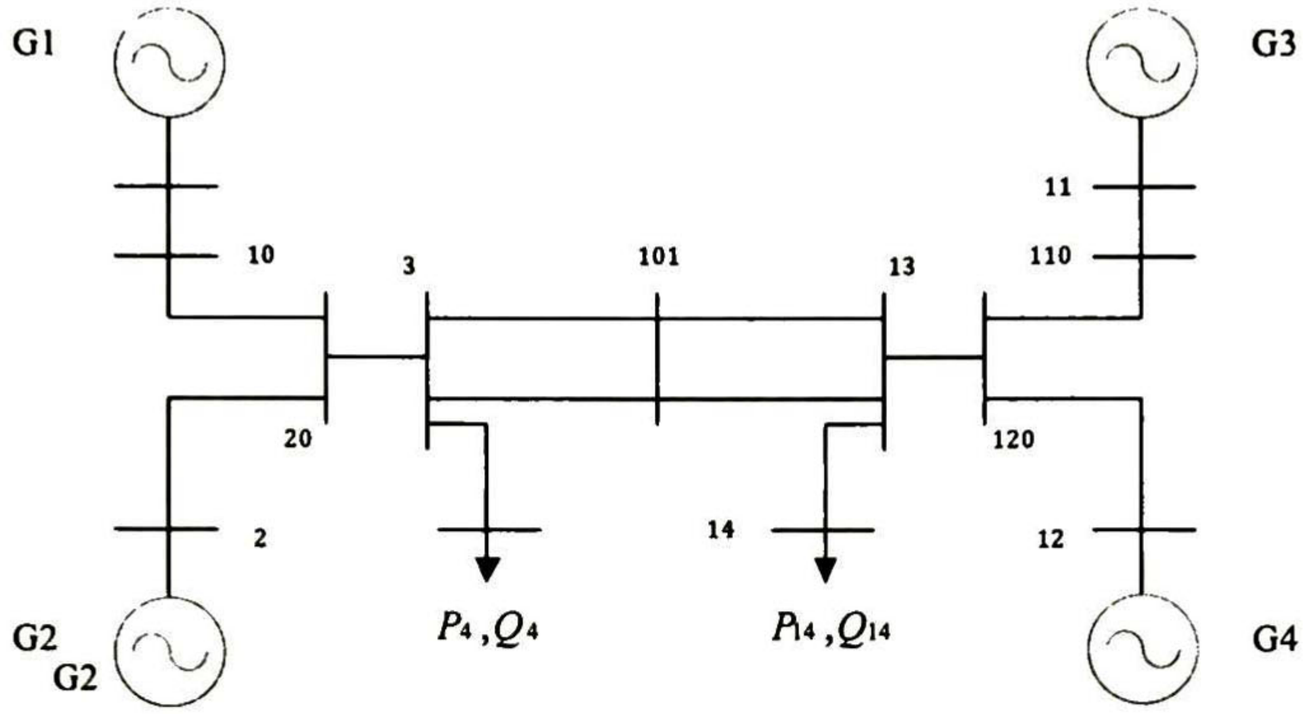

Figure 7.8. Single line diagram of two-area test system

The reactive load power Q_4 and Q_{14} also have a stochastic time-dependent fraction of load representing ambient variations, this reactive power is modeled as a zero-mean white noise with standard deviation given by 1% of the corresponding nominal reactive power demand at nodes 4 and 14.

7.4.1 Problem Description

For this particular case of study, four different stochastic forcing functions are used to drive the system dynamics; these functions are denoted as ξ_{P4}– ξ_{Q4} and ξ_{P14}– ξ_{Q14}. The numerical sub-index denotes the location of the perturbations (see Figure 7.8).

From previous theory the state ensemble average energy can be decomposed as

$$E^{\infty}{}_{x} = S_{x1} + S_{x2} + S_{x3} + S_{x4} \,. \tag{7.8}$$

Two different y-output variables are of interest in this example: the power flow variables (V_i and θ_i) and the set of active power flows through transmis-

sion lines between all the possible pairwise combinations of buses i and j,(P_{ij}). It follows that the energy associated to the power flow variables $E^{\infty}{}_{y\text{-}V\theta}$ can be decomposed as:

$$E^{\infty}{}_{y-V\theta} = S_{1y-V\theta} + S_{2y-V\theta} + S_{3y-V\theta} + S_{4y-V\theta}\,. \tag{7.9}$$

Similarly, for $E^{\infty}{}_{y\text{-}Pij}$

$$E^{\infty}{}_{y-Pij} = S_{1y-Pij} + S_{2y-Pij} + S_{3y-Pij} + S_{4y-Pij}\,. \tag{7.10}$$

Instead of directly calculating the values of the coefficients on the *rhs* of the energy expressions, this example focuses on the fraction of the ensemble average energy E^{∞} uniquely associated to random variations of load at nodes 4 and 14 respectively.

For $E^{\infty}{}_{x}$ define the ratios:

$$R_{4x} = \frac{S_{x1} + S_{x3}}{S_{x1} + S_{x2} + S_{x3} + S_{x4}} \text{ and } R_{14x} = \frac{S_{x2} + S_{x4}}{S_{x1} + S_{x2} + S_{x3} + S_{x4}}, \tag{7.11}$$

that represent the theoretical mean value of these portions of energy.

For $E^{\infty}{}_{y\text{-}V\theta}$, the portions of energy associated with the forcing functions ξ_{P4}- ξ_{Q4} and ξ_{P14}- ξ_{Q14}, given by

$$R_{14y-V\theta} = \frac{S_{y1-V\theta} + S_{y3-V\theta}}{S_{y1-V\theta} + S_{y2-V\theta} + S_{y3-V\theta} + S_{y4-V\theta}} \text{ and } R_{14y} = \frac{S_{y2-V\theta} + S_{y4-V\theta}}{S_{y1-V\theta} + S_{y2-V\theta} + S_{y3-V\theta} + S_{y4-V\theta}}\,. \tag{7.12}$$

respectively.

Similarly, for the ensemble average energy $E^{\infty}{}_{y\text{-}Pij}$, we can write

$$R_{14y-Pij} = \frac{S_{y1-Pij} + S_{y3-Pij}}{S_{y1-Pij} + S_{y2-Pij} + S_{y3-Pij} + S_{y4-Pij}} \text{ and } R_{14y-Pij} = \frac{S_{y2-Pij} + S_{y4-Pij}}{S_{y1-Pij} + S_{y2-Pij} + S_{y3-Pij} + S_{y4-Pij}}, \tag{7.13}$$

where coefficients S_{x1}-S_{x4} and S_{y1}-S_{y4} are as defined in Chapter4.

The theoretical numerical values of R_{4x}-r_{14x}, $R_{4y\text{-}V\theta}$-$r_{14y\text{-}V\theta}$ and $R_{4y\text{-}Pij}$-$R_{14y\text{-}Pij}$ are displayed in Table 7.3

Table 7.3. Theoretical ratios

Ratios	*Values*
R_{4x}	0.3033
R_{14x}	0.6967
$R_{4y\text{-}V\theta}$	0.3053
$R_{14y\text{-}V\theta}$	0.6947
$R_{4y\text{-}Pij}$	0.3229
$R_{14y\text{-}Pij}$	0.6771

7.4.2 Numerical procedure and results

An extensive number of numerical simulations (N_t) have been performed to assess results R_{4x}-R_{14x}, $R_{4y\text{-}V\theta}$-$R_{14y\text{-}V\theta}$ and $R_{4y\text{-}Pij}$-$R_{14y\text{-}Pij}$ in Table 7.1 Based on the principle of superposition for linear systems, three different groups of simulations were conducted

1) Computation of the energy E_T of the power system under statistically steady state conditions when the system was driven by the full-set of forcing functions $\{\xi_{P1},\xi_{P2},\xi_{Q1},\xi_{Q2}\}$. For demonstrative purposes, comparative results from one single linear and non-linear simulation are shown in Figure 7.9 through Figure 7.11

2) Similar to the previous case but now considering that the system was perturbed by $\{\xi_{P4}\ \xi_{Q4}\}$; the energy computed in that case in denoted as E_4.

3) Similarly, when the system was forced by $\{\xi_{P14}\ \xi_{Q14}\}$; the energy computed in this case is denoted as E_{14}.

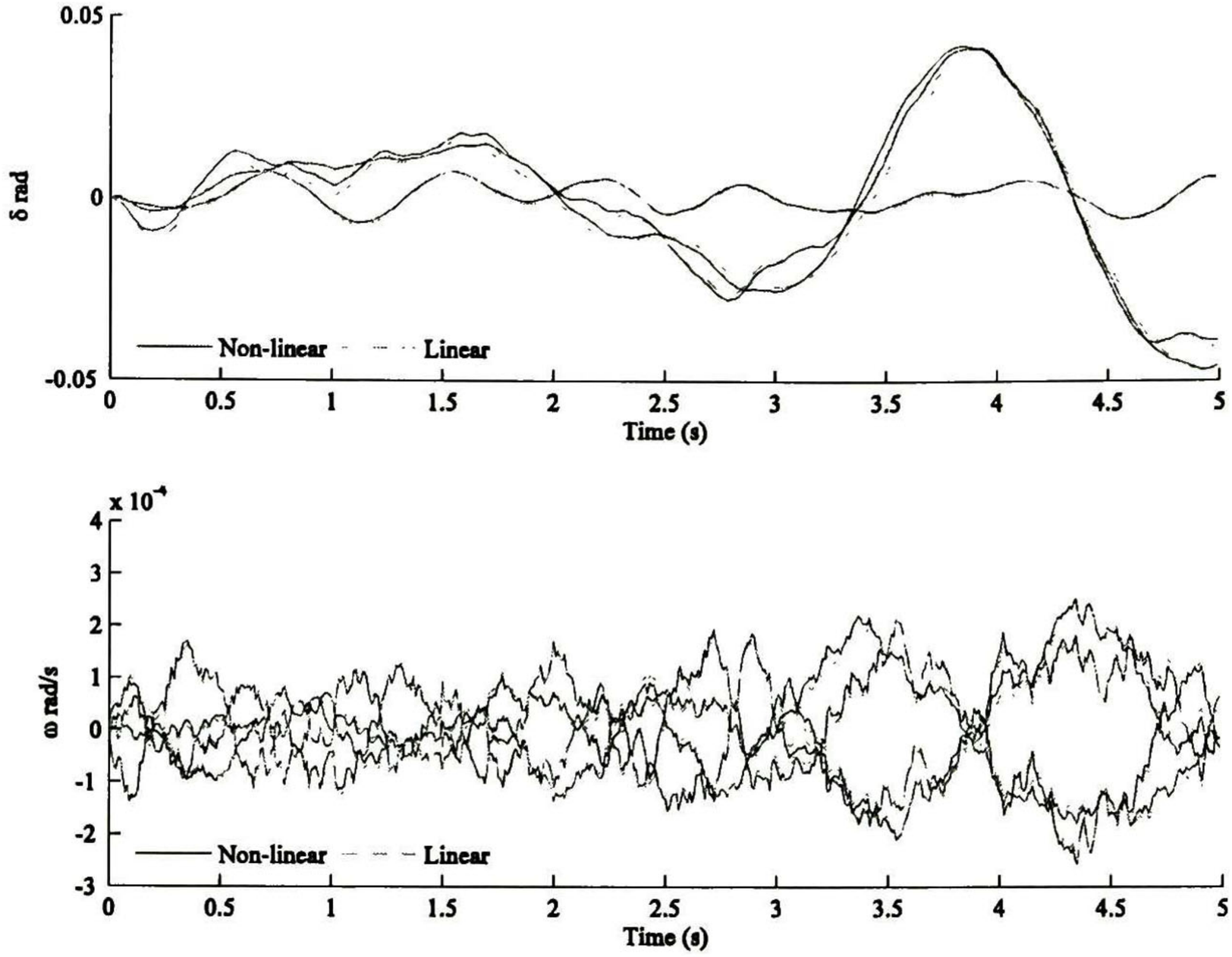

Figure 7.9. State Response of the two-area test system Δt=0.01s. T=5 s.

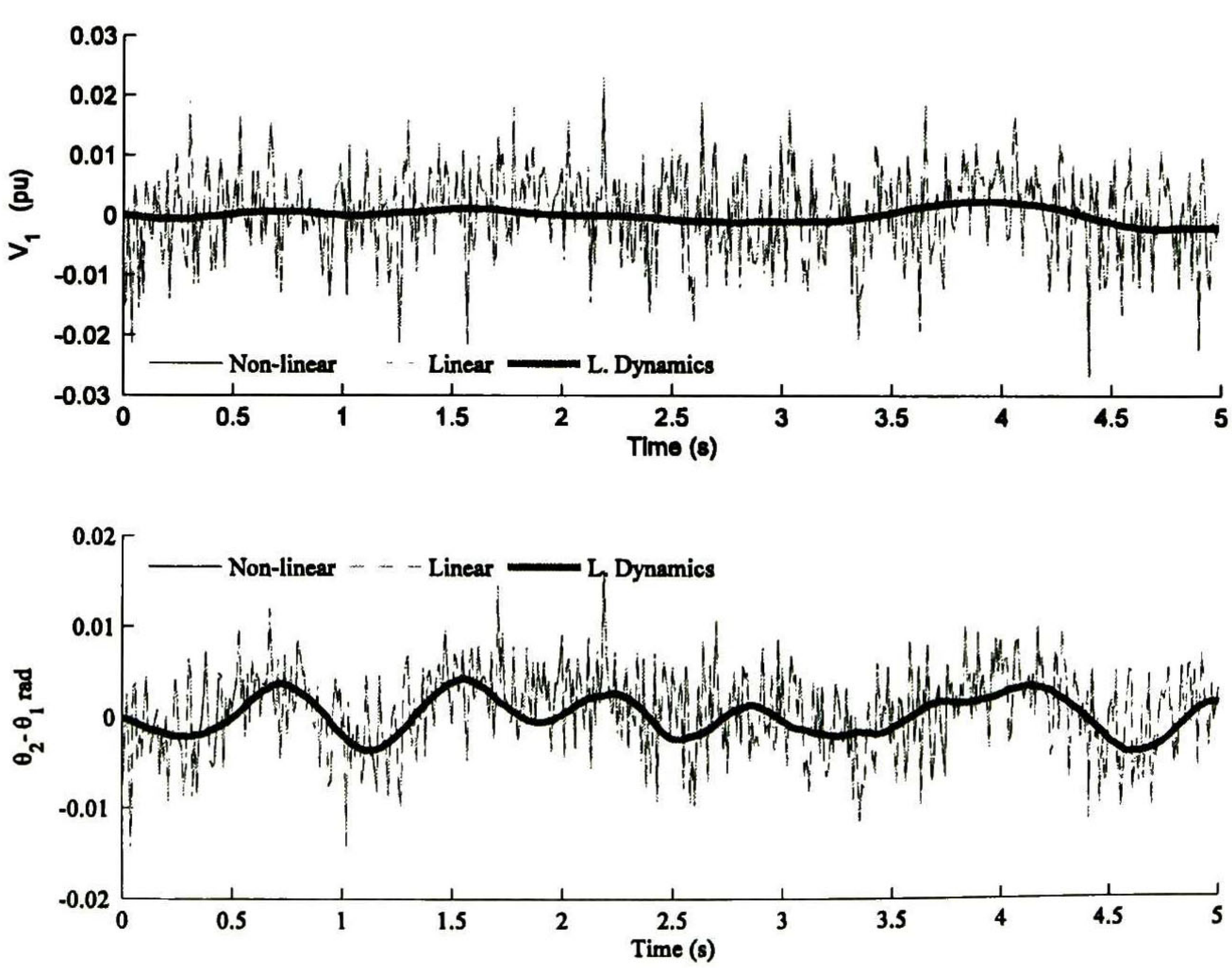

Figure 7.10. Illustrative power flow variables of the two-area test system Δt=0.01s. T=5 s.

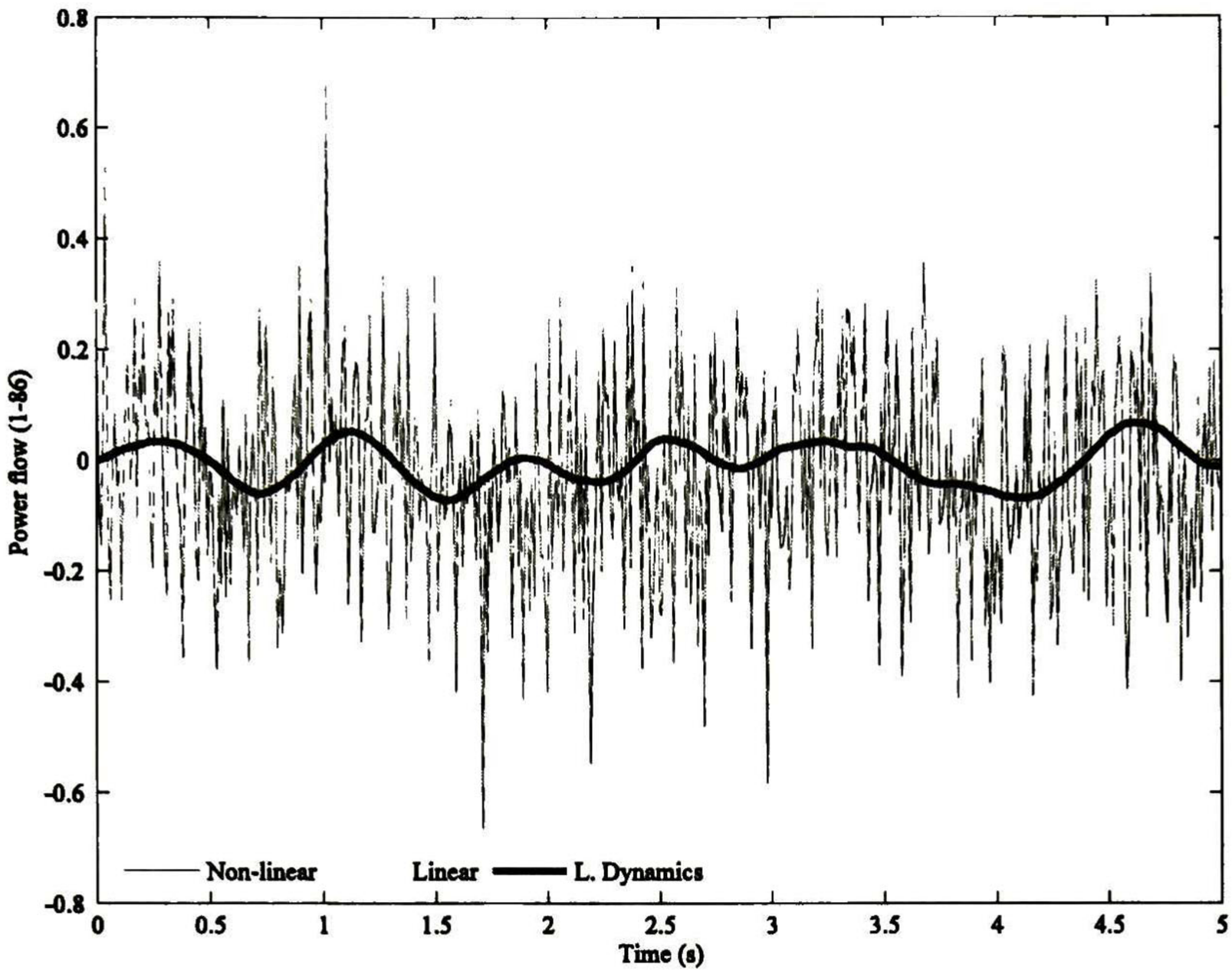

Figure 7.11. Ilustrative active power flow of the two-area test system Δt=0.01s. T=5 s.

Results E_T^k, E_4^k and E_{14}^k obtained from the *k-th* numerical simulation are used to estimate the ratios $R_4^k = E_4^k/E_T^k$ and $R_{14}^k = E_{14}^k/ E_T^k$ for each of the k=1,2,...,N_t. simulations performed. Thus, the statistical sample mean and variance of these N_t. results are used to validate results, R_{4x}-R_{14x} , $R_{4y\text{-}V\theta}$-$R_{14y\text{-}V\theta}$ and $R_{4y\text{-}Pij}$ -$R_{14y\text{-}Pij}$.

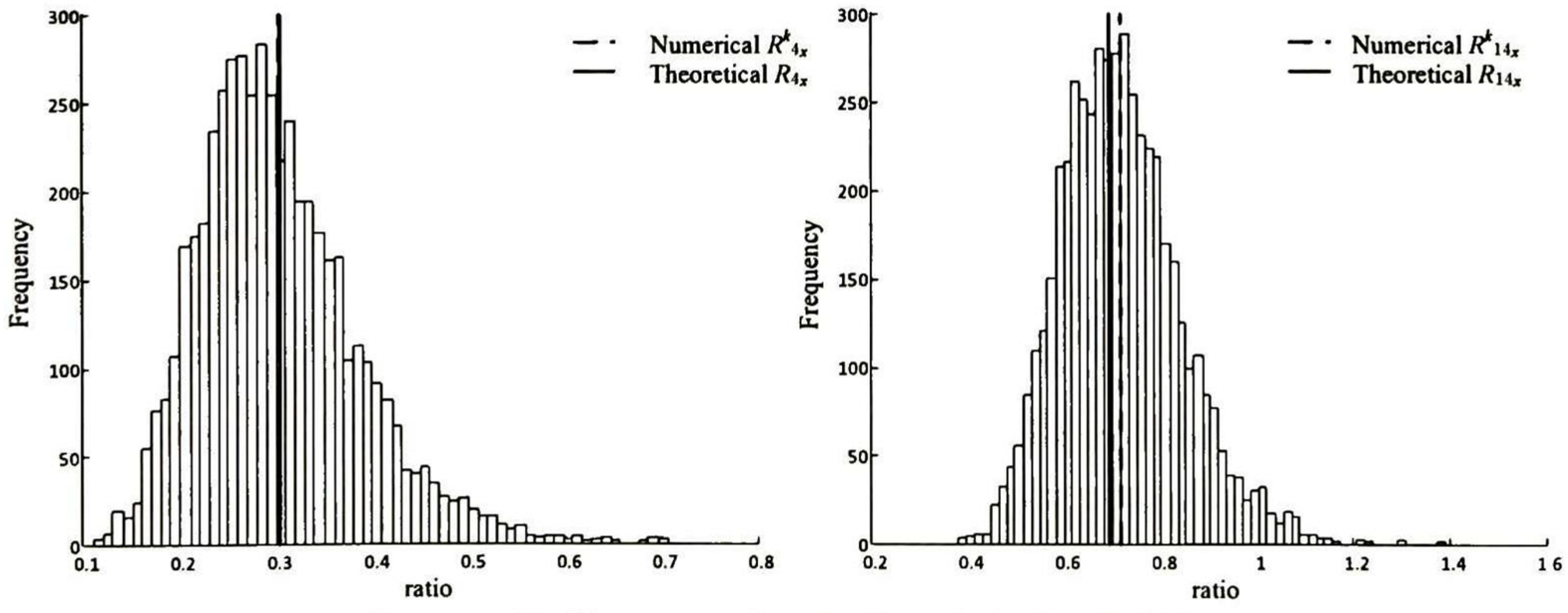

Figure 7.12. Energy ratios R_{4x}-R_{14x} Δt=0.01s T=300 s.

Data collected from simulations is graphically displayed as histograms in Figure 7.14, Figure 7.13 and Figure 7.12. The mean and standard deviation of the estimated ratios R^k_{4x}-R^k_{14x} , $R^k_{4y\text{-}V\theta}$-$R^k_{14y\text{-}\ V\theta}$ and $R^k_{4y\text{-}Pij}$ -$R^k_{14y\text{-}\ Pij}$ for k=1,2,…,N_t have been included.

Figure 7.12 shows the distribution of ratios R^k_{4x}-R^k_{14x} (k=1,2,…,N_t) respectively; the data was obtained from N_t =5000 simulations. As can be seen in this Figure, the peak of data is near to the theoretical results R_{4x}-R_{14x} (Table 7.3) and the data spread from 0.2 to 0.4 for R^k_{4x} and from 0.5-0.9 for R^k_{14x} . Moreover, the mean value of data is close to the theoretical values R_{4x}-R_{14x}.

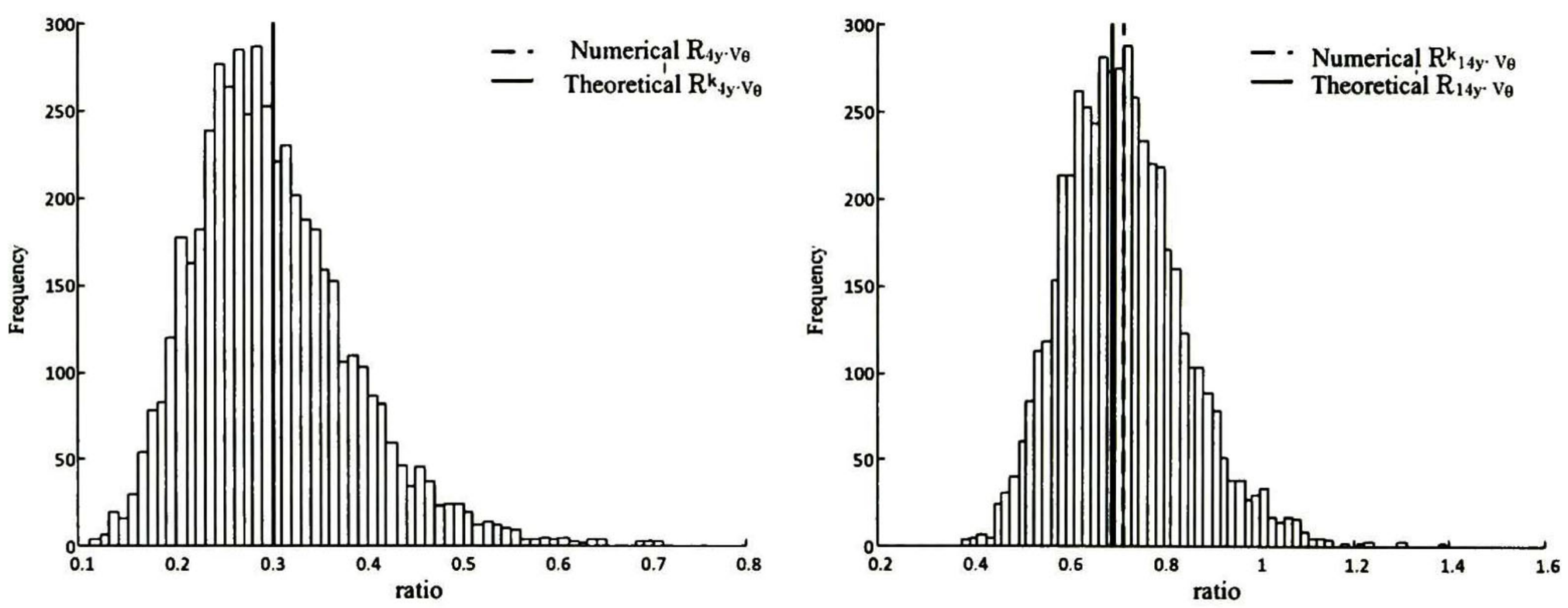

Figure 7.13. Energy ratios $R_{4y\text{-}V\theta}$-$R_{14y\text{-}\ V\theta}$ Δt=0.01s T=300 s.

Similar results are obtained for the ratios $R^k_{4y\text{-}V\theta}$-$R^k_{14y\text{-}\ V\theta}$ (k=1,2,…,N_t) where data is symmetrically distributed around the theoretical results $R_{4y\text{-}V\theta}$-$R_{14y\text{-}\ V\theta}$, see Figure 7.13

In Figure 7.14 is observed an important difference between the mean value of of the numerical ($R^k_{4y\text{-}Pij}$, $R^k_{14y\text{-}\ Pij}$ k=1,2,…,N_t) and the theoretical ($R_{4y\text{-}Pij}$, $R_{14y\text{-}\ Pij.}$) ratios however for both cases the data is distributed around the theoretical ratios.

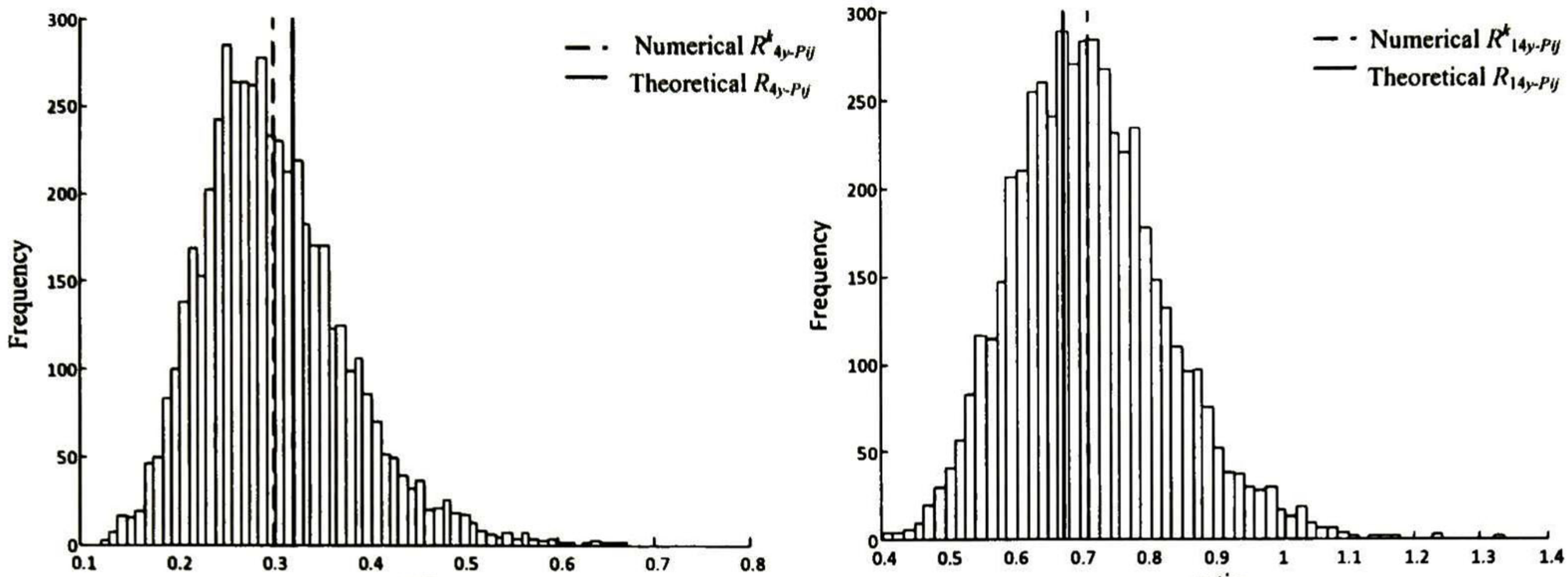

Figure 7.14. Energy ratios $R_{4y\text{-}Pij}$ - $R_{14y\text{-}Pij}$ Δt=0.01s T=300 s.

Table 7.4. Statistics of numerical results 5000 Experiments Δt=0.01

	Theoretical ratio	*mean*	*variance*	*Standard deviation*
R_{4x}	0.3033	0.3024	0.0067	0.0820
R_{14x}	0.6967	0.7184	0.0156	0.1250
$R_{4y\text{-}V\theta}$	0.3053	0.3039	0.0068	0.0827
$R_{14y\text{-}V\theta}$	0.6947	0.7171	0.0158	0.1257
$R_{4y\text{-}Pij}$	0.3229	0.3024	0.0056	0.0748
$R_{14y\text{-}Pij}$	0.6771	0.3024	0.0129	0.1136

More research about the convergence of numerical results to the theoretical ones needs to be performed, e.g., further analytic research about the probability density function describing the energy ratios R_x and R_y would be of vital importance to accurately measure the effect of stochastic small-load variations in the power system dynamical response.

However, for practical purposes, results presented in this example demonstrate that theory developed for the identification of predominant stochastic forcing functions converge to the expected value of all the possible ratios

R_x and R_y; thus, the stochastic optimals procedure can be used in a more realistic power system model to gain insight into the effect of load perturbations to the dynamic behavior of the system.

7.5 Application to a 46-Machine, 189-bus test system

A more realistic power system model is analyzed in this case of study. Details of the system characteristics and base case condition are given in [3]. For this example, it is assumed that stochastic ambient variations of load are modeled as white noise processes whit a standard deviation given by 1% of the corresponding nominal active and reactive power demand. There exist 91 loads spread all over the grid, and 46 classical model generators.

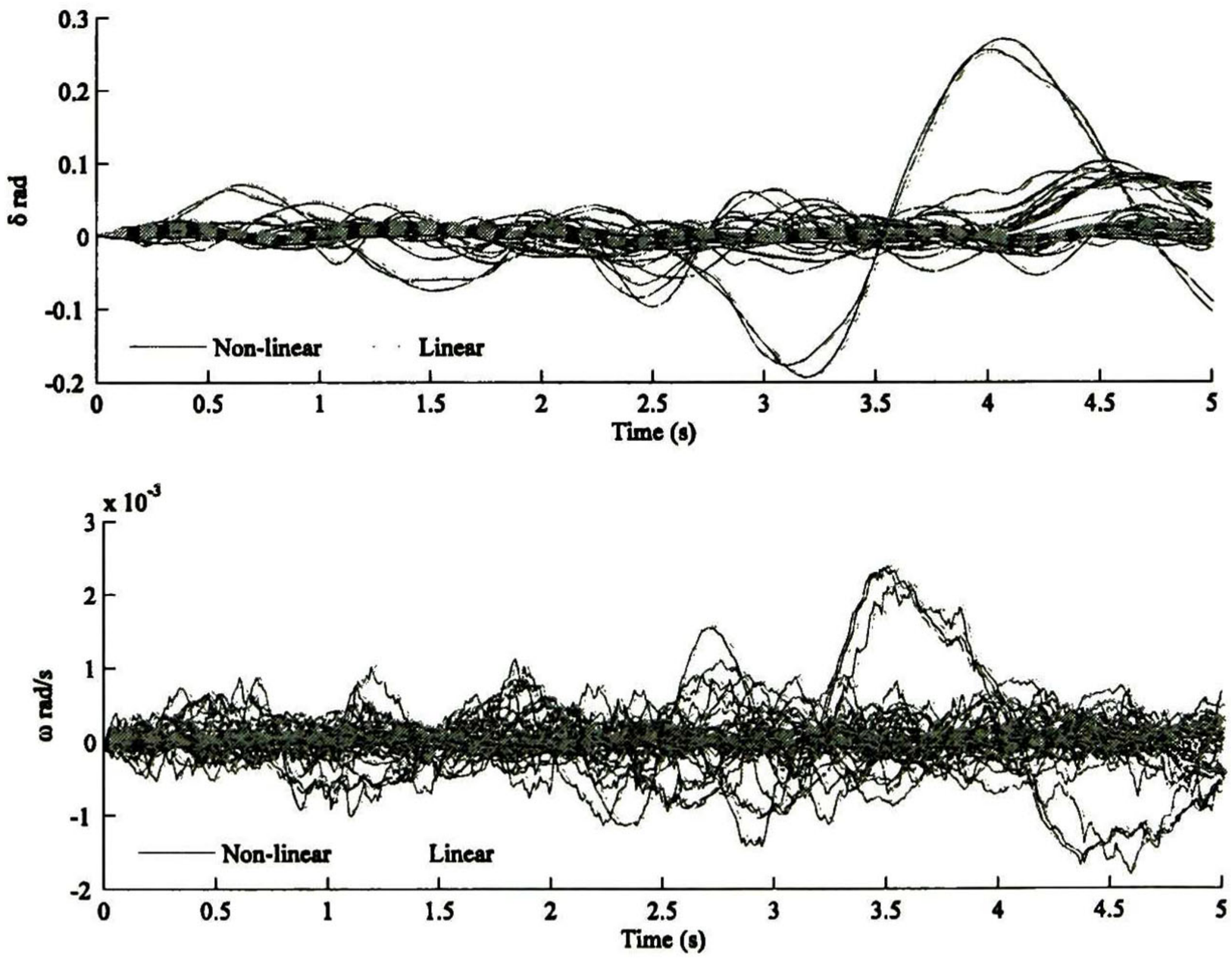

Figure 7.15 . State response of the 46-machine 189-bus test system Δt=0.01s. T=5 s.

For illustrative purposes, Figure 7.15 gives the complete system state response to the stochastic excitation already described. Furthermore, some illustrative algebraic variables (V ,θ and P_{ij}) are also displayed in Figure 7.16 and Figure 7.17 ; the corresponding modal content of these responses is shown in

solid line in each of the cases. As can be seen in these figures, for small-amplitude noise excitation the linear model accurately described the power system dynamic behavior.

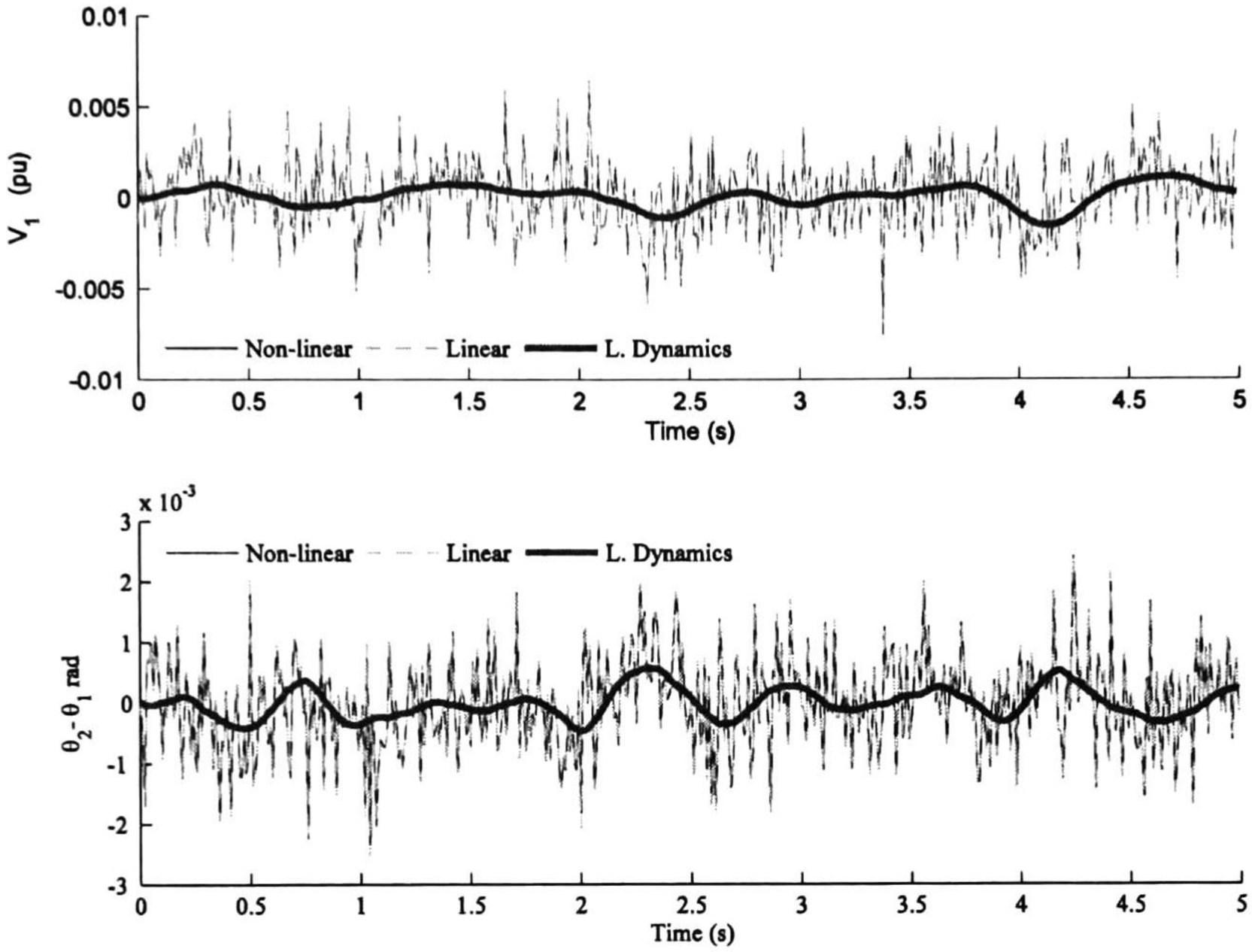

Figure 7.16 . Illustrative power flow variables of the 46-machine 189-bus test system Δt=0.01s. T=5 s.

With the aim of make a compact representation of data, loads have been labeled according to its appearance in a standard bus data matrix used in power flow studies, e.g., P_1 has been associated to the active power load at the node 47 and its respective part modeling stochastically forced variations has been denoted as $\xi_{P-1}(t)$ and so on.

Figure 7.18 shows the spatial pattern of the active and reactive nominal load at different busses. Table 7.6 displays the eleven most important loads with their corresponding labels and the associated physical node to which they are connected.

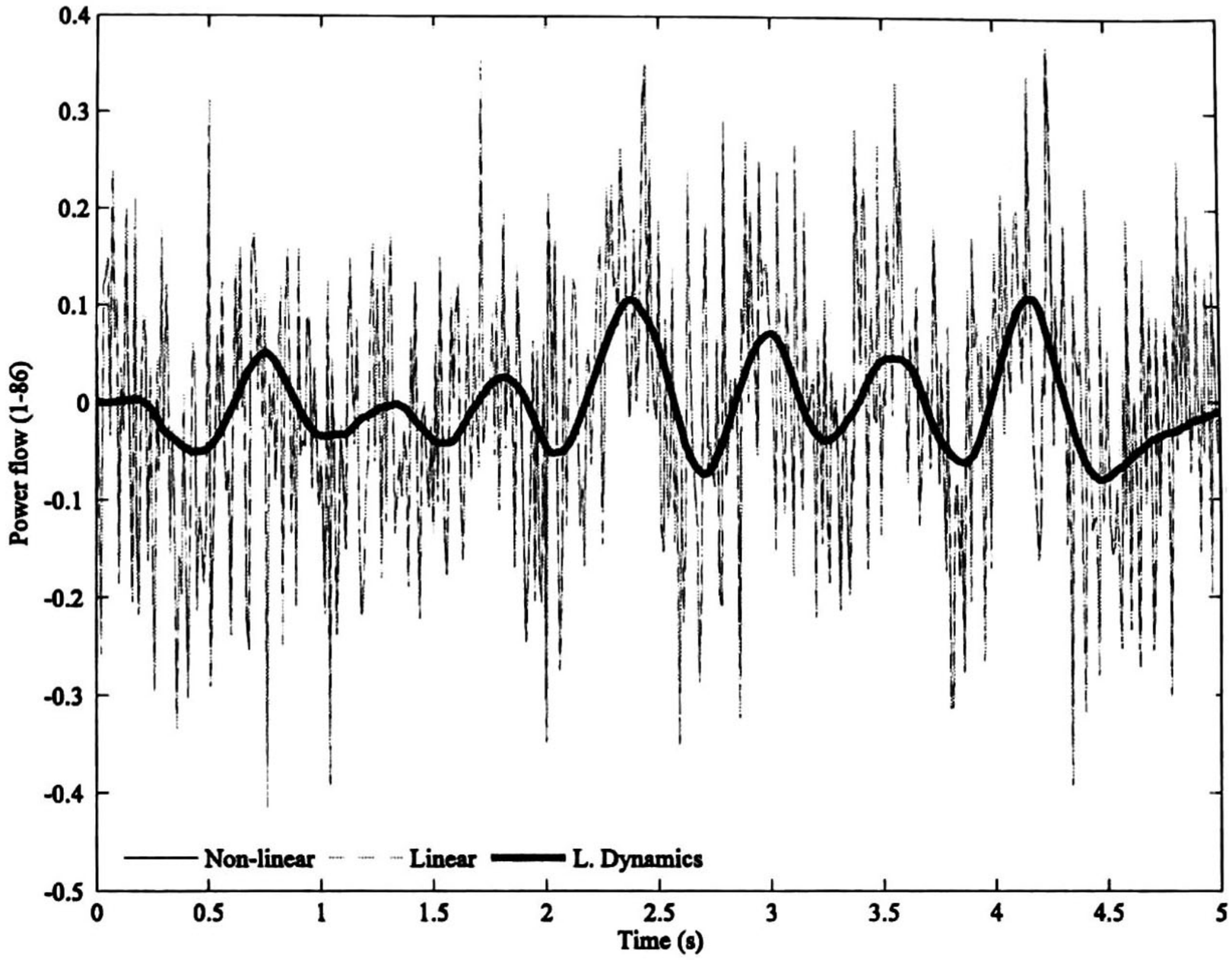

Figure 7.17 . Illustrative active power flow of the 46-machine 189-bus test system Δt=0.01s. T=5 s.

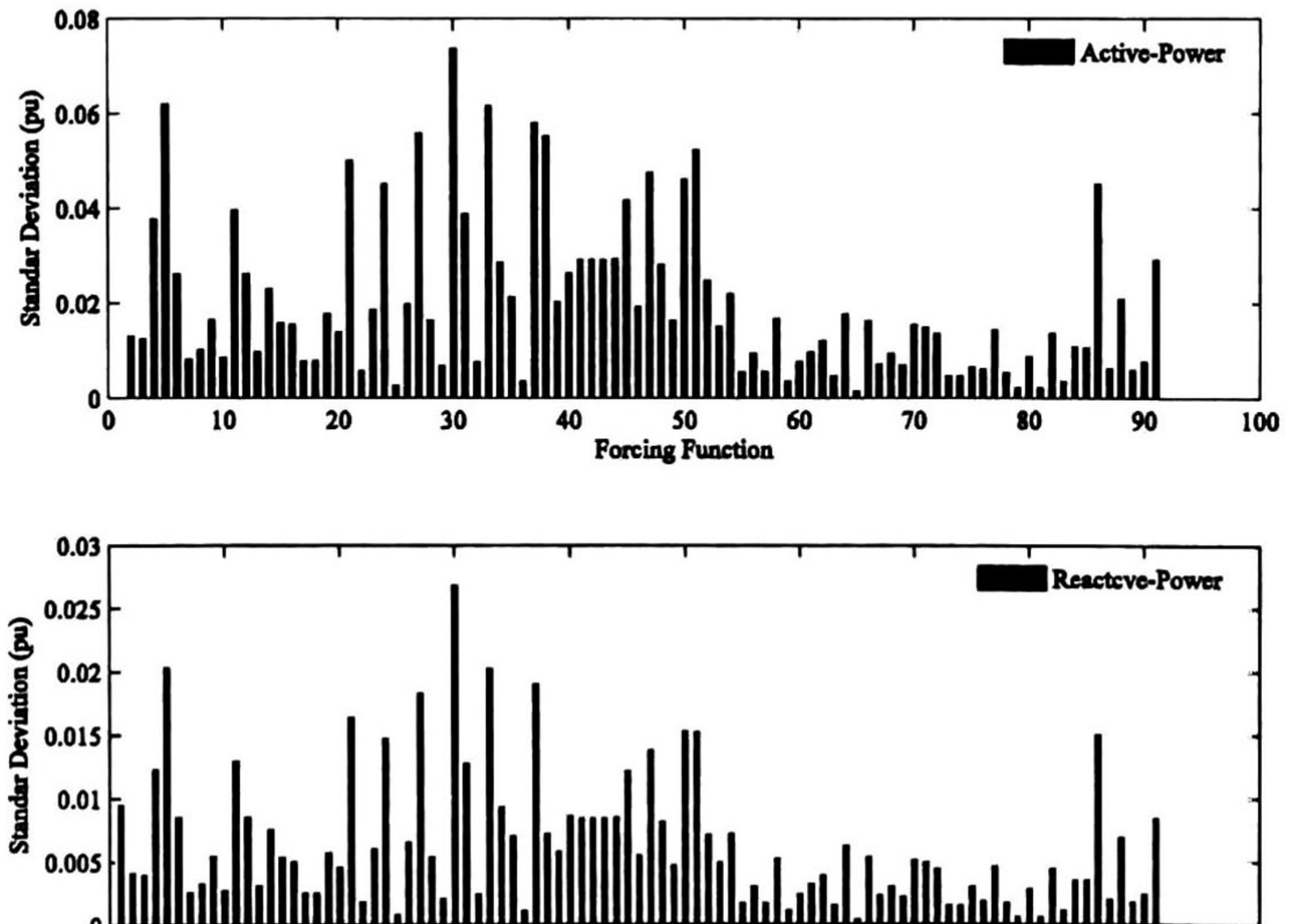

Figure 7.18 Intensity level of the stochastic forcing functions

Furthermore, in order to know the spatial distributions **f**, that allow the highest growth of perturbation, the power system under study is excited by a set of forc-

ing functions { $\xi^{*}_{P\text{-}1},\ldots,_{P\text{-}91}$, $\xi^{*}_{Q\text{-}1}$,...., $\xi^{*}_{Q\text{-}91}$}, which has the property of being composed by white noise processes whit the same intensity (Homogeneous excitation). Results are displayed in Figure 7.19 and Table 7.6

Table 7.5. Largest load demand values (Figure 7.18)

Ranking	*Load Label*	**Physical Node*	λP(pu)
1	30	96	0.0741
2	5	51	0.0624
3	33	103	0.062
4	37	109	0.0584
5	27	93	0.0562
6	38	111	0.0556
7	51	131	0.0527
8	21	83	0.0504
9	47	125	0.0480
10	50	129	0.0465
11	**86	180	0.0455

*Bus data
** Predominant Stochastic Forcing function

Ranking	*Load Label*	**Physical Node*	λQ(pu)
1	30	96	0.0270
2	5	51	0.0205
3	33	103	0.0204
4	37	109	0.0192
5	27	93	0.0185
6	21	83	0.0166
7	50	129	0.0155
8	51	131	0.0154
9	**86	180	0.0152
10	24	87	0.0149
11	47	125	0.0140

*Bus data
** Predominant Stochastic Forcing function

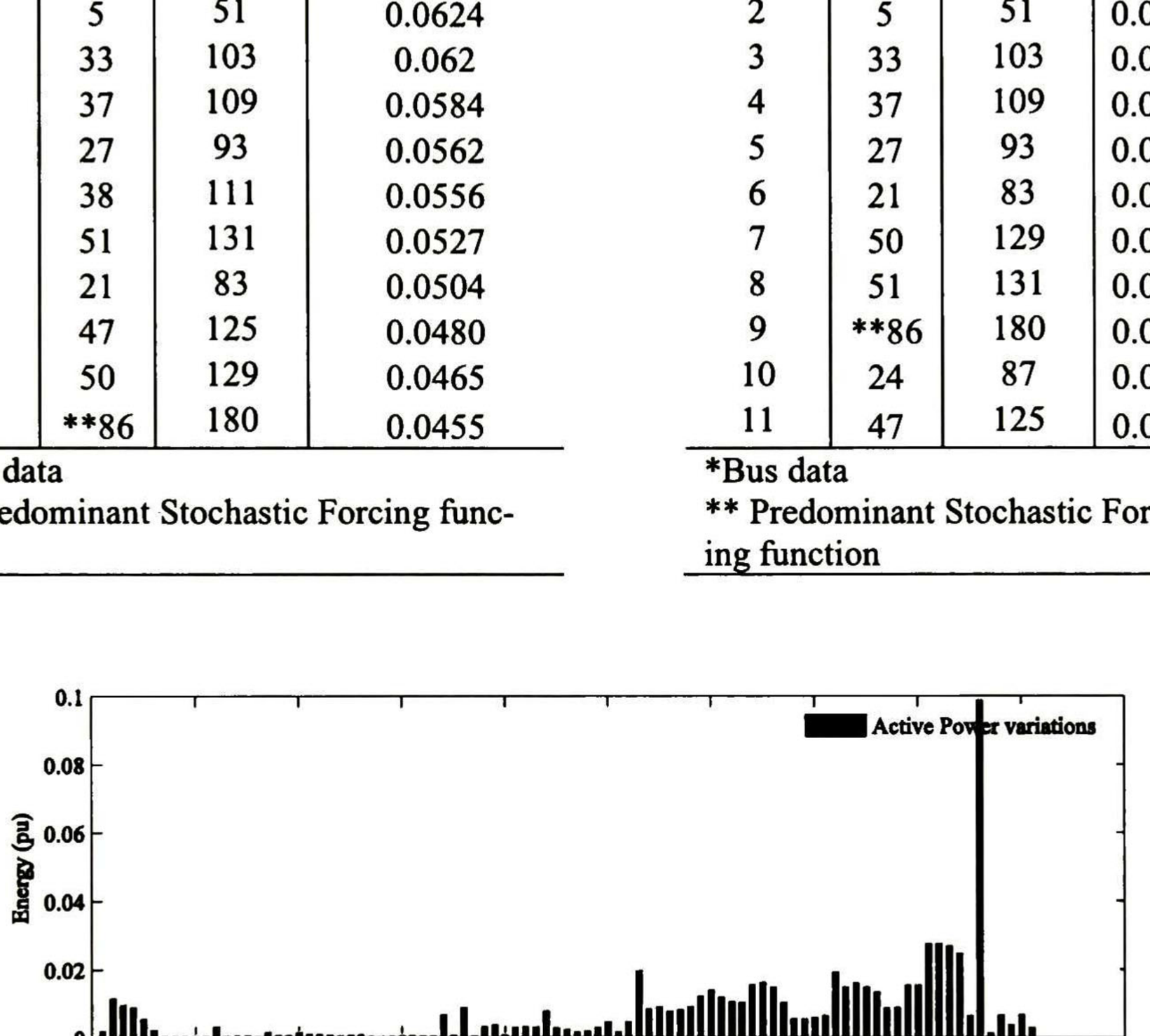

Figure 7.19 Effect of spatial distribution of the stochastic forcing functions on energy distribution

Figure 7.19 suggest that $\mathbf{f}_{P\text{-}86}$ and $\mathbf{f}_{Q\text{-}86}$ for $\xi_{P\text{-}86}$ and $\xi_{Q\text{-}86}$ respectively, have the large components in direction of the most important stochastic optimals see section 5.2); therefore, changes of load at this node, have a major impact on system dynamic behavior.

Table 7.6. Most important stochastic forcing functions (Homogeneous excitation). Figure 7.19

Position	ξ^*_P	**Physical Node*	*Energy*(pu)
1	86	180	0.0991
2	81	174	0.0279
3	82	175	0.0278
4	83	176	0.027
5	84	178	0.0249
6	53	135	0.0198
7	72	162	0.0195
8	65	151	0.0166
9	74	164	0.0164
10	64	150	0.0158

Position	ξ^*_Q	**Physical Node*	*Energy*(pu)
1	86	180	0.0239
2	53	135	0.0108
3	66	152	0.0077
4	84	178	0.0075
5	61	147	0.0074
6	83	176	0.0072
7	67	153	0.007
8	63	149	0.007
9	82	175	0.007
10	64	150	0.0069

Derived from the study previously presented, it is observed that perturbations associated with active power variations have a higher impact on system dynamic response than the reactive components. In turn, Table 7.6 shows that the energy associated with $\xi_{P\text{-}86}$ is almost 2.4 higher than the energy impulse by $\xi_{Q\text{-}86}$. Furthermore, functions labeled by 53-86 drive most of the state response energy.

7.5.1 Predominant stochastic forcing functions

The combined effect of size and spatial distribution of load perturbations is assessed in this section; these two properties have been computed separately in the previous subsection. The distribution of the state response energy according to the functions driving the system is displayed in Figure 7.20.

As a result of the characteristics of vectors $\mathbf{f}_{P\text{-}86}$ and $\mathbf{f}_{Q\text{-}86}$ (see Figure 7.20), It can be observed that the forcing functions associated with $\xi_{P\text{-}86}$- $\xi_{Q\text{-}86}$ impulse

account for 50% of the total energy. Figure 7.21 shows a histogram that groups data from 100 linear simulations; here, R_{86} represents the theoretical ratio of the energy that is driving by $\xi_{P\text{-}86}$- $\xi_{Q\text{-}86}$, and therefore, these results are concentrated near to $R_{86} = 0.5060$.

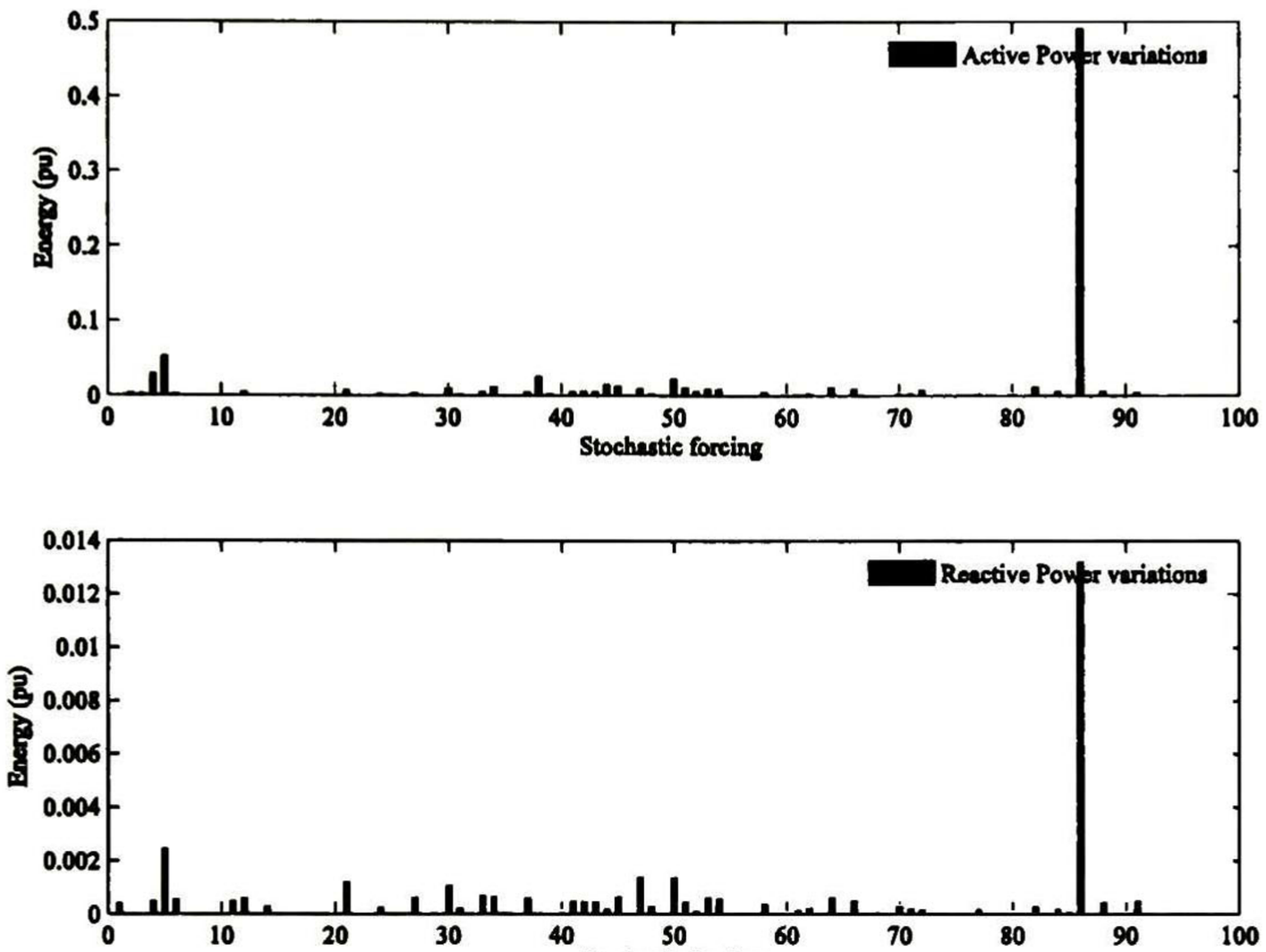

Figure 7.20 Combined effect of intensity level and spatial distribution of the stochastic forcing functions on energy distribution

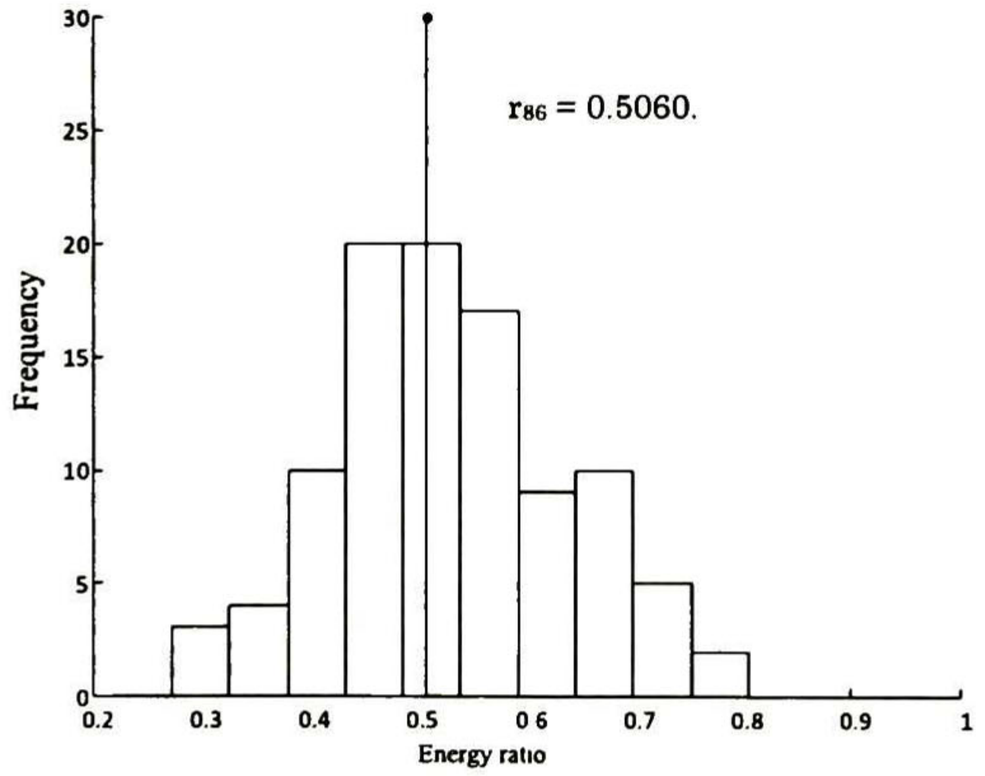

Figure 7.21 Numerical assessment of the energy forced by $\xi_{P\text{-}86}-\xi_{Q\text{-}86}$ Δt=0.01s. T=300 s.

In Figure 7.19 it is observed that according to their location, $\xi_{P\text{-}86}(t)$-$\xi_{Q\text{-}86}(t)$, are the most important active and reactive forcing functions respectively, although they are not the functions with the highest intensity (see Figure 7.18-

Furthermore, in order to know the spatial distributions **f**, that allow the highest growth of perturbation, the power system under study is excited by a set of forcing functions $\{ \xi^*_{P\text{-}1,\ldots,P\text{-}91}, \xi^*_{Q\text{-}1}, \ldots, \xi^*_{Q\text{-}91}\}$, which has the property of being composed by white noise processes whit the same intensity (Homogeneous excitation). Results are displayed in Figure 7.19 and Table 7.6

Table 7.5), their particular spatial distributions $\mathbf{f}_{P\text{-}86}$ and $\mathbf{f}_{Q\text{-}86}$ allow them to significantly impulse the dynamical state response of the model under study.

Table 7.7. Most important stochastic forcing functions (Figure 7.20)

Position	ξ_P	**Physical Node*	*Energy*(pu)
1	86	180	0.4927
2	5	51	0.0544
3	4	50	0.0319
4	38	111	0.0269
5	50	129	0.0247
6	44	120	0.0171
7	34	105	0.0143
8	45	122	0.0137
9	82	175	0.0131
10	51	131	0.0125

Position	ξ_Q	**Physical Node*	*Energy*(pu)
1	86	180	0.0133
2	5	51	0.0025
3	47	125	0.0015
4	50	129	0.0014
5	21	83	0.0013
6	30	96	0.0011
7	33	103	0.0008
8	34	105	0.0007
9	45	122	0.0007
10	27	93	0.0007

According to the results presented in this section, critical stochastic forcing functions can be found.

7.5.2 Modal components of energy (global perspective)

In section 5.3 a methodology was proposed to decompose the ensemble average energy of the state and output responses in terms of modal components.

In the following, this methodology was implemented to determine the dominant modes of the ambient response of the 189-bus, 46-machine test system, when 1 % of stochastic perturbation of both, active and reactive load is used to excite the system.

Based on expression (5.7) (see Chapter 5), Figure 7.22 shows the modal components of energy as a function of the mode frequencies. There, it is observed that the three slowest linear modes at f=0.3996 Hz, f=0.5630 Hz and f=0.7098 Hz, captures 83.92 % of the system energy.

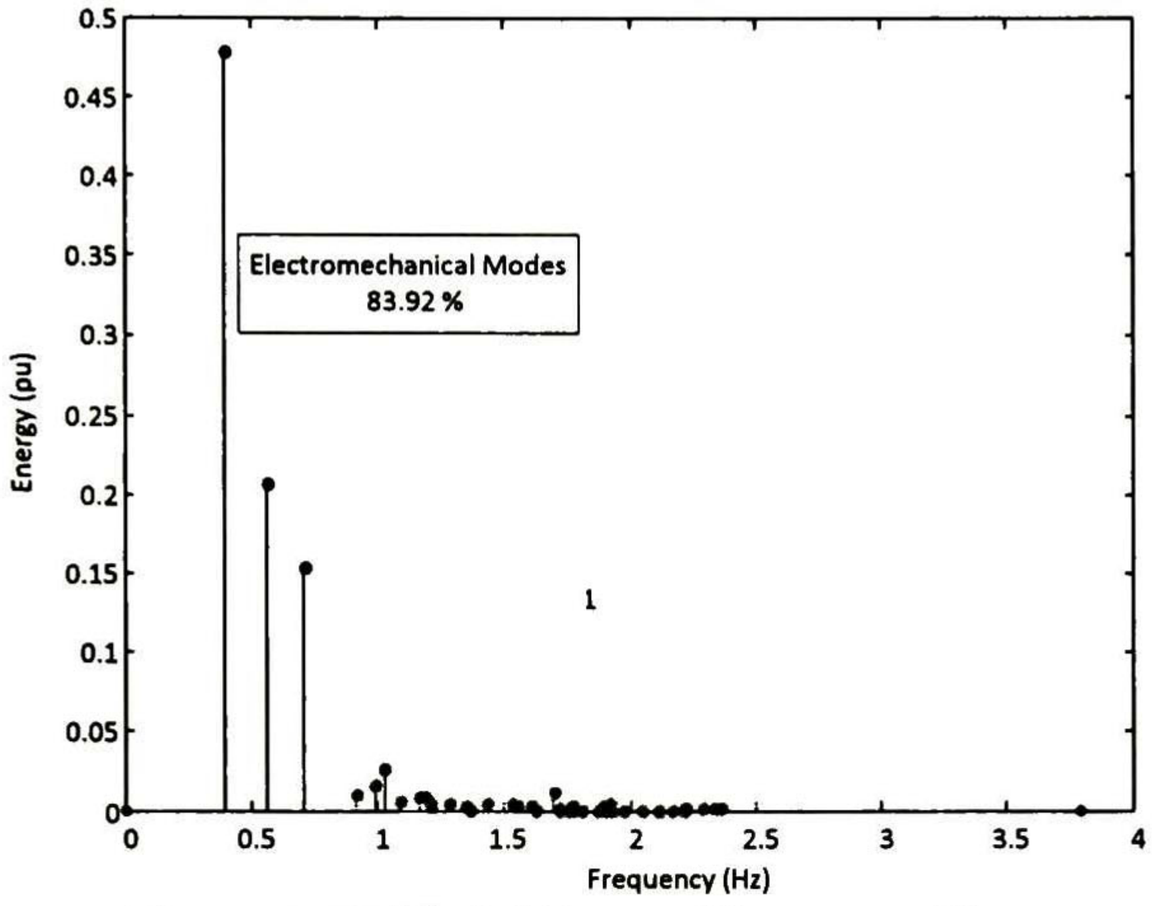

Figure 7.22 Modal Energy Decomposition

Table 7.8. The five most energetic modes

Eigenvalue	*Frequency (Hz)*	*Energy (pu)*
λ_1	0.3996	0.4782
λ_2	0.5630	0.2072
λ_3	0.7098	0.1538
λ_4	1.0310	0.0271
λ_5	0.9898	0.0168

These results, validate that presented in Section 7.2, where it was graphically demonstrated that the speed-based mode shapes associated to the dominant modes of the system response, present characteristic features observed in the mode shapes associated to the two slowest linear modes (λ_1 and λ_2).

This study also demonstrates that from the perspective of modal energy components, the three inter-area modes (λ1, λ2, and λ3) are the most energetic modes that underlie system response.

7.5.3 Modal components of energy (local perspective) observability index

Consider a vector of observations y, for example, active power flows at major transmission lines. For the model under study, 169 transmission lines, 37 power transformers and 46 machine transformers are included in the line data of the system. All of these elements are considered as paths of power transfer; however for practical purposes only the 169 power flows through the 169 transmission lines can be used to be monitored by wide area measurement systems.

The methodology used to give an index of modal observability consists, basically, of decomposing the total ensemble energy (see section 5.3) of certain set of measurements in elemental contributions (individual measurements); each individual energy term is decomposed in modal energy terms. The data collected through this brute forced method is sorted in categories uniquely associated to a single mode. Thus, it is possible to make an individual mode analysis to detect the measurements where certain mode has the strong level of energy. This methodology is described in Figure 7.23.

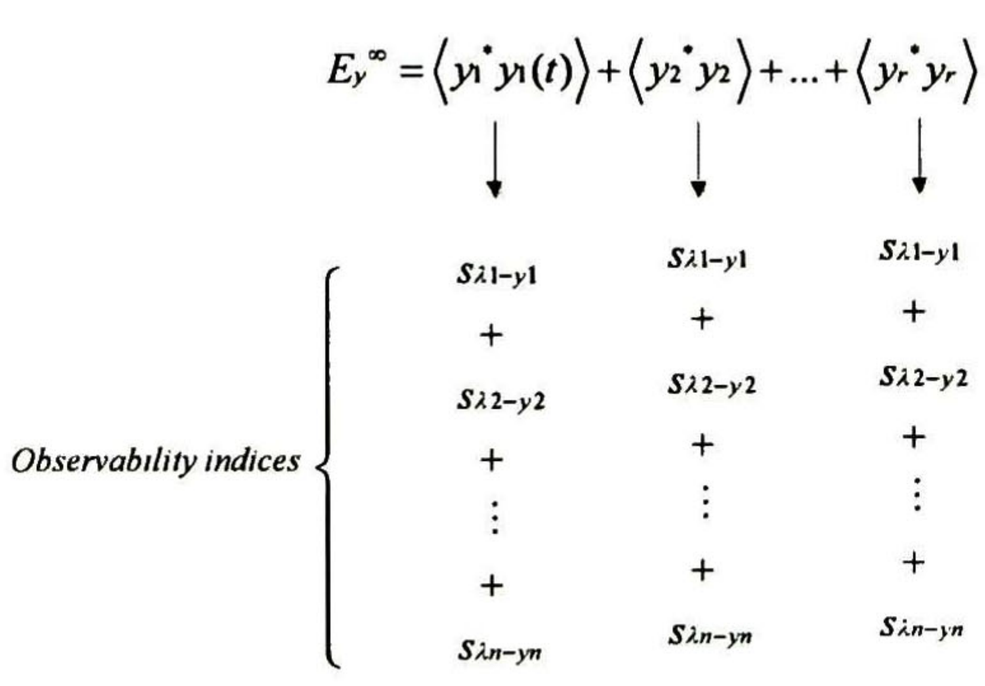

Figure 7.23 Proposed observability indices

The following figures present the results obtained from this approach; results are compared with results obtained from modal observability indices in reference [12].

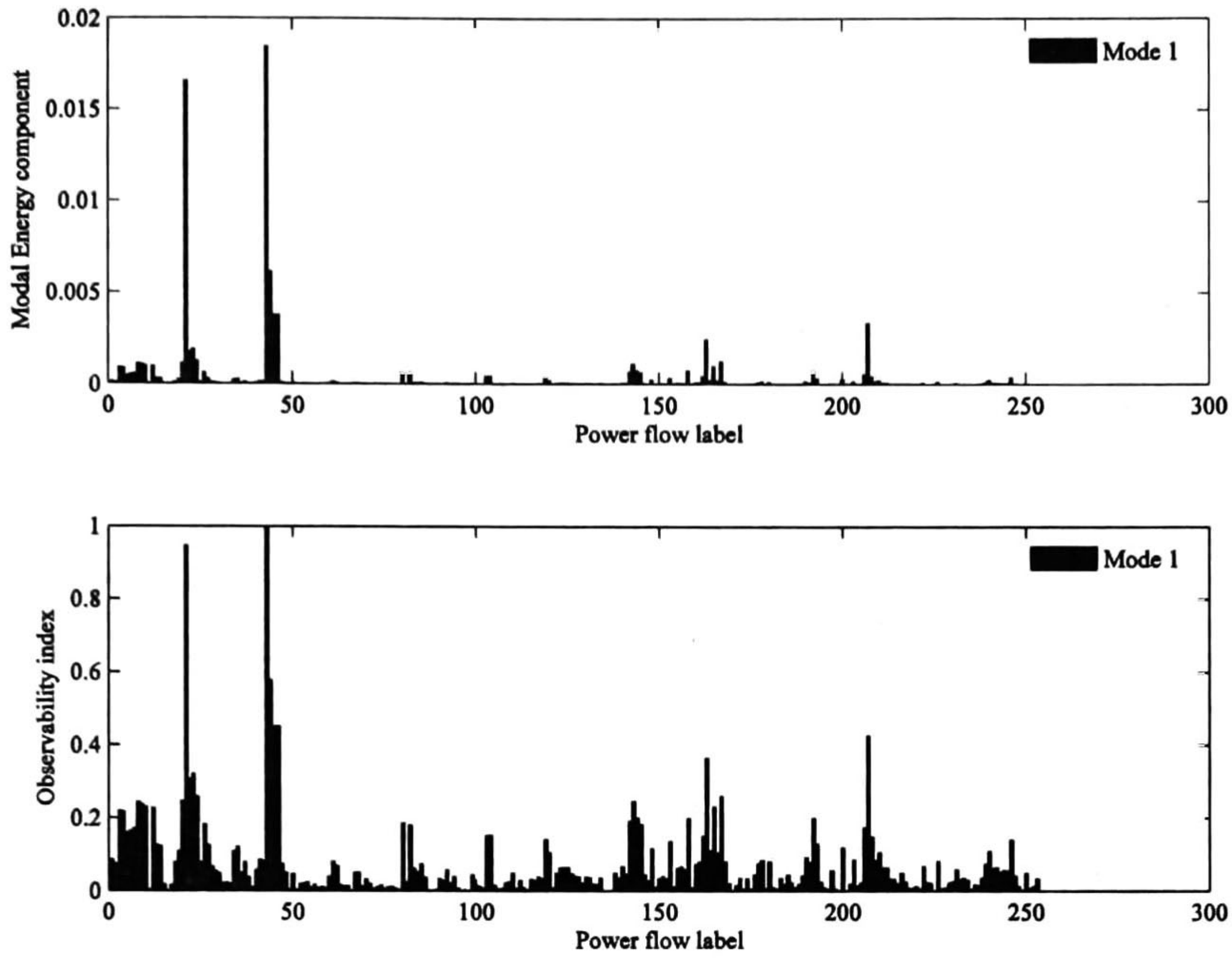

Figure 7.24 Modal energy decomposition mode 1 power flow

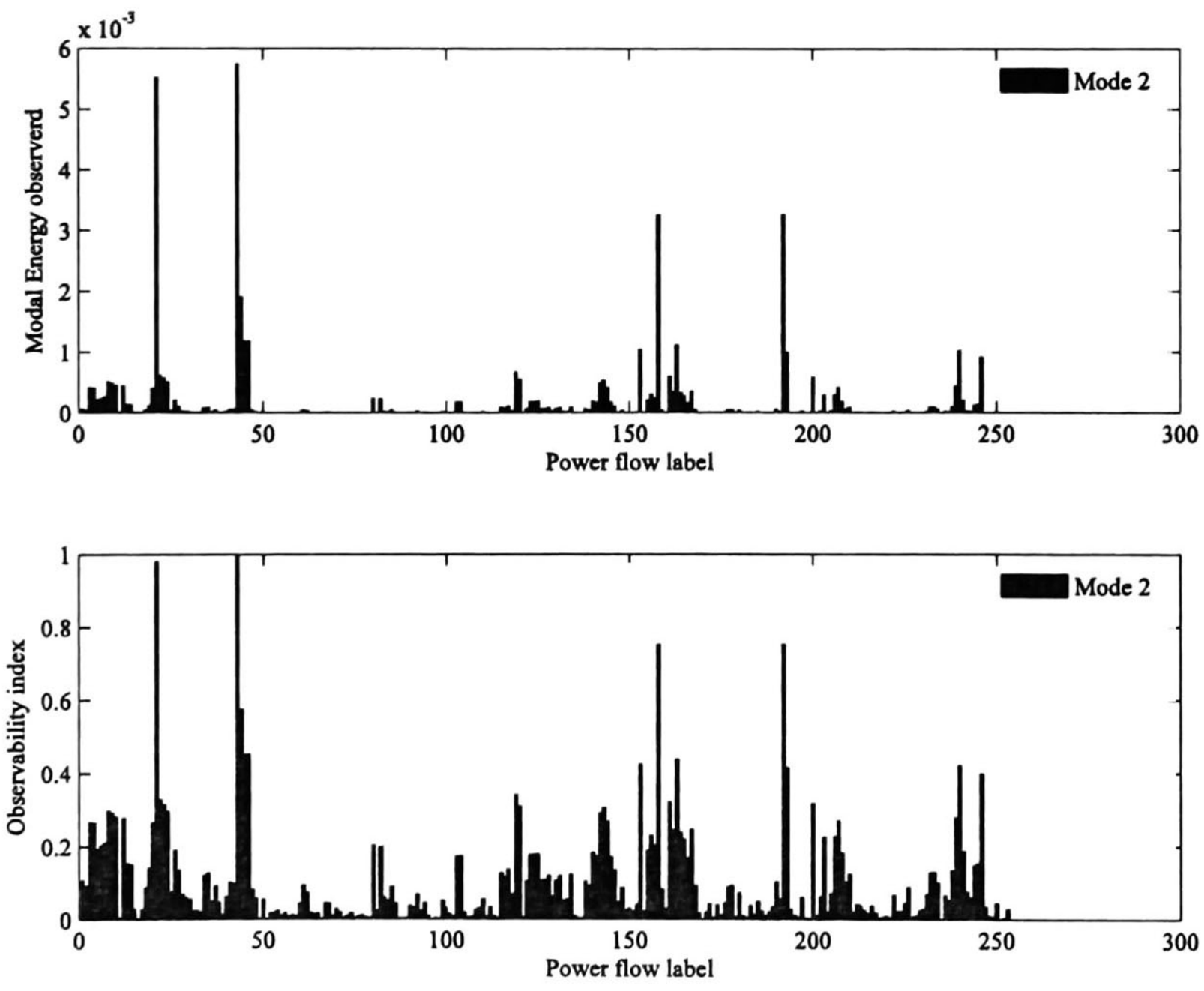

Figure 7.25 Modal energy decomposition mode 2 power flow

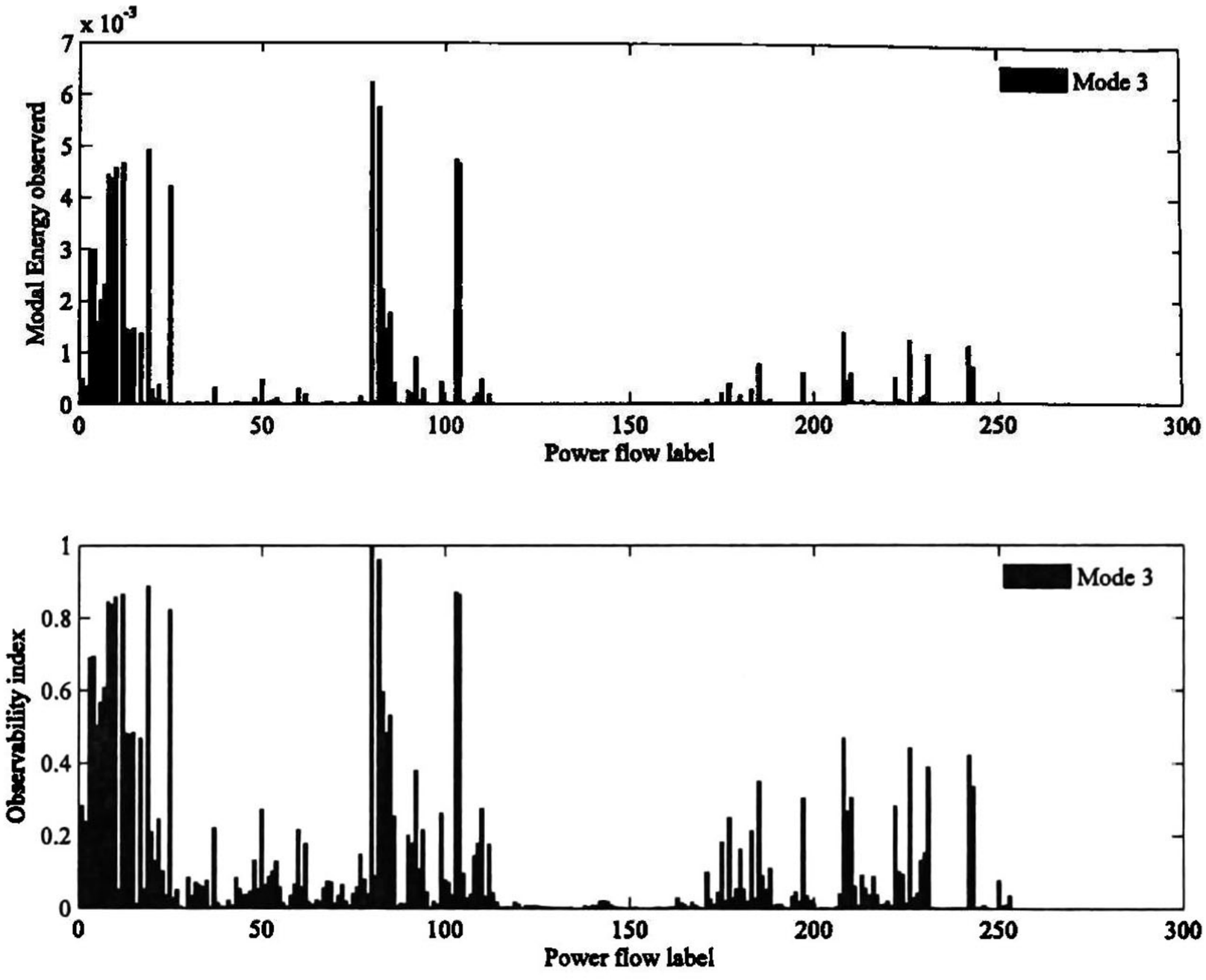

Figure 7.26 Modal energy decomposition mode 3 power flow

Based on Figure 7.24 and Figure 7.25 , it is known that mode 1 and mode 2 present almost the same pattern of energy distribution. However, the total energy associated to mode 1 is higher than the total energy of the mode 2 (see Table 7.9).

From Figure 7.24 and Table 7.9 it is evident that the power flow where is mode 1 is most observable is the active power flow between nodes 182-86 (label 43 in Figure 7.24). For the case of mode 2, it is observed that the power flow between nodes 181-174 (label 158 in Figure 7.25) is a suitable option for monitoring this linear mode of frequency 0.5630 Hz; in contrast to other power flows in this particular case Mode 2 has a stronger presence than Mode 1 i.e, the swing phenomena associate to Mode 2 is not corrupted by swings associate to the Mode 1, which is a desirable characteristic for the optimal monitoring of Mode 2.

Although for the ensemble average state energy , mode 2 presents a higher level of excitation than mode 3, for the case of power flow observations, Mode 3 seems to be more observable than mode 1 and mode 2, this fact is deduced from the total level of energy of the modes displayed at the bottom of Table 7.9.

In Figure 7.26 it is seen that the energy distribution of mode 3 presents a dense concentration in the lines labeled as 1-25. This fact gives the high level of energy to this mode with respect to the rest of the linear modes.

Table 7.9. Power flow energy-observability

	Mode 1				*Mode 2*				*Mode 3*			
		Line				*Line*				*Line*		
Ranking	*label*	*From*	*To*	*Energy*	*label*	*From*	*To*	*Energy*	*label*	*From*	*To*	*Energy*
1	43	182	86	0.0185	43	182	86	0.0058	80	110	113	0.0062
2	21	75	86	0.0166	21	75	86	0.0055	82	113	102	0.0057
3	44	182	185	0.0062	*192	181	180	0.0033	19	64	78	0.0049
4	46	184	182	0.0038	158	181	174	0.0033	103	127	130	0.0047
5	45	185	184	0.0038	44	182	185	0.0019	12	69	64	0.0047
6	*207	185	186	0.0033	46	184	182	0.0012	104	130	89	0.0047
7	163	185	159	0.0024	45	185	184	0.0012	10	53	69	0.0046
8	23	75	77	0.0019	163	185	159	0.0011	8	51	55	0.0044
9	22	75	84	0.0017	153	164	171	0.001	9	53	55	0.0044
10	167	159	166	0.0012	*240	180	33	0.001	25	89	78	0.0042
			**Total	0.0891			**Total	0.0467			**Total	0.0894

*Transformer data

** Total computed whit 256 active power flows not showing in the Table

These examples illustrate the ability of the proposed modal analysis framework to assess the extent and distribution of modal energy.

7.6 References.

[1] Kundur, P. (1994). Power system stability and control (Vol. 7). N. J. Balu, & M. G. Lauby (Eds.). New York: McGraw-hill.

[2] Rogers, G. (2012). Power system oscillations. Springer Science & Business Media.

[3] Messina, A.R.; Vittal, V., "Nonlinear, non-stationary analysis of interarea oscillations via Hilbert spectral analysis,' *Power Systems, IEEE Transactions on* , vol.21, no.3, pp.1234,1241, Aug. 2006 doi: 10.1109/TPWRS.2006.876656

[4] Ayon, J. J., Barocio, E., & Messina, A. R. (2015). Blind extraction and characterization of power system oscillatory modes. Electric Power Systems Research, 119, 54-65.

[5] Kloeden, P. E., Platen, E., & Schurz, H. (2012). Numerical solution of SDE through computer experiments. Springer Science & Business Media.

[6] Zhou, N., Pierre, J. W., & Wies, R. W. (2003, October). Estimation of low-frequency electromechanical modes of power systems from ambient measurements using a subspace method. In *Proceedings of the North American Power Symposium*. Sn.

[7] Zhou, N., Pierre, J., & Hauer, J. (2008, July). Initial results in power system identification from injected probing signals using a subspace method. In Power and Energy Society General Meeting-Conversion and Delivery of Electrical Energy in the 21st Century, 2008 IEEE (pp. 1-1). IEEE.

[8] Liu, G., & Venkatasubramanian, V. M. (2008, May). Oscillation monitoring from ambient PMU measurements by frequency domain decomposition. In Circuits and Systems, 2008. ISCAS 2008. IEEE International Symposium on (pp. 2821-2824). IEEE.

[9] Wang, K., & Crow, M. L. (2011, July). Numerical simulation of stochastic differential algebraic equations for power system transient stability with random loads. In Power and Energy Society General Meeting, 2011 IEEE (pp. 1-8). IEEE.

[10] Wang, K., & Crow, M. L. (2011, July). Numerical simulation of stochastic differential algebraic equations for power system transient stability with random loads. In Power and Energy Society General Meeting, 2011 IEEE (pp. 1-8). IEEE.

[11] Liu, Y. F., Ju, P., Wu, F., Yu, Y. P., & Zhang, J. Y. (2014, October). Computation comparisons of power system dynamics under random excitation. In Power System Technology (POWERCON), 2014 International Conference on(pp. 752-758). IEEE.

[12] Chan, S. M. (1984). Modal controllability and observability of power-system models. International Journal of Electrical Power & Energy Systems, 6(2), 83-88.

Chapter 8
General Conclusions

This chapter summarizes the main results of this thesis and identifies opportunities for future research.

8.1 Conclusions

The work described in this thesis, presents a new analytical approach to assessing the effect of stochastically excited small disturbances, on system dynamic behavior. Across the different examples the consistency of results obtained from the proposed methodology was demonstrated:

-The mode shape extracted from POD analysis for the predominant mode in the system response identifies both, the swing patterns as well as the machines most involved in the oscillations under ambient operating conditions. The analytic result obtained from the proposed model-based approach was compared whit results obtained from a measure-based method applied to simulation data. Results show the feasibility of the proposed method.

-The energy-based theory developed in this dissertation allows to directly estimate the energy associated to the dominant linear modes that underlie the system behavior. These results are in concordance with results obtained from POD analysis. In both cases, it is concluded that inter-area modes predominantly underlie the oscillatory dynamics of the system response to stochastically excited load disturbances.

-The spatial distribution of the stochastic forcing functions plays an important role in determining the influence of stochastic perturbations in the variance of system dynamic behavior. The concept of stochastic optimals and the proposed methodology used to find the prevalent randomly behaved perturbations, provide valuable information to find and understand hidden system characteristics such as high level of energy associated to one single input. However, further research is needed to establish physical interpretation of these results.

As was presented in section 7.5, an energy-based observability index is proposed. Results are comparable with observability indices that have been developed for linear system representations in the field of control theory.

8.2 Future work

Derived from previously discussed theory, suggestions for future areas of research are listed as follow:

In order to make the actual formulation compatible with widely adopted approaches rely in structure preserving model, an analytic structure-preserving framework for realistic power system models is needed.

-The inclusion of SDE continuous models to describe more general sources of random excitation, such as intermittent power generation, is a problem of practical interest that requires further analytical research.

The identification of predominant forcing functions modeled as SDE, can be considered as a direction of future research to formulate model input reduction techniques that allows a comprehensive analysis of realistic power systems that includes countless sources of uncertainty.

Appendix A

Ringdown Analysis

Ringdown algorithms use transient (large disturbance) system responses to estimate modal parameters require existence of transient responses in the system, which makes their application difficult in continuous (near real-time) mode estimation.

Prony analysis[1]-[11] is a classical approach to modal identification based on the (parametric) frequency domain representation of measured signals. Other ringdown analysis algorithms have been successfully applied to power-system data. These include the Minimal Realization algorithm first introduced in [12], the Eigenvalue Realization Algorithm (ERA) [13], the Matrix-Pencil method and the Hankel Total Least Squares (HTLS) In frequency-domain there are two linear methods that have been used, these are: frequency-domain identification and [14] z-transform identification [15].

The methods mentioned above, are considered as linear approaches. However, there also exist methods that recognize that power systems transient responses are inherently non-linear, these include methods in the frequency domain such as: frequency domain pattern recognition (FDPR)[16], the short time Fourier transform (STFT) [17], and in recent times the digital Taylor Fourier transform (DTFT) [18]

There also exist another group of non-linear parametric methods that determines instantaneous values of frequency and damping, and example of techniques composed this group are Hilbert Analysis [19] and Wavelets [20].

References.

[1] Hauer, J. F., Demeure, C. J., & Scharf, L. L. (1990). Initial results in Prony analysis of power system response signals. Power Systems, IEEE Transactions on, 5(1), 80-89.

[2] Scharf, L. L. (1991). Statistical signal processing (Vol. 98). Reading, MA: Addison-Wesley.

[3] Pierre, D. A., Trudnowski, D. J., & Hauer, J. F. (1992). Identifying linear reduced-order models for systems with arbitrary initial conditions using Prony signal analysis. Automatic Control, IEEE Transactions on, 37(6), 831-835.

[4] Hauer, J. F. (1991). Application of Prony analysis to the determination of modal content and equivalent models for measured power system response. Power Systems, IEEE Transactions on, 6(3), 1062-1068.

[5] Pierre, D. A., Trudnowski, D. J., & Hauer, J. F. (1992). Identifying linear reduced-order models for systems with arbitrary initial conditions using Prony signal analysis. Automatic Control, IEEE Transactions on, 37(6), 831-835.

[6] Trudnowski, D. J., Donnelly, M. K., & Hauer, J. F. (1993). Advances in the identification of transfer function models using Prony analysis. In American Control Conference (No. 30, pp. 1561-1562).

[7] Smith, J. R., Fatehi, F., Woods, C. S., Hauer, J. F., & Trudnowski, D. J. (1993). Transfer function identification in power system applications. Power Systems, IEEE Transactions on, 8(3), 1282-1290.

[8] Trudnowski, D. J. (1994). Order reduction of large-scale linear oscillatory system models. Power Systems, IEEE Transactions on, 9(1), 451-458

[9] Trudnowski, D. J., Johnson, J. M., & Hauer, J. F. (1998, June). SIMO system identification from measured ringdowns. In American Control Conference, 1998. Proceedings of the 1998 (Vol. 5, pp. 2968-2972). IEEE.

[10] Trudnowski, D. J., Johnson, J. M., & Hauer, J. F. (1999). Making Prony analysis more accurate using multiple signals. Power Systems, IEEE Transactions on, 14(1), 226-231.

[11] Kamwa, I., Grondin, R., Dickinson, E. J., & Fortin, S. (1993). A minimal realization approach to reduced-order modelling and modal analysis for power system response signals. Power Systems, IEEE Transactions on, 8(3), 1020-1029.

[12] Sanchez-Gasca, J. J., & Chow, J. H. (1997). Computation of power system low-order models from time domain simulations using a Hankel matrix. Power Systems, IEEE Transactions on, 12(4), 1461-1467.

[13] Liu, G., Quintero, J., & Venkatasubramanian, V. (2007, August). Oscillation monitoring system based on wide area synchrophasors in power systems. InBulk Power System Dynamics and Control-VII. Revitalizing Operational Reliability, 2007 iREP Symposium (pp. 1-13). IEEE.

[14] Vanhuffel, S., Chen, H., Decanniere, C., & Vanhecke, P. (1994). Algorithm for time-domain NMR data fitting based on total least squares. Journal of Magnetic Resonance, Series A, 110(2), 228-237.

[15] Poon, K. P., & Lee, U. C. (1988). Analysis of transient stability swings in large interconnected power systems by Fourier transformation. Power Systems, IEEE Transactions on, 3(4), 1573-1581.

[16] Ostojić, D. R., & Heydt, G. T. (1991). Transient stability assessment by pattern recognition in the frequency domain. Power Systems, IEEE Transactions on,6(1), 231-237.

[17] Ostojić, D. R. (1993). Spectral monitoring of power system dynamic performances. Power Systems, IEEE Transactions on, 8(2), 445-451.

[18] de la O, S., Antonio, J., Ramirez, J. M., Zamora Mendez, A., & Paternina, M. R. A. Identification of Electromechanical Modes Based on the Digital Taylor-Fourier Transform.

[19] Messina, A. R., & Vittal, V. (2006). Nonlinear, non-stationary analysis of interarea oscillations via Hilbert spectral analysis. Power Systems, IEEE Transactions on, 21(3), 1234-1241.

[20] Ruiz-Vega, D., Messina, A. R., & Enríquez-Harper, G. (2005). Analysis of interarea oscillations via non-linear time series analysis techniques. Proc. of 15th PSCC, Liege, 22-26.

Appendix B
Supplementary Definitions and Derivations

B.1 Unit function impulse

a) Definition of the Unit Function Impulse [1]

$$\delta(t) = \lim_{\varepsilon \to 0} \delta_\varepsilon(t) \quad \text{for } t \neq 0 \tag{B.1.1}$$

$$\delta_\varepsilon(t) = \begin{cases} 0, & |t| > \varepsilon \\ \dfrac{1}{2\varepsilon}, & |t| > \varepsilon \end{cases} \quad \text{for } t \neq 0 \tag{B.1.2}$$

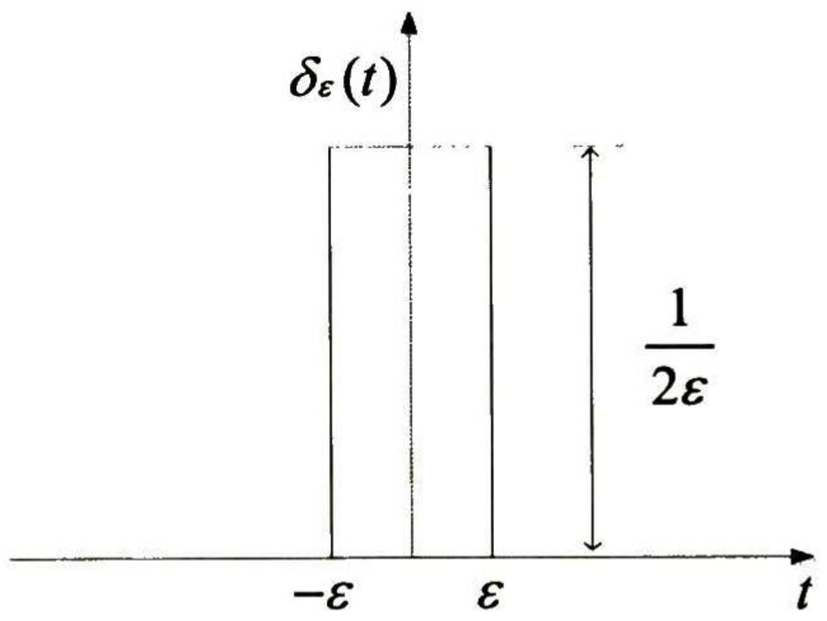

Figure A.1.1 Definition of the impulse function

This definition implies that

$$\int_{t_1}^{t_2} \delta(t-\tau)d\tau = \begin{cases} 1, & t_1 < t < t_2 \\ 0, & t_1 > t \text{ or } t > t_2 \end{cases} \tag{B.1.3}$$

This function also satisfies [1]

$$\delta(t) = 0 \quad \text{for } t \neq 0 \tag{B.1.4}$$

$$\int_{-\infty}^{\infty} \delta(t)dt = 1 . \qquad \text{(B.1.5)}$$

b) Multiplication of a Function by an Impulse [1]

Since the impulse $\delta(t)$ exists only at t=0 and the value of a general deterministic function $\varphi(t)$ at t=0 is $\varphi(0)$, then

$$\varphi(t)\delta(t) = \varphi(0)\delta(t) . \qquad \text{(B.1.6)}$$

Similarly, if $\delta(t)$ is multiplied by and impulse$\phi(t\text{-}T)$ (impulse located at t=T), then

$$\varphi(t)\delta(t-T) = \varphi(T)\delta(t-T) . \qquad \text{(B.1.7)}$$

Provided $\varphi(t)$ is continuous at t=T.

c) Sampling Property of the Unit Impulse Function [1]

From (B.1.6) and (B.1.5) it follows that

$$\int_{-\infty}^{\infty} \varphi(t)\delta(t)dt = \varphi(0) . \qquad \text{(B.1.8)}$$

From (B.1.7) and (B.1.5) it follows that

$$\int_{-\infty}^{\infty} \varphi(t)\delta(t-T)dt = \varphi(T) . \qquad \text{(B.1.9)}$$

In these definitions is assumed that the function $\varphi(t)$ is continuous at the instant where the impulse is located.

d) Important definitions particular case of ito-integrals (*undefined cases*) [2]

Integrals involving delta functions, it frequently occurs in the study of stochastic differential equations that the argument of the delta function is equal either the upper or the lower limit of the integral, that is, we find integrals like

$$I_1 = \int_{t_1}^{t_2} f(t)\delta(t-t_1)dt . \qquad \text{(B.1.10)}$$

or

$$I_2 = \int_{t_1}^{t_2} f(t)\delta(t - t_2)dt \,. \tag{B.1.11}$$

and various conventions can be made concerning the value of such integrals. In reference [4] is proved that

$$I_1 = \int_{t_1}^{t_2} f(t_1)dt \,. \tag{B.1.12}$$

or

$$I_2 = 0 \,. \tag{B.1.13}$$

Corresponding to counting all the weight of a delta function at a lower limit of an integral, and none of the weight at the upper limit.

B.2 Leibniz integration rule

The Leibniz rule for differentiating an integral [3], in its general form is written as

$$\frac{d}{dt}\left(\int_{g(t)}^{h(t)} F(x,t)dx\right) = \left\{F[h(t),t]\dot{h}(t) - F[g(t),t]\dot{g}(t)\right\} + \int_{g(t)}^{h(t)} \frac{\partial F(x,t)}{\partial t}dx \,, \tag{B.2.1}$$

although it is seldom if ever used in such generality. Usually, either the limits are constants, or the integrand is independent of time t. Frequent cases are

$$\frac{d}{dt}\left(\int_a^t F(x)dx\right) = F(t) \,, \frac{d}{dt}\left(\int_a^{\infty} F(x,t)dx\right) = \int_a^{\infty} \frac{\partial F(x,t)}{\partial t}dx \,. \tag{B.2.2}$$

B.3 Exponential function

The term $e^{\mathbf{A}t}$ can be formally defined by the convergent power series as [4],

$$e^{\mathbf{A}t} = \mathbf{I} + t\mathbf{A} + \frac{1}{2}t^2\mathbf{A}^2 + \cdots \tag{B.3.1}$$

From this result the term $\mathbf{A}^H e^{\mathbf{A}^H(t-s')}$ also can be expanded as

$$\mathbf{A}^H e^{\mathbf{A}^H(t-s')} = \mathbf{A}^H\left(\mathbf{I} + (t-s')\mathbf{A}^H + \frac{(t-s')^2}{2}\left(\mathbf{A}^H\right)^2 + \cdots\right)$$
$$= \left(\mathbf{I} + (t-s')\mathbf{A}^H + \frac{(t-s')^2}{2}\left(\mathbf{A}^H\right)^2 + \cdots\right)\mathbf{A}^H \qquad \text{(B.3.2)}$$
$$= e^{\mathbf{A}^H(t-s')}\mathbf{A}^H$$

where is demonstrated that $\mathbf{A}^H e^{\mathbf{A}^H(t-s')} = e^{\mathbf{A}^H(t-s')}\mathbf{A}^H$

B.4 Expansion of $\xi^* \psi \xi$

Having a n-dimensional vector ξ and a matrix ψ of dimensions $n \times n$, then the product $\xi^* \psi \xi$ can be expanded as

$$\xi^* \psi \xi = \sum_i^n \sum_j^n \xi_i \xi_j \psi_{ij} \qquad \text{(B.4.1)}$$

where ξ_i is the *i-th* element of the vector ξ, i.e. $\xi = [\ \xi_1\ \xi_2\ \ldots\ \xi_n\ ]^T$ and ψ_{ij} is the ij-th element of the matrix ψ.

Let matrix ψ be written in terms of their column components ψ_i as $\psi = [\ \psi_1\ \psi_2\ \ldots\ \psi_n\ ]$. Expansion of the product $\xi^* \psi \xi$, yields

$$\xi^* \psi \xi = [\xi^* \psi_1 \quad \cdots \quad \xi^* \psi_n] \begin{bmatrix} \xi_1 \\ \vdots \\ \xi_n \end{bmatrix} = \xi_1 \xi^* \psi_1 + \cdots + \xi_n \xi^* \psi_n \qquad \text{(B.4.2)}$$

and (B.4.1) is obtained.

B.5 Optimization problem

Given (5.9), find a set of n-dimensional normalized vectors, $\{\mathbf{f}_{sox\text{-}1}, \mathbf{f}_{sox\text{-}2}, \ldots, \mathbf{f}_{sox\text{-}n}\}$ that maximize, $E^{\infty}_{so\text{-}x}$, i.e.,

If,

$$E^{\infty}_{so-x} = trace\left(\mathbf{F}_{so}{}^H \mathbf{B}_x{}^{\infty} \mathbf{F}_{so}\right) = \sum_{i=1}^{n} \mathbf{f}_{sox-i}{}^H \mathbf{B}_x{}^{\infty} \mathbf{f}_{sox-i} \,. \qquad \text{(B.4.3)}$$

Then

$$\text{Maximize } E^{\infty}_{so-x}. \tag{B.4.4}$$

Subject to

$$\mathbf{f}_{sox-i}{}^{H}\mathbf{f}_{sox-i} = 1. \tag{B.4.5}$$

By using the Laplace Multipliers [5] the optimization problem without restrictions can be recast as

$$\max\left[\sum_{i=1}^{n}\mathbf{f}_{sox-i}{}^{H}\mathbf{B}_{x}{}^{\infty}\mathbf{f}_{sox-i} - \sum_{i=1}^{n}\lambda_{sox-i}\left(\mathbf{f}_{sox-i}{}^{H}\mathbf{f}_{sox-i} - 1\right)\right] \tag{B.4.6}$$

Further, by defining the functions

$$\zeta_1(\mathbf{f}_{sox-1},\mathbf{f}_{sox-2},\ldots,\mathbf{f}_{sox-n}) = \sum_{i=1}^{n}\mathbf{f}_{sox-i}{}^{H}\mathbf{B}_{x}{}^{\infty}\mathbf{f}_{sox-i} \tag{B.4.7}$$

and

$$\zeta_2(\mathbf{f}_{sox-1},\mathbf{f}_{sox-2},\ldots,\mathbf{f}_{sox-n}) = \sum_{i=1}^{n}\lambda_{so-i}\left(\mathbf{f}_{sox-i}{}^{H}\mathbf{f}_{sox-i} - 1\right) \tag{B.4.8}$$

Then the objective function is now redefined in terms of (B.4.7)-(B.4.8) is rewritten as

$$\zeta(\mathbf{f}_{sox-1},\mathbf{f}_{sox-2},\ldots,\mathbf{f}_{sox-n}) = \zeta_1(\mathbf{f}_{sox-1},\mathbf{f}_{sox-2},\ldots,\mathbf{f}_{sox-n}) - \zeta_2(\mathbf{f}_{sox-1},\mathbf{f}_{sox-2},\ldots,\mathbf{f}_{sox-n}) \tag{B.4.9}$$

To find the optimal $\mathbf{f}_{so\text{-}i}$ is needed to derivate the objective function with respect to the vector of interest, thus

$$\frac{d}{d\mathbf{f}_{sox-i}}\zeta = \frac{d}{d\mathbf{f}_{sox-i}}\zeta_1 - \frac{d}{d\mathbf{f}_{sox-i}}\zeta_2 \tag{B.4.10}$$

From result (B.4.2) in is easily proved that

$$\frac{d}{d\mathbf{f}_{sox-i}}\zeta = \frac{d}{d\mathbf{f}_{sox-i}}\mathbf{f}_{sox-i}{}^{H}\mathbf{B}^{\infty}\mathbf{f}_{sox-i}$$
$$= \frac{d}{d\mathbf{f}_{sox-i}}\sum_{j=1}^{n}\sum_{k=1}^{n}\mathbf{f}^{j}{}_{sox-i}b^{\infty}{}_{jk}\mathbf{f}^{k}{}_{sox-i} \qquad \text{(B.4.11)}$$
$$= \frac{d}{d\mathbf{f}_{sox-i}}\left[\sum_{j=1}^{n}\left(\mathbf{f}^{j}{}_{sox-i}\right)^{2}b_{jj} + 2\sum_{J=1}^{n-1}\sum_{k=i+1}^{n}\left(\mathbf{f}^{J}{}_{sox-i}\right)b^{\infty}{}_{jk}\left(\mathbf{f}^{k}{}_{sox-i}\right)\right]$$

where $b_{jk}{}^{\infty}$ is jk-th element of $\mathbf{B}_x{}^{\infty}$ and $\mathbf{f}^{j}{}_{so\text{-}i}$ is the j-th element of vector $\mathbf{f}_{so\text{-}i}$ and the symmetry of the matrix $\mathbf{B}_x{}^{\infty}$ has been exploited. Since the derivative of the objective function (scalar function) is with respect to a vector, it results in a vector, then the l-th component of this result is found to be,

$$\frac{d}{d\mathbf{f}^{l}{}_{sox-i}}\left[\left(\mathbf{f}^{l}{}_{sox-i}\right)^{2}b_{ll} + 2\sum_{\substack{j=1\\ j\neq l}}^{n}\left(\mathbf{f}^{l}{}_{sox-i}\right)b^{\infty}{}_{lj}\left(\mathbf{f}^{J}{}_{sox-i}\right)\right] = 2\sum_{J=1}^{n}\left(b^{\infty}{}_{lj}\mathbf{f}^{j}{}_{sox-i}\right) \qquad \text{(B.4.12)}$$

It follows easily that,

$$\frac{d}{d\mathbf{f}_{sox-i}}\zeta = 2\mathbf{B}^{\infty}\mathbf{f}_{sox-i} \qquad \text{(B.4.13)}$$

The second derivative in the *rhs* of (B.4.10) can be obtained following a similar procedure. Straightforward analysis leads to

$$\frac{d}{d\mathbf{f}_{so-i}}\zeta_2 = 2\lambda_{sox-i}\mathbf{f}_{sox-i} \qquad \text{(B.4.14)}$$

Finally substituting (B.4.13)-(B.4.14) in (B.4.10) the *i-th* general vector satisfies

$$\mathbf{B}^{\infty}\mathbf{f}_{sox-i} = \lambda_{sox-i}\mathbf{f}_{sox-i}\,. \qquad \text{(B.4.15)}$$

and the complete solution of (B.4.6) is composed by the set of eigenvectors of $\mathbf{B}_x{}^{\infty}$

B.6 Dyadic expansion of the exponential function

From the basic theory of linear algebra the following identities are well known

$$\mathbf{AV} = \mathbf{V}\Lambda\,. \qquad \text{(B.4.16)}$$

And

$$\mathbf{WA} = \mathbf{W}\Lambda . \tag{B.4.17}$$

Where the matrices $\mathbf{V}=\text{col}[\mathbf{v}_1,\mathbf{v}_2,\ldots,\mathbf{v}_n]$, $\mathbf{W}=\text{row}[\mathbf{w}_1^T,\mathbf{w}_2^T,\ldots,\mathbf{w}_n^T]=\mathbf{V}^{-1}$ are the matrices containing the right and left eigenvectors of matrix **A** respectively, and $\Lambda=\text{diag}[\lambda_1,\lambda_2,\ldots,\lambda_n]$ contains the eigenvalues of **A** in its main diagonal. Matrix **A** can be factorized as

$$\mathbf{A} = \mathbf{V}\Lambda\mathbf{W} . \tag{B.4.18}$$

Furthermore **A** and $e^{\mathbf{A}t}$ can be written as dyadic expansion of left and right eigenvectors [6]:

$$\begin{aligned}
\mathbf{A} &= [\mathbf{v}_1 \quad \ldots \quad \mathbf{v}_n]\begin{bmatrix} \lambda_1 & & \\ & & \\ & & \lambda_n \end{bmatrix}\begin{bmatrix} \mathbf{w}_1^T \\ \vdots \\ \mathbf{w}_n^T \end{bmatrix} \\
&= [\lambda_1\mathbf{v}_1 \quad \ldots \quad \lambda_n\mathbf{v}_n]\begin{bmatrix} \mathbf{w}_1^T \\ \vdots \\ \mathbf{w}_n^T \end{bmatrix} \\
&= \sum_{i=1}^{n} \lambda_i \mathbf{v}_i \mathbf{w}_i^T
\end{aligned} \tag{B.4.19}$$

and

$$\begin{aligned}
e^{\mathbf{A}t} &= \mathbf{I} + t\mathbf{A} + \frac{1}{2}t^2\mathbf{A}^2 + \ldots \\
&= \mathbf{I} + t(\mathbf{V}\Lambda\mathbf{W}) + \frac{1}{2}t^2(\mathbf{V}\Lambda^2\mathbf{W}) + \ldots \\
&= \mathbf{V}\mathbf{W} + \mathbf{V}\Lambda\mathbf{W} + \frac{1}{2}t^2(\mathbf{V}\Lambda^2\mathbf{W}) + \ldots \\
&= \sum_{i=1}^{n}\mathbf{V}_i\mathbf{W}_i^T + \sum_{i=1}^{n}\lambda_i\mathbf{V}_i\mathbf{W}_i^T + \sum_{i=1}^{n}\frac{1}{2}t^2\lambda_i^2\mathbf{V}_i\mathbf{W}_i^T + \ldots \\
&= \sum_{i=1}^{n}(1 + t\lambda_i + \frac{1}{2}t^2\lambda_i^2 + \ldots)\mathbf{V}_i\mathbf{W}_i^T \\
&= \sum_{i=1}^{n} e^{\lambda_i t}\mathbf{V}_i\mathbf{W}_i^T
\end{aligned} \tag{B.4.20}$$

References.

[1] Lathi, B. (1998). Signal processing and linear systems. Oxford University Press, USA.

[2] Gardiner, C. W. (1986). *Handbook of stochastic methods for physics, chemistry and the natural sciences*. Springer series in synergetics, 13, 149-168.

[3] Flanders, H. (1973). Differentiation under the integral sign. American Mathematical Monthly, 615-627.

[4] Moler, C., & Van Loan, C. (1978). Nineteen dubious ways to compute the exponential of a matrix. SIAM review, 20(4), 801-836

[5] Bertsekas, D. P. (2014). Constrained optimization and Lagrange multiplier methods. Academic press.

[6] Chan, S. M. (1984). Modal controllability and observability of power-system models. International Journal of Electrical Power & Energy Systems, 6(2)

Appendix C

Brief Review on Proper Orthogonal Decomposition

C.1 Proper orthogonal decomposition

The proper orthogonal decomposition (POD) provides a basis for the modal decomposition of an ensemble of functions, such as data obtained from measurements of observed phenomena. The most striking of its properties is optimality: POD provides the most efficient way of capturing the dominant components of an infinite-dimensional process with only finitely few modes [1]-[5]

More precisely, assume that $u(x,t_j)$, j=1,2,…,N denotes a sequence of observations on some domain $x \in \Omega$ where x is a vector of spatial variables, and t_j is the time at which the observations are made. The POD procedure determines empirical orthogonal functions (EOFs), $\varphi_i(x)$ (i=1,2,…,∞), such that the projection onto the first EOF's (a low order representation)[1],[2].

$$u(x,t_j) = \sum_{i=1}^{p} a_i(t)\varphi_i(x). \tag{C.1.1}$$

is optimal in the sense that the average least squares truncation error, ε

$$\varepsilon = \left\langle \left\| u(x,t_j) - \sum_{i=1}^{p} a_i(t)\varphi_i(x) \right\|^2 \right\rangle \quad p \le N \tag{C.1.2}$$

is minimized. In (C.1.2) $\|\cdot\|$ denotes the L^2-norm and $\langle\cdot\rangle$ represents the ensemble average symbol. Also, in (C.1.1) the time-dependent coefficients may be interpreted as modal coordinates.

The discrete version of $u(x,t_j)$ can be defined as matrix data that captures its spatio-temporal characteristics, let **X** be defined as

$$\mathbf{X} = [\mathbf{x}_1 \quad \mathbf{x}_2 \quad \cdots \quad \mathbf{x}_n]. \tag{C.1.3}$$

where each column of $\mathbf{X}$, $\mathbf{x}_i$, is an N-dimensional vector of the form

$$\mathbf{x}_i = [u(x_i, t_1) \quad u(x_i, t_2) \quad \cdots \quad u(x_i, t_N)]^T, i = 1,2,...,n. \tag{C.1.4}$$

The vector $\mathbf{x}_i$ can be interpreted as sequence of observations at times $t_1,\ldots,t_N$ made at the x_i location.

Furthermore, the discrete version of (C.1.2) can be recast as

$$\varepsilon = \frac{1}{n}\sum_{j=1}^{n}\left\|\mathbf{x}_i - \sum_{k=1}^{p} a_{ik}\varphi_k\right\|^2 \quad p \le N \tag{C.1.5}$$

where φ_k is the discrete version of the continuous function $\varphi_k(t)$ and a_{jk} is a coefficient to be determined from write $\mathbf{x}_i$ as a linear combination of the EOF's, i.e.,

$$\mathbf{x}_i = \sum_{k=1}^{N} a_{ik}\varphi_k \ , \tag{C.1.6}$$

in addition, in (C.1.2) the ensemble average operator have been substituted by the sample mean. It can be demonstrated that the optimal solution of (C.1.5) converges to a linear equation of the form [1],[2].

$$\mathbf{C}_c\varphi = \lambda_{EOF}\varphi \tag{C.1.7}$$

where $\mathbf{C}_c$ is an $N \times N$ matrix defined as

$$\mathbf{C}_c = \frac{1}{n}\mathbf{X}^T\mathbf{X} \tag{C.1.8}$$

The eigenvectors φ of $\mathbf{C}_c$ are the empirical orthogonal functions (EOF's), and they represent an ordered decomposition of the data matrix $\mathbf{X}$, which in an statistical sense allows to characterize the variation present in the data set trough a group of uncorrelated variables which are ordered so that the first few retain most of the variation present in all the original variables. In this way, the most important EOF's, are that eigenvectors of $\mathbf{C}_c$ corresponding to the greatest eigenvalues λ_l, and they can conform a reduced basis $\{\varphi_1 \varphi_2 \ldots \varphi_p\}$ $p<n$ that optimally spans the space generated by $\{\mathbf{x}_1,\mathbf{x}_2,\ldots,\mathbf{x}_n\}$..

C.2 The method of snapshots

The method of snapshots is a procedure that is appropriate to follow when the number of samples in $\mathbf{x}_i$ is much greater than the number of spatial locations where they are taken , i.e., for $N >> n$. This approach reduces the computational burden from an N-dimensional eigenvalue problem to an n-dimensional one.

Under the assumption of linear independence of the vectors of the set $\{\mathbf{x}_1,\mathbf{x}_2,\ldots,\mathbf{x}_n\}$ each EOF can be expressed as linear combination of the columns of **X**, thus

$$\varphi_i = \sum_j^n w_{ij}\mathbf{x}_j \quad i=1,2,\ldots,n, \tag{C.1.9}$$

and by substituting this expression into (C.1.7), a new eigenvalue problem can be formulated [1],[2] as a solution of (C.1.5), and it is expressed as

$$\mathbf{C}_s\mathbf{w} = \lambda\mathbf{w}\,, \tag{C.1.10}$$

where $\mathbf{C}_s$ is an $n\times n$ matrix defined as

$$\mathbf{C}s = \frac{1}{N}\mathbf{X}\mathbf{X}^T \tag{C.1.11}$$

and their eigenvectors **w**, are the Proper Orthogonal Modes (POMs) and the associated eigenvalues λ are the Proper Orthogonal Values (POVs).As was mentioned for the EOF's the POMs associated to the components that most captures the variation of the matrix data **X** are those eigenvectors associated to the greatest eigenvalues POVs.

C.3 Energy relations

Following reference [1] , the energy of a vector sequence $\mathbf{x}_i$ building an $N\times n$ matrix is defined by the Frobernious norm

$$E(C) = \sum_{i=1}^{N}\sum_{j=1}^{n}\|\mathbf{x}_i\|^2 = \sum_{k=1}^{n}\lambda_k \tag{C.1.12}$$

Defining the total energy as E

$$E = \sum_{k=1}^{n} \lambda k \tag{C.1.13}$$

The energy of an eigenvalue, λi can be expressed as Ei

$$(\lambda / E) \times 100\% \tag{C.1.14}$$

References.

[1] Messina, A. R., & Vittal, V. (2007). Extraction of dynamic patterns from wide-area measurements using empirical orthogonal functions. Power Systems, IEEE Transactions on, 22(2), 682-692.

[2] Barocio, E., Pal, B. C., Thornhill, N. F., & Messina, A. R. (2014). A dynamic mode decomposition framework for global power system oscillation analysis.

[3] Holmes, P., Lumley, J. L., & Berkooz, G. (1998). Turbulence, coherent structures, dynamical systems and symmetry. Cambridge university press.

[4] G Kerschen, G., Golinval, J. C., Vakakis, A. F., & Bergman, L. A. (2005). The method of proper orthogonal decomposition for dynamical characterization and order reduction of mechanical systems: an overview. Nonlinear dynamics,41(1-3), 147-169.

[5] Buljak, V. (2011). Inverse analyses with model reduction: proper orthogonal decomposition in structural mechanics. Springer Science & Business Media.

Appendix D

Numerical Integration of Stochastic Differential Equations

D. 1 Numerical integration of stochastic differential equations

The study of power systems under ambient operating conditions take into account phenomena that is stochastic in nature. Therefore, models formulated for this purpose differ from the deterministic models commonly used, and special features of them must be carefully interpreted, a vast number of references can be found that explain the theory involved in the solution of the so called stochastic differential equations (SDE) [1]-[4]

In this section a brief description of one of the multiple schemes to SDE solution is reviewed, this with the aim of make a clear exposition of the numerical validation of the theoretical results developed in this research.

D. 2 Implicit euler scheme

The simplest implicit scheme solution of stochastic differential equations is the Euler scheme, it has a wide range of step sizes suitable for the approximation of stochastic dynamical systems, in particular those involving vastly different time scales [1].

Consider a stochastic differential equation of the form

$$dx = f(x)dt + \alpha dW \tag{C.1.15}$$

Where $f(x)$ is a deterministic nonlinear function and the term αdW, the diffusion term that represents the stochastic part of model (C.1.15), the solution of it can be obtained by using the discrete recursive formula [1]

$$X_{n+1} = X_n + hf_{n+1} + \alpha_n \Delta W_n \tag{C.1.16}$$

In (C.1.16) $t_0=0<t_1=\Delta t<\ldots<t_k=k\Delta t<\ldots<T=N\Delta t$ is the discretized version of the continuous interval of time $t\epsilon$ [0 T]; thus, $X_{n+1}=x(t_{n+1})$, $X_n=x(t_n)$, $f_{n+1}=f(t_{n+1})$, and ΔW_n are increments of a standard Wiener process, for details in the formulation of (C.1.15)-(C.1.16) the reader can consult references [1]- [5].

For multi-dimensional linear stochastic differential systems, (C.1.15) takes the form given by

$$dx = Axdt + FdW \tag{C.1.17}$$

Being x an n-dimensional vector and dW an m-dimensional standard Winner process [1], A and F are matrices of appropriate dimensions. From (C.1.16) it follows that for the multidimensional linear case,

$$X_{n+1} = X_n + hAX_{n+1} + \alpha_n \Delta W_n \tag{C.1.18}$$

and solving for X_{n+1}, then

$$X_{n+1} = (I - hA)^{-1}(X_n + \alpha_n \Delta W_n) \tag{C.1.19}$$

For numerical validation of the analytical results developed in this thesis, the implicit Euler scheme is widely used in Chapter 7.

References.

[1] Kloeden, P. E., Platen, E., & Schurz, H. (2012). Numerical solution of SDE through computer experiments. Springer Science & Business Media.

[2] Holden, H., Øksendal, B., Ubøe, J., & Zhang, T. (1996). Stochastic partial differential equations (pp. 141-191). Birkhäuser Boston.

[3] Gardiner, C. W. (1985). Handbook of stochastic methods (Vol. 4). Berlin: Springer.

[4] Kloeden, P. E., & Pearson, R. A. (1977). The numerical solution of stochastic differential equations. The Journal of the Australian Mathematical Society. Series B. Applied Mathematics, 20(01), 8-12.

[5] Higham, D. J. (2001). An algorithmic introduction to numerical simulation of stochastic differential equations. SIAM review, 43(3), 525-546.

CENTRO DE INVESTIGACIÓN Y DE ESTUDIOS AVANZADOS DEL I.P.N.
UNIDAD GUADALAJARA

El Jurado designado por la Unidad Guadalajara del Centro de Investigación y de Estudios Avanzados del Instituto Politécnico Nacional aprobó la tesis

Un Enfoque Estadístico a la Estimación Modal de Sistemas de Potencia Sujetos a Excitación Ambiente

del (la) C.

Juan Antonio MEDINA ROSAS

el día 24 de Agosto de 2015.

Dr. José Manuel Cañedo Castañeda
Investigador CINVESTAV 3C
CINVESTAV Unidad Guadalajara

Dr. Federico Sandoval Ibarra
Investigador CINVESTAV 3C
CINVESTAV Unidad Guadalajara

Dr. Arturo Román Messina
Investigador CINVESTAV 3C
CINVESTAV Unidad Guadalajara

Dr. José Raúl Loo Yau
Investigador CINVESTAV 3B
CINVESTAV Unidad Guadalajara